BACKGROUND UV IN THE 300 TO 400 nm REGION AFFECTING THE EXTENDED RANGE DETECTION OF RADIOACTIVE MATERIAL

by

WILLIAM CAREY WEST

A DISSERTATION

Submitted in partial fulfillment of the requirements for requirements
for the degree of Doctor of Philosophy in the
Department of Mechanical Engineering
in the Graduate School of
The University of Alabama

TUSCALOOSA, ALABAMA

2010

ABSTRACT

The desire to find alternative methods for the detection of radioactive material at extended ranges has resulted in an increased interest in the detection of the air fluorescence resulting from the alpha or beta radioactive particle's interaction with molecules of air. Air fluorescence photons travel further than the radioactive particles, allowing for detections at longer distances. However, any detection of the ultraviolet (UV) air fluorescence is dependant on overcoming natural and man-made background UV to achieve favorable signal to noise ratios.

This research describes laboratory and field experiments conducted to determine the background UV in the 300 to 400 nm region of the electromagnetic spectrum for certain detection scenarios, and number of UV air fluorescence photons required to achieve detections with a certain confidence limit. The reflective, scintillation, and transmissive UV characteristics of some common materials are discussed and their contribution to a successful detection explored. Additionally, the contributions to the UV background from natural and man-made light sources are investigated. The successful outside optical detection of alpha and beta radioactive isotopes in the 300 to 400 nm region is possible in the lower part of the spectral region (i.e., near 316 nm), when there is no UV light from man-made sources in that band and only natural light exists. Alpha sources (i.e., ^{241}Am) equal to or larger than 1.017 curies, theoretically can be detected with 95% confidence during nighttime scenarios with moonless overcast skies at a distances of 20 meters at 316 nm with the optical system assumed for these calculations. Additionally, where scintillators are available that can be employed near ^{90}Sr

radioactive sources, the detectable activities can be reduced by factors as high as 250. This allows for detections of sources in the millicuries. Tests results are presented for several common materials (e.g., polypropylene, high density polyethylene, low density polyethylene, etc.) that scintillate in the presence of ^{90}Sr and can be used to achieve gains in the 100s in the air fluorescence bands centered on 316 nm and 337 nm.

LIST OF ABBREVIATIONS AND SYMBOLS

B	Background UV
Bq	Becquerel, 2.703 x 10^{-11} curies
CCD	Charge Coupled Device
C.I.E	Commission Internationale de l'Eclairage
CDL	Lower critical limit
cos	Cosine
d	Distance from the radioactive source to the collector
HDPE	High density polyethylene
IUPAC	International Union of Pure and Applied Chemistry
L_c	Lower limit of detection
LDPE	Low density polyethylene
MFP	Mean free path, the distance between successive interactions
MDNC	Minimum detectable number of counts
MDNP	Minimum detectable number of photons
mCi	Millecurie = 3.7 x 10^7 disintegrations per second
N_2	Second positive of excited nitrogen molecule
N_2^+	First negative ion of excited nitrogen
$N_{s_{\min}}$	Minimum detectable number of counts of the fluorescence signal
N_s	Fluorescence signal

N_T	Total fluorescence signal
$N_{B.}$	Background signal
PMT	Photomultiplier tube
PNNL	Pacific Northwest Laboratory
PVC	Polyvinyl chloride
r	Radius of collector
S	Signal
SNR	Signal to noise ratio
S_S	Scintillation signal (counts/minute)
S_{Fbop}	Air fluorescence, back of material, outside the perimeter (cts/minute)
S_{Fbt}	Air fluorescence, back of material, transmitted through (cts/minute)
S_{Ff}	Air fluorescence signal in front of the material (cts/minute)
S_B	Background noise signal (S_B) (cts/minute)
$S_{SFbopFbtFfB}$	Total signal = scintillation + air fluorescence + background
$S_{SFbopFfB}$	Total signal – fluorescence behind material transmitted through material
$S_{FbopFfB}$	$S_{Fbop} + S_{Ff} + S_B$ = Signal fluorescence plus background minus S_{Fbt}
TSA	Transportation Security Agency
USGS	U.S. Geological Survey
UV	Ultraviolet
UV-A	315 to 400 nm region of ultraviolet
UV-B	Ultraviolet in the 280 to 315 nm region
UV-C	Ultraviolet in the 100 to 280 nm region
$\bar{X}^2$	Mean squared

x_a	Some threshold value
x_{bi}	Mean of a blank
x_L	Smallest measure of concentration
σ^2	Variance
σ	Standard deviation
σ_o	Standard deviation when signal is zero
σ_{bi}	Standard deviation of blank
$\sigma_{instrument\_dark\_count}$	Standard deviation of instrument dark count
θ_0	Angel between optical axis and solid angle boundary
Ω	Solid Angle

ACKNOWLEDGMENTS

I wish to thank my advisor, Dr. Daniel J. Fonseca, whose patience and support never wavered. He provided timely and sound advice as I negotiated the academic hurdles to complete this dissertation. I would also like to thank Dr. Willard C. Schreiber Jr., Dr. Clark Midkiff Jr., and Dr. Timothy A. Haskew, for their patience and support throughout my academic career. I want to give a special thanks to Dr. Chris Winstead for allowing me to use the resources of the Signal Research Center to conduct my research and always providing timely advice as I struggled to overcome many technical problems and equipment shortages. Additionally, to each committee member, I give special thanks. During my recent illness, each member of my committee provided the moral support necessary to for me to continue by research. Your kind thoughts and support were instrumental in my determination to finish my research. Lastly, I would like to thank my family. Throughout my long and varied academic career, you have always been there for me. You have motivated me when my spirits were low and have always shown pride in my achievement. I truly appreciate the love and support you have provided.

CONTENTS

ABSTRACT……ii

LIST OF ABBREVIATIONS AND SYMBOLS ……..iv

ACKNOWLEDGMENTS .. ……vii

LIST OF TABLES…….....xi

LIST OF FIGURES……xii

1. INTRODUCTION…….....1

1.1 Background.....2

1.2 Problem Statement…….....9

1.3 Objectives of Research…… ……..…. 9

2. LITERATURE SEARCH…… ……12

2.1 The Background UV Problem 13

2.2 Historical Background of Optical Detection Methods…….....13

2.3 Sources of Background.....17

2.3.1 Air fluorescence from materials in the vicinity of the irradiator 18

2.3.2 Air fluorescence from the earth's surface, and other materials/structures....20

2.3.3 UV photons from solar radiation, lights, scintillation, and reflected UV 20

2.3.3.1 Background UV photons from solar radiation 20

2.3.3.2 Background UV photons from man-made lights..…….....21

2.3.3.3 Photons produced from material scintillation 26

2.3.3.4 Photons reflected into the detectors field of view 29

2.3.4 Other UV Background 31

2.4 Literature Search Summary 32

3. SIGNAL DETECTION 34

3.1 Statistics of Signal Detection 34

3.2 Solid Angle 38

3.3 Collection System 40

4. SCINTILLATION OF STUDIED MATERIALS 42

4.1 Source Deployment Devices 43

4.2 Methodology of Scintillation Testing 46

4.3 Air Fluorescence Images of ^{241}Am 51

4.4 Air Fluorescence Images of ^{90}Sr 53

4.5 Scintillation of Materials by ^{241}Am 55

4.5.1 Tests Setup 56

4.5.2 Tests Results 57

4.5.3 Tests Conclusion 59

4.6 Scintillation of Materials by ^{90}Sr 60

4.6.1 Test Setup 61

4.6.2 Test Results 63

4.6.3 CCD Image of Scintillation by ^{90}Sr 66

4.6.4 Tests Conclusions 68

5. REFLECTIVE CHARACTERISTICS OF STUDIED MATERIALS 70

5.1 Back Reflective Characteristics of Studied Materials 70

5.2 Spectral Reflective Characteristics of Studied Materials.....74

5.3 Conclusion 77

6. TRANSMISSIVE CHARACTERISTICS OF STUDIED MATERIALS…..……81

6.1 First Transmission Technique …….……82

6.2 Second Transmission Technique Using a Spectrometer …….……84

6.3 Conclusions.....86

7. OUTDOOR BACKGROUND LEVELS ……..88

7.1 Solar Background…….88

7.2 Nighttime Optical Background Levels of Potential Targets…….....…93

7.2.1 Test Setup for the Nighttime Optical Background……...……...94

7.2.2 Background Surveys of Potential Targets……..……..94

7.3 Man-made Clutter Other Than Lighting … .....……116

7.4 Conclusion 117

8. CONCLUSIONS AND OPPORTUNITIES FOR FUTURE WORK 119

8.1 Conclusions.....119

8.2 Opportunities for Future Work 123

REFERENCES 126

LIST OF TABLES

2.1 Levels of Activities from Natural Sources in Common Construction Materials.....19

2.2 General Lighting Sources 22

2.3 Properties of some common scintillation materials.....28

3.1 Probability Values and Confidence Limits.....37

4.1 Studied Materials.....46

5.1 Reflective Tests Materials 73

6.1 Transmissive Tests Materials 82

6.2 Percent Transmission Compared to Air.....83

6.3 Percent Transmission Compared to Air Using a Spectrometer 86

7.1 Reference Solar Spectral Irradiance from ASTM G173-3 at Sea Level 90

7.2 Photon Flux Density..... 91

7.3 CDL and MDNP for Daylight Operations.....92

7.4 CDLs and MDNPs for Nighttime Operations 92

8.1 Prediction of ^{241}Am Activity Required at 316 nm for Daytime Scenarios.....122

8.2 Prediction of ^{241}Am Activity Required at 316 nm for Nighttime Scenarios 122

LIST OF FIGURES

1.1 Fluorescence spectrum generated by the electrons impact in nitrogen 6

1.2 Optical system field-of-view effect on air fluorescence detection 7

2.1 Spectral Irradiance of terrestrial direct beam solar radiation 21

2.2 Linear Spectral Irradiance at 1000 LUX of: A) Quartz Hal Capsule, B) MR16 with Cover/Glass, and C) T8 Lamp 23

2.3 Logarithmic Spectral Irradiance at 1000 LUX OF: A) Quartz Hal Capsule B) MR16 with Cover/Glass, and C) T8 Lamp 23

2.4 UV Spectral Irradiance at 1000 LUX Comparing Ce/Ti Doped Quartz and Undoped Quartz Capsules 24

2.5 UV Spectral Irradiance of Sun at 30 degrees from Zenith Compared to a 120 W Par-38 and a 400 Watt HP Hg Lamp 24

2.6 UV Spectral Irradiance at 1000 LUX for 400 W Hg, MH and HPS Lamps 25

2.7 UV Spectral Irradiance at 1000 LUX for three Par-38 Lamps and a 150 W Quartz Halogen Capsule 25

2.8 UV Spectral Irradiance at 1000 LUX for Dichroic and Aluminum MR16's, one with Cover Glass 26

2.9 Reflectance of Light Gray Brick 30

2.10 Reflectance of Dark Red Brick 30

2.11 Reflectance of Gray and Red Brick 31

3.1 Point Source and Collector 39

3.2 Cooler with PMT, Filter Wheel, and 100 mm Lens 41

3.3 CCD Camera and 100 mm Lens 41

4.1 Irradiator #1 with source in the exposed position 44
4.2 Irradiator #2 with source in unshielded position 45
4.3 Source angled to the surface of the studied material, Setup #1 47
4.4 Source placed behind studied material, Setup #2 47
4.5 Signal with effects of scintillation shielded 50
4.6 Air fluorescence image collected by CCD 52
4.7 Air fluorescence image overlaid on source holder 52
4.8 Air fluorescence aura around ^{241}AM 53
4.9 ^{63}Ni air fluorescence image color enhanced 54
4.10 ^{63}Ni air fluorescence image color enhanced overlaid on image of holder 55
4.11 ^{241}Am on material surface used to determine $S_{SFbopFfB}$ 56
4.12 ^{241}Am with material shield to measure $S_{FbopFfB}$ 57
4.13 Scintillation of Studied Materials with ^{241}Am 58
4.14 Air Fluorescence of ^{241}Am 59
4.15 Scintillation – Air Fluorescence Ratio 59
4.16 Test material over ^{90}Sr source 61
4.17 Scintillation of Studied Materials with ^{90}Sr 64
4.18 Air Fluorescence of ^{90}Sr 65
4.19 Scintillation – Air Fluorescence Ratio 65
4.20 Total Scintillation – Air Fluorescence Ratio 66
4.21 HDPE Scintillation 5 Minute Exposure 67
4.22 Polypropylene Scintillation 5 Minute Exposure 67
4.23 LDPE Scintillation 5 Minute Exposure 68

5.1 Spectrometer, Deuterium Lamp, Probe, and Test Block....71
5.2 Reflectivity Standard (RS50) Halon 72
5.3 Back Reflectivity Setup....72
5.4 Reflectance Back at 45 Degrees on Aluminum, Brick and Concrete 73
5.5 Reflectance Back at 45 Degrees on Translucent Materials and Plastics....74
5.6 Reflectance Back at 45 Degrees on Wood/Paper Products....74
5.7 Test Block with Probe Mounted on Top at 90 degrees 75
5.8 Specular Reflective Characteristics Setup....76
5.9 Specular Reflectance Wood/Paper Products 76
5.10 Specular Reflectance of Translucent Materials and Plastics....77
5.11 Specular Reflectance of Brick and Concrete....77
6.1 Test Sample between the PMT and the 4 inch Lens 83
6.2 Test Material between Deuterium Lamp and the Spectrometer....84
6.3 Transmission Test Stand 85
6.4 Transmission Curves for Materials in Table 6.1 85
7.1 ASTM G173-3 Irradiance Data (Global Tilt)....89
7.2 Extended Range Detection where $d >> r$ 94
7.3 Strip Mall Lights – Houston....96
7.4 Strip Mall Lights – Hattiesburg....97
7.5 Strip Mall Lights - Tuscaloosa 97
7.6 Supermarket Parking Lights - Houston....98
7.7 Supermarket Parking Lights – Hattiesburg 98
7.8 Supermarket Parking Lights – Tuscaloosa....99

7.9 Drug Stores - Houston 99
7.10 Drug Stores – Hattiesburg 100
7.11 Drug Stores – Tuscaloosa 100
7.12 Restaurant Lighting – Houston 101
7.13 Restaurant Lighting – Hattiesburg 101
7.14 Restaurant Lighting – Tuscaloosa 102
7.15 Convenience Store Lighting – Hattiesburg 102
7.16 Convenience Store Lighting – Tuscaloosa 103
7.17 Mall Lighting – Houston 103
7.18 Mall Lighting – Hattiesburg 104
7.19 Mall lighting – Tuscaloosa 104
7.20 Hospital Lighting – Houston 105
7.21 Hospital Lighting – Hattiesburg 105
7.22 Hospital Lighting – Tuscaloosa 106
7.23 Bank Parking – Houston 106
7.24 Bank Parking – Hattiesburg 107
7.25 Bank Security Lighting – Houston 107
7.26 Bank Security Lighting – Hattiesburg 108
7.27 Bank Teller – Houston 108
7.28 Bank Teller – Hattiesburg 109
7.29 Fast Food Parking – Houston 109
7.30 Fast Food Parking – Hattiesburg 110
7.31 Home Improvement Lighting – Houston 110

7.32 Home Improvement Lighting – Hattiesburg 111
7.33 Post Office Lighting – Houston 111
7.34 Post Office Lighting – Hattiesburg 112
7.35 Hotel Lighting (Parking)- Hattiesburg 112
7.36 Hotel Lighting (Parking)- Hattiesburg 113
7.37 Hotel Security Lights – Hattiesburg 113
7.38 Hotel Security Lights – Hattiesburg 114
7.39 Auto Dealer Lighting – Houston 114
7.40 Auto Dealer Lighting – Hattiesburg 115
7.41 Street Lights – Houston 115
7.42 Street Lights – Hattiesburg 116
7.43 Commonly Available Outdoor Lights 116
7.44 Clutter from a Stun Gun Arc, a Lighter, and a Propane Flame 117

CHAPTER 1

INTRODUCTION

The purpose of the research is to examine the optical detection of alpha and beta radioactive sources in the 300 to 400 nm region of the electromagnetic spectrum in the presence of selected common materials and background ultraviolet light (UV). In doing so, one must not only understand the effects of solar and man-made radiation sources, but also look at how different materials in the path of alpha and beta radiation affect the induced UV air fluorescence, resulting from the radiation, and integrate those effects in the optical detection and imaging processes for radioactive contamination. This research analyzes the air fluorescence produced by alpha and beta radiation at distances exceeding currently used detection devices. While the air fluorescence produced from the effects of alpha and beta radiation occurs in close proximity to the radioactive source, fluorescence produced from the effects of gamma radiation is spread over a much larger volume. Thus, the air fluorescence from alpha and beta radiation is more easily brought into the field of view of the collection instruments. This makes optical detection methods more efficient for small alpha and beta sources than for small gamma sources.

Using reflective and refractive single photon counting optical sensors and advanced imaging techniques, radioactive contamination can be mapped and identified as alpha (Baschenko 2004 and Lamadie et al. 2004) and beta radiation (Leybourne et al. 2010) at extended distances. The utilization of optical detection methods requires a good understanding of background UV sources and their associated fluctuations. To understand the UV background,

contributions to the background signal due to solar radiation, man-made lighting, and material scintillation are examined, as well as the transmissive and reflective properties of different materials in the path from the optical detector to the radioactive source. The conducted study enhances the development of a decision support tool for identifying radioactive contamination.

1.1 Background

Modern radiation detection systems limit the detection of the radiation from the radioactive material, to the range of travel of the radiation in air. These ranges are approximately 4 cm for alpha, up to 10 m for beta, and 10s to 100s of meters for gamma. For small gamma sources, detection is limited, generally, to ranges of tens of meters depending on the size of the instrument, allowable weight, cost, measurement time, mass and composition of the target, required confidence, and shielding. Current detection systems use scintillation and semiconductor technologies to detect the radioactive particle arriving at the collecting instrument. For purposes of the current research, background levels are analyzed to understand their effects in the detection of alpha and beta radiation.

The Alpha particle is a helium nucleus consisting of two neutrons and two protons, and is 7,300 times heavier than an electron (Shapiro 2002). The particle is a lower speed particle than the electron, and it has a high linear energy transfer (Shapiro 2002). Consequently, it has a range much less than electrons with comparable energies. A typical alpha particle has energy of 5 MeV, and will travel about 3.5 cm in air, compared to 415 cm for a beta particle with a fifth as much energy (Shapiro 2002).

Beta particles are high-speed electrons emitted from the nuclei of atoms during the decay process and slow down as they lose energy. The electron is ejected as a neutron is

transformed into a proton (Shapiro 2002). The commonly used beta emitters ^{3}H, ^{14}C, ^{45}Ca, ^{32}P, and ^{90}Sr have a range in air of 0.006, .305, .610, 8.84 meters (i.e., 0.02, 1, 2, 20, and 29 feet), respectively (Shapiro 2002).

Gamma rays are electromagnetic radiation of uncharged ionizing particles emitted by the radioactive nuclei in the form of energy packets, called photons. All gamma rays travel at the speed of light (Shapiro 2002). Their speed is not reduced with a decrease in energy. Gamma rays lose energy through chance encounters with atoms. They could lose all or only part of their energy. If energy remains, the gamma ray continues to travel at the speed of light as a lower energy photon (Shapiro 2002). Thus, it is possible for some gamma rays to travel greater distances than alpha or beta particles. There is a finite probability that some gamma rays can pass through a medium. This probability is dependent on the energy of the gamma ray, the composition of the medium, and the thickness of the medium (Shapiro 2002). Although the mean free path (MFP), the average distance the photon travels between successive interactions (Tsoufanidis 1995), in air having a density of 1.225 kg/m^2 exceeds one hundred meters for a 1 MeV gamma ray, the detectability of the signal is limited by the spherical spreading of the radiation, the attenuation due to air, and background radiation. Considering only spherical spreading, the signal experiences a $1/d^2$ fall-off as the photons travel a distance d (Shapiro 2002).

This research program is focused on detecting the effects (air induced fluorescence) of the radiation on the atmosphere surrounding a radioactive source. Radiation interacting with the atmosphere can create ionized and neutral molecules, and the emission of ultraviolet photons from excited atmospheric species (Davidson and O'Neil 1964, Bunner 1964 and 1967).

A number of experiments have clearly established that radiation stimulates "air fluorescence" in the ultraviolet region of the spectrum, and that the fluorescence is dominated by

the emissions from N_2 second positive and the N_2+ first negative transitions in the 300 to 400 nm band (Bunner 1964 and 1967, O'Neil and Davidson 1964 and 1968, Ave et al. 2007). Physicists from the University of Utah were the first to detect fluorescence light from cosmic ray showers in 1976 (History of Air Fluorescence Technique, http://www.telescopearray.org/outreach/history.html). Experiments are continuously being conducted to precisely measure air fluorescence efficiencies (Huntemeyer 2003 and Waldenmaier, Blumer, and Klages 2008).

The capability of alpha, beta, and gamma radiation to stimulate air fluorescence allows for a detection of contamination from the presence of radioactive materials, including contamination from nuclear accidents, radiation dispersal devices or equipment in nuclear production facilities. Extensive laboratory experiments have been performed in recent years, and the results of these experiments used to design optical systems appropriate for the long range detection of radioactive materials. Long-range tests were performed using alpha and beta emitting radionuclides in 2009 at the Y-12 National Security Complex in Oak Ridge, Tennessee (Leybourne et al., 2010). These field tests demonstrated that appropriately designed optical systems using effective spectral filtering are capable of detecting these materials at ranges orders of magnitude larger than today's best commercial devices. The field tests also suggested the importance of obtaining a picture of the target area in the visible spectrum to locate possible background UV sources. Once the location of background UV sources is known, it may be possible to narrow the collection instrument's field of view or reposition the instrument to reduce the background UV. Additionally, an image of the air fluorescence aura can be overlaid on the picture of the target area to a give a spatial understanding of the contamination.

Although field tests have validated that the collection of UV photons can be accomplished, with the proper filtering of noise, at distances exceeding 150 meters, the sources

of the background UV are not completely understood. In addition to the effects of solar radiation and man-made lighting, the capability of common materials to transmit and reflect UV can have an impact on a definitive detection. Additionally, the scintillation of these materials in the UV can also be a contributor to the observed signal. Because the reflective, transmissive, and scintillation contributions of materials vary by wavelength, the contributions due to these common materials can enhance or limit the detection at one wavelength, and have the opposite effects at other wavelengths.

The characterization of the aura produced by these radionuclides and the development of prediction tools is dependent upon understanding the effects of materials prone to scintillate in the radiation path, how these materials reflect or attenuate radiation and air induced fluorescence, and the effects of background UV. This research examines common sources of background UV in the 300 to 400 nm range of the electromagnetic spectrum. The scintillation, reflective, and transmissive effects of common materials, some found in nuclear and industrial production facilities, are examined in ambient air in the path of the radiation, and the air induced fluorescence resulting from the radiation collected. This research integrates those effects with other background UV sources (i.e., solar and man-made lighting) to determine the possibility of achieving a definitive detection.

Air fluorescence (see Figure 1.1) primarily results from emissions from excited nitrogen molecules and ions, namely the N_2 second positive and N_2^+ first negative transitions (Bunner 1964 and 1967, Davidson and O'Neil 1968, Kakimoto 1996, and Nagano et al. 2001). The 300-400 nm spectral emissions are widely used for detecting air fluorescence because of the high fluorescence yields at 316 nm, 337 nm, 354 nm and 391 nm as shown in Figure 1.1 (Baschenko 2004 and Lamadie et al. 2004). High background levels limit the detection of air fluorescence,

and require careful optical filtering for transmitting emission spectral bands and rejecting background light. When radioactive materials are shielded by other materials (e.g., shipping containers, storage containers, etc.), charged-particle alpha and beta radiation emissions are attenuated by the container material, suggesting that detecting radioactive material in the containers through the optical detection of air fluorescence will be dependent upon air fluorescence generated by gamma rays. A leak in containment may permit sufficient quantities of alpha and beta radiation to escape allowing for a detection. Gamma rays are photons, not charged particles as described above, but the Compton scattering of gamma rays from nitrogen or oxygen molecules in the atmosphere leads to significant ionization and thus the emission of electrons. These emitted electrons subsequently can cause air fluorescence emissions.

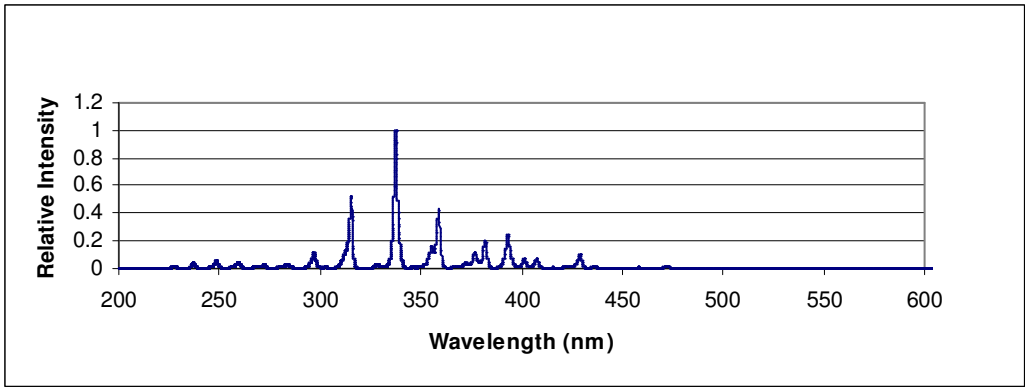

Figure 1.1: Fluorescence spectrum generated by the electrons impact in nitrogen. Source: Data from O'Neil and Davidson (1968).

Figure 1.2 illustrates the optical system field-of-view effect on the air fluorescence generated around a point source. For gamma radiation, the radiation flux (i.e., the signal detected by standard gamma direct radiation detectors) falls off approximately as $1/d^2$ (Shapiro 2002), where d is the distance from the radiation source. Because gamma radiation can travel 100s of meters (Leybourne et al. 2009), and air fluorescence is generated along the path as the radiation interacts with the molecules of air, the air fluorescence signal in the field-of-view will

decrease at a rate less than $1/d^2$. The air fluorescence volumes generated by alpha and beta sources, where the radiation travels a few centimeters to a few meters, respectively, will be smaller than those for a gamma source with the same activity (Leybourne et al. 2009). Thus, the air fluorescence from alpha and beta radiation can more easily be collected with an instrument having a narrower field-of-view; while a larger field-of-view instrument is required for gamma sources (Leybourne et al. 2009). Additionally, as the instrument in Figure 1.2 moves farther away from the gamma source to capture a greater portion of the fluorescence volume, more background UV comes into the field-of-view. Therefore, optical detection methods are more appropriate for alpha and beta sources than for similar activity gamma sources.

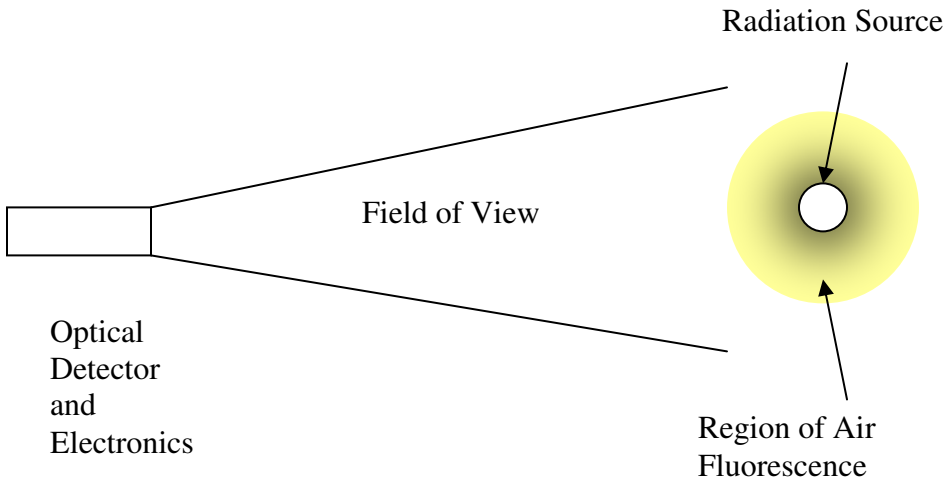

Figure 1.2: Optical system field-of-view effect on air fluorescence detection

For a particular wavelength, the signal received by the detector is studied to determine:

1) The contribution of the air fluorescence produced by the atmospheric effects of the radioactive source,
2) The contribution due to background noise from other UV sources,
3) The contribution due to scintillation in the path from other materials, and

4) The effects of the transmissive and reflective properties of materials in the field of view

Detecting beta emitters and alpha emitters using direct (conventional) detection methods requires placing the detectors in close proximity to the actual radioactive material. Mapping a ^{90}Sr contamination event using direct detection of the beta radiation would require examining surfaces at ranges less than 8.84 meters (maximum range for ^{90}Sr beta in air according to Shapiro 2002). Mapping an alpha source would require the placement of the detector within a few centimeters (maximum range of alpha in air according to Shapiro, 2002) of the source of the contamination. Safety considerations dictate a long-distance detection system that can map large areas while ensuring personnel safety.

Ukrainian and French scientists have demonstrated the ability of using optical detection methods to image radioactive sources (Baschenko 2004 and Lamadie et al. 2004). The Ukrainian scientists imaged an alpha source in the presence of a high activity gamma source on film strip at a distance of 30 meters (Baschenko 2004). French researchers placed an electrodeposited ^{241}Am source at a distance of 0.6 meter in front of a CCD camera, and obtained a good image after an exposure time of 1 hour (Lamadie et al. 2004). Further tests using ^{238}Pu yielded an image after an exposure time of 5 hours. Additionally, the transmissive properties were examined for a one millimeter thick surface of Triplex, Polycarbonate, and Plexiglas, yielding transmission values relative to the same air thickness of 91, 92, and 97 percent, respectively (Lamadie et al. 2004). The Ukrainian and French tests validate the imaging concept in the 300 to 400 nm wavelength portion of the UV spectrum, but both suffer from the limitation of only being able to image in total darkness.

1.2 Problem Statement

This study addresses the following two unknowns: (1) Can the air fluorescence signal of a radioactive source in the UV from 300 to 400 nm be distinguished from other background UV, suggesting the possibility of a decision support matrix to distinguish radioactive sources from other UV sources for particular background scenarios (e.g., background conditions that include a radioactive source in the presence of common materials and UV from solar and commercial lighting)? (2) Can material scintillation in the UV due to the presence of radioactive sources be used to enhance the detection of the radioactive material?

1.3 Objectives of the Research

The study involves five main objectives:

(1) Examine common materials (i.e., plywood, concrete (smooth and textured), brick, aluminum, paper products, plastic materials, Polycarbonate, and Plexiglas) in the presence of radioactive sources (^{241}Am and ^{90}Sr) to determine the resulting contributions due to the material scintillation and air fluorescence photon emission in the UV spectrum from 300 to 400 nm.

(2) Examine common translucent materials (i.e., plastic covers, polycarbonate, and Plexiglas) in the presence of radioactive sources (^{241}Am and ^{90}Sr) to determine the resulting contributions due to the transmission of the air fluorescence photon emission in the UV spectrum from 300 to 400 nm.

(3) Examine the reflective characteristics of common materials (i.e., plywood, smooth and textured concrete, brick, aluminum, paper products, plastic materials,

Polycarbonate, and Plexiglas) in the presence of background UV light from 300 to 400 nm. Then, determine the likelihood of detecting radioactive sources (^{241}Am and ^{90}Sr) in the presence of the UV light.

(4) Determine outdoor background levels using a mini-spectrometer and use the detection levels established during the outdoor background surveys to determine the possibility of detecting the presence of radioactive material.

(5) Determine the possibility of a prediction tool for relevant isotopes' (i.e., ^{241}Am and ^{90}Sr) air induced fluorescence signals in the presence of common materials and background lighting conditions for specific optical test systems. Using the General Lighting Irradiance Curves (Bergman et al. 1995), outdoor background surveys, and the efficiency peaks from Bunner (1967) and Waldennaier (2008), determine the activity of the sources that are detectable, with 95% confidence, for particular background conditions.

Objectives 1 and 2 are accomplished using:

a. An optical system with known solid angle of collection and transmission characteristics

b. Dwell times that allow consistent and reasonable statistics.

c. Multiple photo-detectors (i.e., CCD camera and photomultiplier tubes) will be used during the scintillation testing. The CCD camera is used to image the spatial extent of the background noise, fluorescence signal, and the scintillation signal.

The PMT is used to collect photons during scintillation, air fluorescence, and transmission tests.

CHAPTER 2

LITERATURE SEARCH

Searches of literature and computerized data bases revealed a small number of literary sources dealing with the background issues associated with using optical identification methods for the detection of air fluorescence in the UV. The available resources point to the difficulty of obtaining a definitive detection in the presence of background UV, and identify the region from 300 to 400 nm as the portion of the spectrum providing the best opportunity of optical detection. Since air fluorescence (see Figure 1.1) primarily results from emissions from excited nitrogen molecules and ions, previous research using optical detection methods has concentrated on wavelengths (316, 337, 354, and 391 nm) of highest fluorescence efficiency. While these wavelengths may provide the best chance of a definitive detection, there exists a possibility that more favorable signal to noise ratios (SNRs) can be obtained at a given wavelength, provided that background spectral distributions are understood. A systematic approach exploring the spectrum in more detail could identify the regions for particular levels of background UV.

The capability of certain materials to transmit or reflect UV is also a consideration. This is especially important in nuclear facilities, where observing contamination through a transparent medium may be desirable (Lamadie et al. 2004). Additionally, the use of common materials as scintillators to provide more favorable signal to noise ratios in the 300 to 400 nm region should be explored. A good scintillator can increase the signal to noise ratio significantly, making detections of small quantities of radioactive materials possible at extended distances.

2.1 The Background UV Problem

The C.I.E (Commission Internationale de l'Eclairage—the International Commission on Illumination) identifies the 100-400 nm region of the Electromagnetic Spectrum as ultraviolet (McCluney, 1994). This region of the spectrum is further broken down into UV-A, extending from 315 to 400 nm, UV-B from 280 to 315 nm, and UV-C from 100 to 280 nm. Because wavelengths shorter than 200 nm are absorbed in air (Bergman, Parham, and McGowan 1995), this portion of the spectrum is of little significance for purposes of air fluorescence, and the UV-C area of interest is reduced to a region from 200 to 280 nm. For the optical detection of air fluorescence from radioactive sources at a particular wavelength, the signal received by the detector must be studied to determine:

1) The contribution of the air fluorescence generated by the atmospheric effects of the radioactive source
2) The contribution due to background noise from other UV sources
3) The contribution due to scintillation in the path from other materials, and
4) The effects, including atmospheric effects, associated with the transmissive and reflective properties of materials in the field of view

2.2 Historical Background of Optical Detection Methods

Investigations of alpha-radioluminescence were carried out by Baschenko in 2004. He indicated that 95 percent of the alpha induced fluorescence fell in a range between 310 to 400 nm (Baschenko 2004). He emphasized that direct detection methods were limited by the mean free path (MFP) of the ionizing radiation particle or photon. The mean free path is defined as the mean distance radiation particles or photons travel without interaction with another particle or molecule. Alpha particles, beta particles, or gamma ray photons with initial energy levels of a

few megaelectron volts would only have a mean free path in the atmosphere of a few centimeters, a few tens of meters, and a few hundred meters, respectively. Baschenko (2004) realized safety considerations indicated a need for new longer range detection methods. He found that the luminescence (fluorescence) from his alpha source was typically in a region 2-3 cm wide around the source. Baschenko (2004) estimated that each alpha particle emitted from a ^{239}Pu source surface resulted in the creation of 30 UV photons in ambient air. He also noted the alpha particles were emitted from the source surface with an angular distribution of $cos^{8}(\theta)$. The spectrum was identified using a 29 mm x 62 mm ^{239}Pu source baked into an enamel plate measuring 35 nm x 70 nm, and an optical detector able to detect down to the single photon level in the 190 to 800 nm spectral range (Baschenko 2004). The alpha-spectrum was determined using an optical imaging system consisting of a spherical mirror, an optical glass transmitting 60 percent of the UV in the 300-400 nm range, a selected film strip for the image, and a protective metal plate for the film to shield the film from gamma ray emissions (Baschenko 2004). The distance from the mirror to the source was 30 meters. To verify the assumption that different alpha and gamma sources produced various brightnesses which would present the possibility of identifying alpha in the presence of gamma, Baschenko (2004) placed six 1 mCi alpha sources on a bar separated by a distance of 5 cm with a 5 mCi ^{60}Co gamma source placed 200 mm aside the center of the 6 alpha sources. Baschenko (2004) obtained an image of the fluorescence enabling him to identify the aura for each alpha source in the presence of the gamma source. Additional calculations were performed showing the possible applicability of the research to the imaging of nuclear material using a CCD area photodetector (Baschenko 2004).

In 2004, French scientists presented results demonstrating the applicability of a CCD detector in alpha imaging in the region between 300 and 400 nm (Lamadie et al. 2004). After

using gamma imaging for nuclear decommissioning operations for over 10 years, the French realized that gamma imaging was not sufficient for all types of contamination present (Lamadie et al. 2004). They explored the detection of ultraviolet radiation emitted by nitrogen when irradiated with alpha particles (Lamadie et al. 2004). Acknowledging the effects that charged particles have in air in the research conducted by O'Neil and Davidson (1968), and the spectral information identified by Bunner (1964) in his study on comic ray detection by air fluorescence, the French (Lamadie et al. 2004) recognized the nitrogen molecule emits electromagnetic radiation primarily in the near ultraviolet portion of the electromagnetic spectrum. The emissions were characterized by the Japanese (Kakimoto et al. 1996) for the main wavelengths of 337.1 nm, 357.7 nm, and 391.4 nm for different charged particles for the nitrogen molecule in air. By placing an electrodeposited 30 kBq ^{241}Am source at a distance of 0.6 meters in front of a CCD camera, cooled with liquid nitrogen and treated to enhance the detection efficiency in the region between 300 and 400 nm, the French (Lamadie et al. 2004) obtained a good image after an exposure time of 1 hour. The aura from the source extended several centimeters from the surface validating the aura seen by Baschenko (2004) in his experiments. Further tests, using a 9.1 cm^2 circular ^{238}Pu source uniformly incorporated in anodized aluminum, demonstrated the ability to image a uniformly contaminated surface at a distance of 20 cm after an exposure time of 5 hours (Lamadie et al. 2004). Of particular interest is Lamadie et al.'s (2004) discussion of the signal to noise ratio (SNR). Defining the SNR as the measure of the net signal amplitude compared to image noise fluctuations (standard deviations), the research team (Lamadie et al. 2004) emphasized the difficulty of locating a 30 kBq 241 Am source where the SNR was less than 1 (SNR < 1).

Additionally, the transmissive properties in the UV for (300 to 400 nm) were examined for a one-millimeter thick surface of Triplex, Polycarbonate, and Plexiglas, yielding transmission values relative to the same thickness of air of 91, 92, and 97 percent, respectively (Lamadie et al. 2004). While the French (Lamadie et al. 2004) validated Baschehko's (2004) proposed practical application for imaging the fluorescence using a CCD camera in the 300 to 400 nm area of interest in a dark environment, the French (Lamadie et al. 2004) effort did not analyze the region in more discrete increments to determine the possibility of obtaining an image with limited background UV.

Hannuksela (2010) discusses the challenges of determining and dealing with background signals and indicates optical detection is promising for safety and security scenarios where UV lighting can be avoided. He uses a portable demonstration device consisting of a 3 inch collector, a photomultiplier tube, and a 40 nm filter (i.e., from Semrock, Inc.), centered on 320 nm, to capture the fluorescence signal peaks at 316 nm and 337 nm from a 1 kBq alpha emitter. Unable to separate the background from the fluorescence signal, he uses the signal in the 299 to 303 nm region as an estimate of the background. For outside detection scenarios, this technique is of little value. Since the background is dropping sharply from 340 nm to 299 nm as shown in Figure 2.1, any estimate for the background at 337 nm, based on a value at 299 to 300 nm, would be an extremely low estimate.

Leybourne et al. (2010) examined possible alternative techniques (other than direct radiation detection) for the stand-off detection of radioactive material and identified optical fluorescence detection techniques as promising. Alpha and beta sources were identified with a confidence of greater than 99% at extended distances. Radioactive sources and dummy sources

were placed on drums 100 meters from the collector and the drums scanned to distinguish the real sources.

Pressure, humidity, and temperature affect the fluorescence efficiency. As the pressure goes from 100 mm Hg to 760 mm Hg in the 337 nm band, which is dominated by N_2 second positive bans, tests show that the fluorescence yields increase (Kakimoto et al. 1996). The opposite is true in the region around 391 nm, which is dominated by the N_2+ first negative. In that region, tests show a decrease in fluorescence efficiency with the increase in pressure (Kakimoto et al. 1996).

As the temperature decreases from 320 to 240 degrees Kelvin at 314 nm, 337 nm, and 354 nm, recent studies have shown a decrease in fluorescence yield (Ave et al. 2007). The opposite is true in the band around 391 nm that is dominated by the N_2+ first negative. This band shows an increase in fluorescence yield (Ave et al. 2007).

With water vapor partial pressures up to 25 hPa, relative humidity 0 to 100%, there is a 20 % decrease in fluorescence yield at 314 nm, 337 nm, 354 nm, and 391 nm (Ave et al. 2007). The band around 391 nm, dominated by the N_2+ first negative, reacts in the same manner as the bands dominated by the N_2 second positive.

Temperature, pressure and humidity will not change rapidly during the proposed study, and will have a negligible effect on the data collected.

2.3 Sources of Background

Knoll's (1979) book titled *Radiation Detection and Measurement* identifies 5 categories of background radiation: (1) radioactivity from the materials of the detector; (2) radioactivity of equipment, supports, and shielding placed in the vicinity of the detector; (3) radiation from the earth's surface, wall of the laboratory, or other far away structures; (4) radioactivity in the air

surrounding the detector; and (5) primary and secondary components of cosmic radiation (Knoll 1979).

Knoll's (1979) categories dealt with the measuring the direct effects of radiation. Since this research focuses on collecting background UV photons created in the target area with the detector placed at extended distances from a radiation source, the direct effects of radiation from materials used to hold the detector are contained in the collector dark count (e.g., photon count with the collector covered to prevent light from entering). Cosmic radiation effects, Knoll's (1979) fifth category, are included in the dark count and background UV count (e.g., counts without the effects of the targeted radioactive material). Thus, if Knoll's (1979) remaining 4 categories are modified to for purposes of this research (i.e., air fluorescence and background UV in the detector's field of view), the resulting modified 4 categories are as follows:

1. Air fluorescence from the radioactivity of the materials used to construct devices (e.g., the irradiator) holding the radiation sources,

2. Air fluorescence from the radioactivity of the equipment, supports, and shielding placed in the vicinity of the irradiator in the field of view of the collector,

3. Air Fluorescence from radiation from the earth's surface, walls of the laboratory, local structures, and far away materials or structures in the field of view of the detector, and

4. UV photons from light sources in the detector's field of view (i.e., to include those from the scintillation of materials), and UV photons reflected from sources outside the detector's field of view back into the detector's field of view

2.3.1 Air fluorescence from materials in the vicinity of the irradiator

Man-made materials are used to construct the irradiator holding the radiation source, equipment, supports, and shielding placed in the vicinity of the irradiator. It has been established that many common construction materials are sources of radiation (Knoll 1979). Shown in Table 2.1 are activities of natural radioactive sources in common construction materials which have a

potential for producing UV photons. These activities are displayed in disintegrations per minute for a gram of the material. In detecting target sources of as small as a millicurie (i.e., where a curie = equal to 3.7 x 10^{10} disintegrations/second or 222 x 10^{10} disintegration per minute), there would have to be a considerable quantity of the material to generate a significant contribution to the background signal. As an example from Table 2.1, a ton (9.068 x 10^5 grams) of Portland Cement would produce 2.227x 10^5 disintegrations per minute from the ^{232}Th in the material, 11.8 x 10^5 disintegrations from the ^{238}U, and 18 x 10^5 disintegrations from the ^{40}K (Knoll 1979).

Table 2.1

Levels of Activities from Natural Sources in
Common Construction Materials

Materials	Disintegration/minute per gram of Material		
	^{232}Th(583keV)	^{238}U	^{40}K
Aluminum (6061 from Harshaw)	0.42	0.4	<0.05
Stainless Steel (304-L)	<0.005	<0.005	<0.02
Magnesium Rod	0.06	<0.04	0.1
Magnesium Ingot	<0.01	<0.002	<0.02
Pyrex Window	0.45	0.27	3.8
Molecular Sieve	4.4	3.0	9.0
Apiezon Q	4.5	4.5	2.7
Cement (Portland)	0.25	1.3	4.5

Source: Data from Knoll 1979

Although, the shear weight of large concrete structures may make these contributions significant when attempting to detect small sources in some applications, precautions will be taken to ensure that the materials used to construct the irradiator and support equipment will not contribute significantly to the air fluorescence. A survey of the test area and materials used to construct the irradiator will be conducted to establish radiation levels.

2.3.2 Air fluorescence from the earth's surface and other materials/structures

Air fluorescence from radiation from the earth's surface, laboratory walls, local materials and structures are not factors in this research exercise since testing is conducted in a controlled environment that has been screened to ensure that the only significant radiation sources are those controlled by the facility. Any air fluorescence from far away materials or structures in the field of view of the detector will become part of the optical background.

2.3.3 UV photons from solar radiation, lights, scintillation, and reflected UV

Background lighting conditions can yield noise levels that mask the signal from the radioactive sources. The light can go directly into the detector/collector from the source, be reflected into the collector from a surface, or be transmitted through some translucent materials.

2.3.3.1 Background UV photons from solar radiation

The spectral irradiance associated with solar radiation is a large component of background light that affects outside detection schemes. McCluney (1994) and ASTM G173-3 (see Figure 2.1) show similar curves for solar direct radiation.

The large number of photons generated by the sun makes utilization of optical signal recognition techniques almost impossible during daylight operations in the spectral region from 300 to 400 nm above 300 nm. However, because the highest relative fluorescence efficiencies (Figure 1.1) of nitrogen are located in the 300 to 400 nm portion of spectrum, prior research has focused on this region (Baschenko 2004, Lamadie et al. 2004, and Hannuksela 2010). Realizing a successful optical detection depended on controlling the solar background, prior studies have

been conducted inside in the dark or in controlled environments (Baschenko 2004, Lamadie et al. 2004, and Hannuksela 2010).

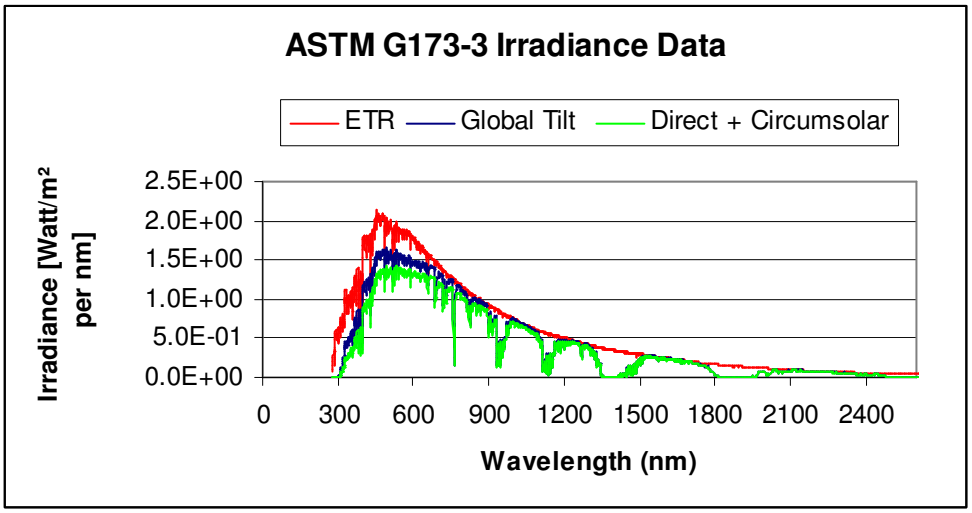

Figure 2.1: Spectral Irradiance of Solar Radiation. Source: Data from ASTM G173-3

2.3.3.2 Background UV photons from man-made lights

Man-made background lights can also be significant contributors to elevated background levels. Manufacturers generally provide spectral plots in the 380-760 nm region of the electromagnetic spectrum (see Spectral Power Distribution Curves at www.gelighting.com/na/ business_ lighting/education_resources/learn_about_light/distribution_curves, 2008). The damage UV-A and UV-B radiation can inflict on the human body has been a point of contention and the subject of a number of studies. Bergman, Parham, and McGowan (1994) presented a paper at the Annual Meeting of the Illuminating Engineering Society providing valuable spectral plots on commercial lighting. These plots and the emission lines in Figure 1.1 are used to study background UV wavelengths for the current study. Table 2.2 is a list of lighting products discussed in the paper by Bergman, Parham, and McGowan (1994). Figures 2.2 through 2.8

provide the spectral irradiance plot for various combination of lighting sources listed in Table 2.2. The data was obtained between 200 and 800 nm using an Atonics OL752 Double Spectrometer with a (PMT) detector (Bergman, Parham, and McGowan 1994).

Table 2.2

General Lighting Sources

Lighting Source
Sun at 30 degrees from zenith
12V/65W HI Quartz Halogen Capsule
12V/75W Quartz Halogen Capsule
I 2V/T5W Ce/Ti Quartz Halogen Capsule'
12V/65W 9006 Glass Halogen Capsule
MR16 50W without cover glass
MR16 50W with cover glass
1 20V/500W Linear Quartz Halogen
120V/350W Linear Quartz Halogen IR
PAR38 120W Incandescent
PAR38 90W Glass Halogen
PAR38 60W Quartz Halogen FR
F4OT12CW
F32T8SP4I US
HLBXF4OSPX35
F32TBSP4I UK
F32T8SP41 US with 280ppm Ce
F32T8SP41 US with 5OOppm Ce
F32T8SP41 US with acrylic diffuser
400W Mercury
400W Metal Halide
400W High Pressure Sodium (HPS)

Source: Bergman, Parham, and McGowan (1994)

Because of the small irradiance values in the UV region (i.e., 200-400 nm), the irradiance values are sometimes plotted on a log scale (see Figure 2.2) versus a linear scale (see Figure 2.3). In addition, manufacturers often use a variety of covers on their lamps to filter out harmful amounts of UV in the UV-B and UV-C regions.

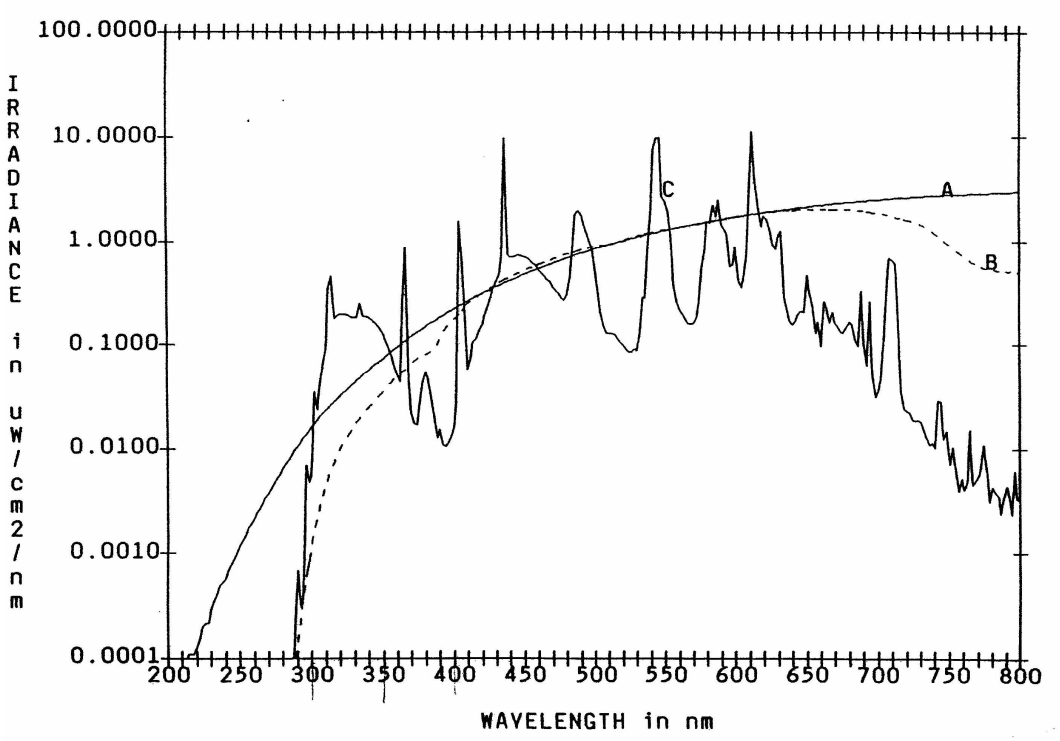

Figure 2.2: Logarithmic Spectral Irradiance at 1000 LUX of: A) Quartz Hal Capsule, B) MR16 with Cover/Glass, and C) T8 Lamp. Source: Figure courtesy of General Electric Corporation.

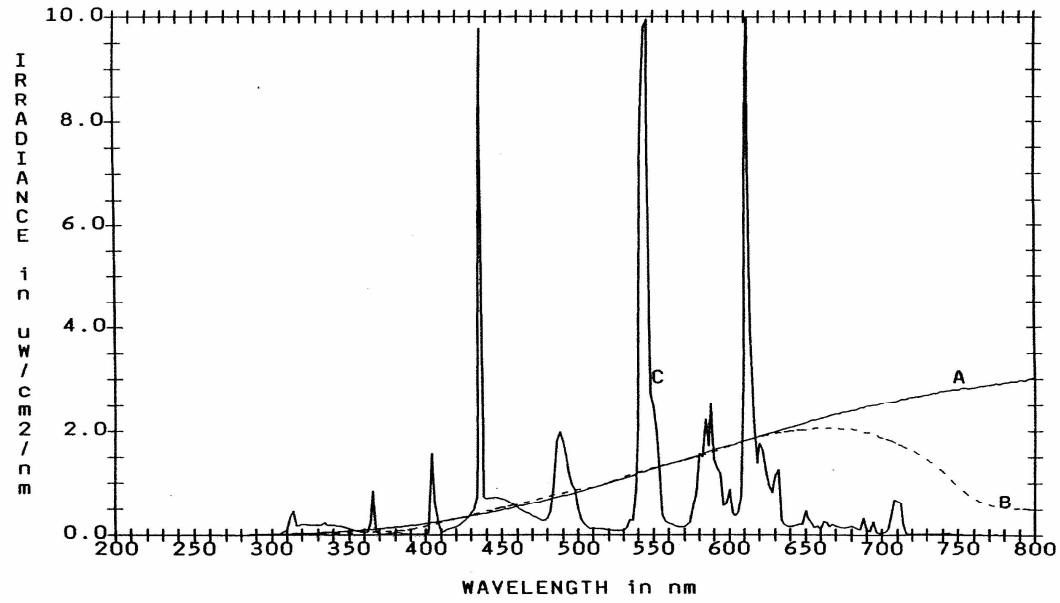

Figure 2.3: Linear Spectral Irradiance at 1000 LUX OF: A) Quartz Hal Capsule, B) MR16 with Cover/Glass, and C) T8 Lamp. Source: Figure courtesy of General Electric Corporation.

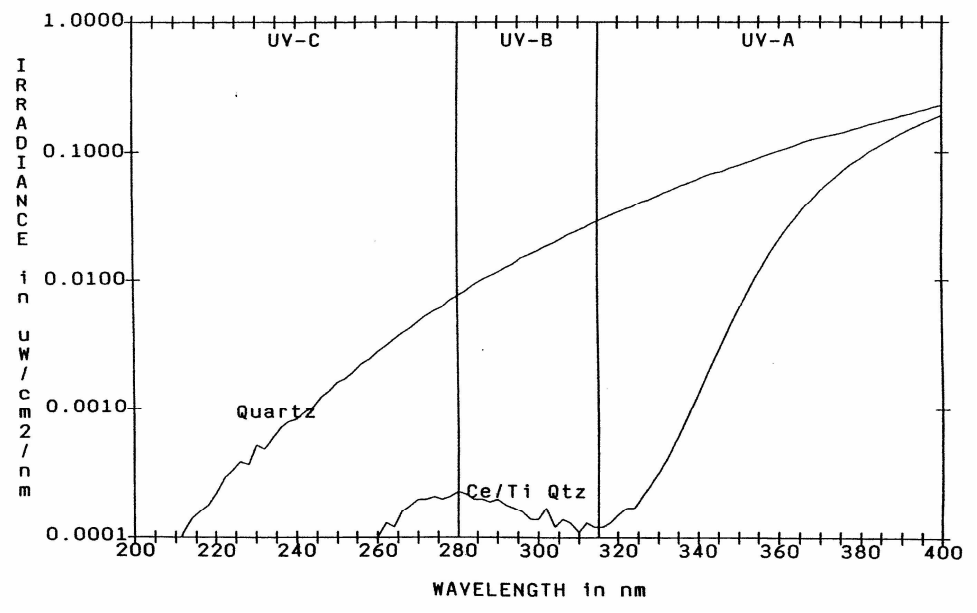

Figure 2.4: UV Spectral Irradiance at 1000 LUX Comparing Ce/Ti Doped Quartz and Undoped Quartz Capsules. Source: Figure courtesy of General Electric Corporation.

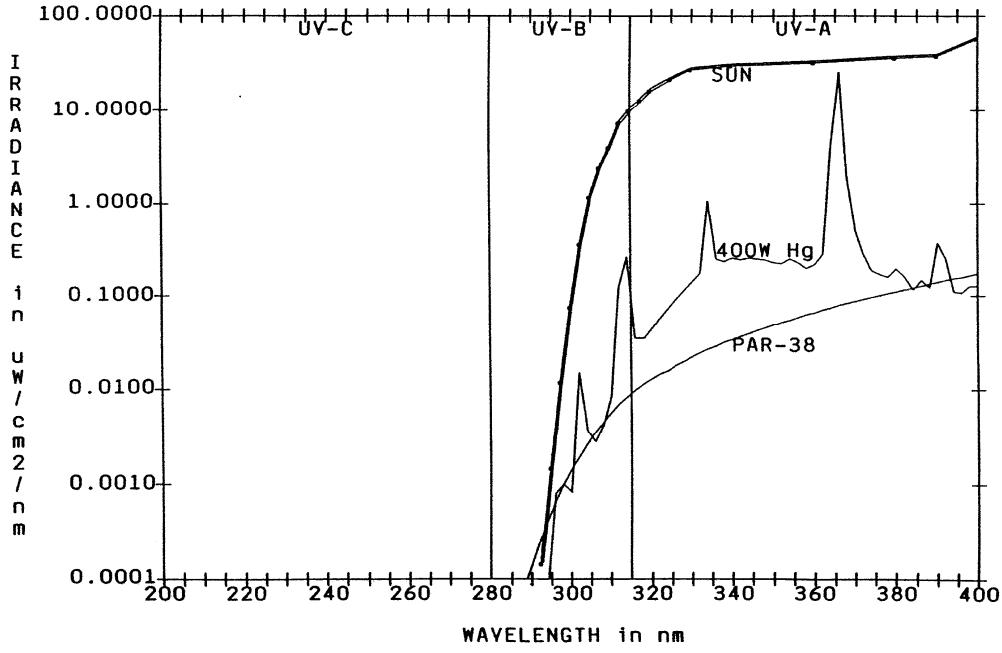

Figure 2.5: UV Spectral Irradiance of Sun at 30 degrees from Zenith Compared to a 120 W Par-38 and a 400 Watt HP Hg Lamp. Source: Figure courtesy of General Electric Corporation.

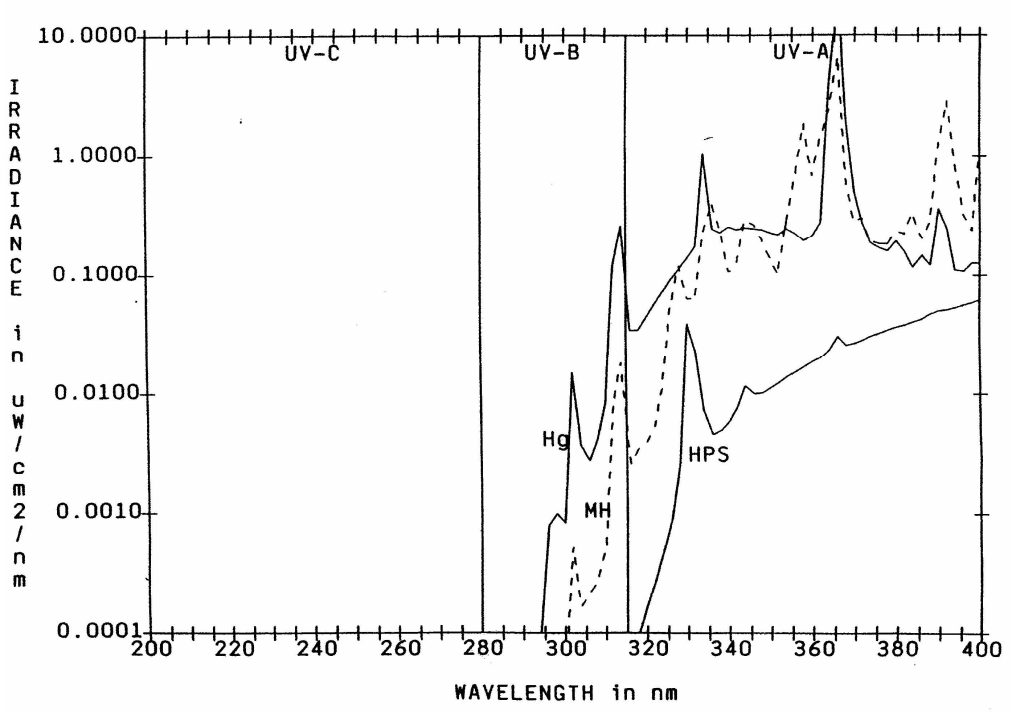

Figure 2.6: UV Spectral Irradiance at 1000 LUX for 400 W Hg, MH and HPS Lamps. Source: Figure courtesy of General Electric Corporation.

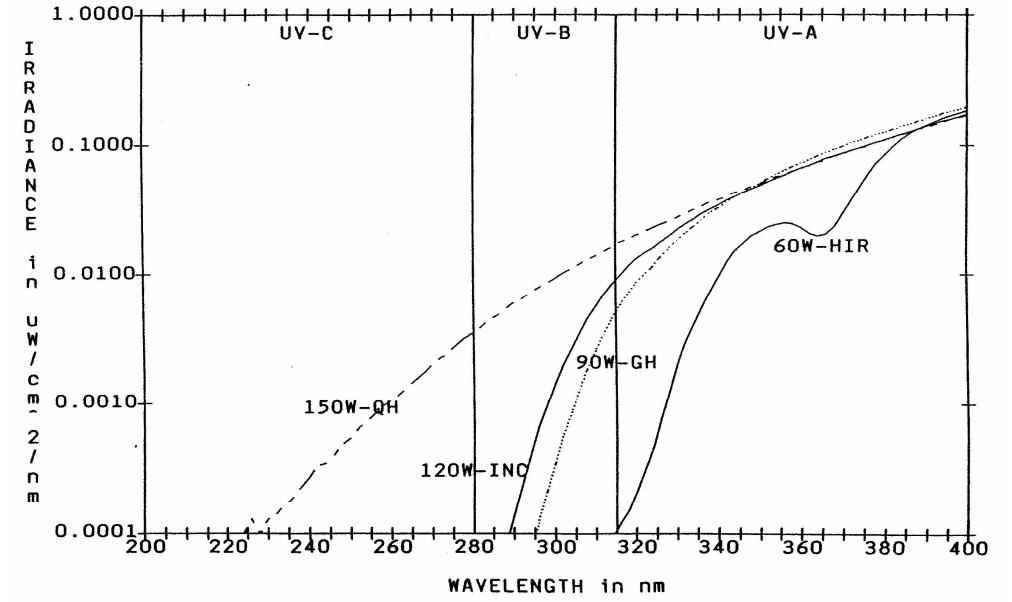

Figure 2.7: UV Spectral Irradiance at 1000 LUX for three Par-38 Lamps and a 150 W Quartz Halogen Capsule. Source: Figure courtesy of General Electric Corporation.

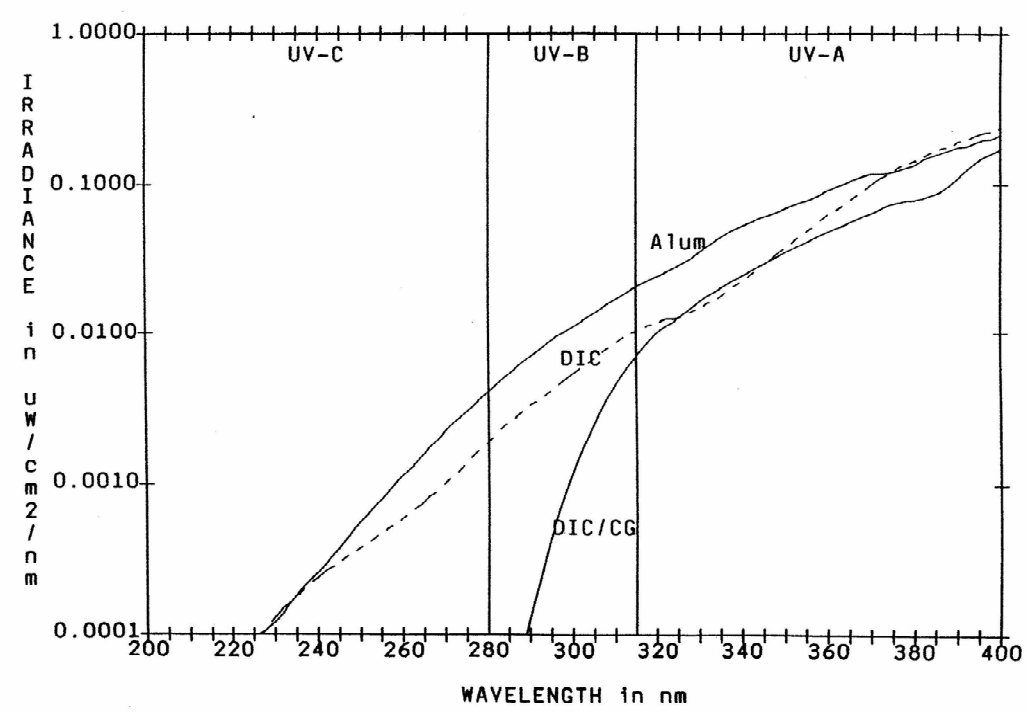

Figure 2.8: UV Spectral Irradiance at 1000 LUX for Dichroic and Aluminum MR16's, one with Cover Glass. Source: Figure courtesy of General Electric Corporation.

2.3.3.3 Photons produced from material scintillation

Scintillation of materials in the field of view is another consideration. The detection of ionizing radiation using scintillation of materials is known as one of most useful methods for the detection of radiation (Knoll 1979). Knoll (1979) identifies 6 quantities of an ideal scintillation material:

1. It should convert the kinetic energy of charged particles into detectable light with high scintillation efficiency

2. This conversion should be linear—the light yield should be proportional to the deposited energy over as wide a range as possible.

3. The medium should be transparent to the wavelength of its own emission for good light collection

4. The decay time of the induced luminescence should be short so that fast signal pulses can be generated

5. The material should be of good optical quality and subject to manufacture in sizes large enough to be of interest as a practical detector

6. Its index of refraction should be near to that of glass (~1.5) to permit efficient coupling of the scintillation light to a photomultiplier tube (Knoll 1979)

Fluorescence and *phosphorescence* are often confused. Knoll (1979) defines fluorescence as the "emission of visible radiation from a substance following its excitation by some means". The emission is usually prompt (delayed fluorescence has a longer emission time) and differs from *phosphorescence* which is characterized by the emission of longer wavelength light (visible light) after excitation through a much longer emission time (Knoll 1979).

Birks (1964) breaks scintillators down into organic scintillators, inorganic scintillators, and gas scintillators. Plastics are included in the organic category. Only a few of these scintillators have maximum emission values in the UV below 400 nm. Sigma Aldrich (2008) lists some properties of common scintillators with maximum emissions between 300 and 400 nm. These are shown in Table 2.3. In practice, scintillation rates in the 10s or 100s, near the material, will greatly increase the chance of a detection of the air fluorescence. Such scintillation values would be of marginal value for uses where the radiation must travel a long distance, d, to reach the scintillation material. This is due to the $1/d^2$ fall-off of the direct radiation signal.

Table 2.3

Properties of some Common Scintillation Materials

Mat'l	Density (g/cm^3)	Emission Max. (nm)	Refractive Index	Decay Constant (ns)	Con-version Efficiency*	Yield (photons /MeV)
Undoped Halides						
BaF_2	4.88	315	1.56	630	16	9,500
		220	1.56	0.8		1,400
CsF	4.64	390		3 – 5	5-7	
CsI	4.51	450	1.80	2/20	4-6	2,000
		305		several µs		varies
Cerium Doped Inorganics						
YAP(Ce)	5.55	350	1.95	27	35 – 40	18,000
LuAP(Ce)	8.4	365	1.94	17		17,000
Glasses						
^{6}Li – glass	2.4 – 2.7	390 – 430	1.55-1.58	60 – 100	4 – 6	3,300 – 5,600
Plastics						
Anthracene	1.25	447		30	43	16,500
Stilbene	1.16	410		4.5	22	8,300

Source: Data from Sigma-Aldrich (2008).

For purposes of the current investigation, common materials (i.e. plywood, concrete (smooth and textured), brick, aluminum, paper products, plastic materials, polycarbonate, and extruded acrylic (i.e., Plexiglas)) are studied to determine if there is light produced from scintillation in 300 to 400 nm region of the UV spectrum when the materials are in the presence of radioactive material (i.e., ^{241}Am and ^{90}Sr). While Table 2.3 only gives the maximum emission values for some common scintillation materials, this is not an exhaustive list. The total photon yield from scintillation when common materials are in the presence of the radioactive materials will depend not only on the quantity and variety of scintillation compounds in the studied material, but also on the scintillators' interactions with other elements in the studied material. This will make the total photon yields from scintillation difficult to predict. Additionally, scintillation can occur, but the light produced may be unable to escape the material. Thus,

laboratory testing is conducted to determine the likely scintillation contributions to the signal for a number of common materials.

2.3.3.4 UV photons reflected into the detectors field of view

Reflected photons from background sources inside and outside the target area are a primary concern. Fluctuations in the background can make a definitive detection impossible for signal to noise ratios less than 1. There is little information available in the region below 350 nm for the reflectance values of common materials. However, above 350 nm, the USGS Digital Spectral Library provides a catalog of spectral plots for the reflectance for different materials. The Library is broken up into 6 classes: Minerals, Mixtures, Coatings, Volatiles, Man-made, and Vegetation (Clark et al. 2007). For purposes of the current research, the "man-made" category can provide useful data from 350nm to 2500 nm in most cases. However, for values below 350 nm, additional testing should be conducted to determine the reflectance. An example of how a material's color affects the reflectance is useful. Using the USGS Digital Spectral Library's database of spectral plots listed under the chapter titled "Man-Made," the user can get plots from 350 nm to 2,500 nm for the reflectance of Light Gray Brick (Figure 2.9) and Dark Red Brick (Figure 2.10). When the data for both colors are plotted on a single graph (Figure 2.11) for the region 350 to 650 nm, the reflectance of the light gray brick is approximately three times the reflectance of the red brick. This example demonstrates the importance of understanding the reflectance of materials. The light surface can increase the background noise to levels where small fluctuations in the noise could masks the air fluorescence signal for small radioactive sources. Repositioning the detector, changing the detection wavelength, and/or reducing the field of view might reduce the effects of reflected noise and improve the Signal to Noise Ratio.

However, if the object is a diffuse reflector, as is the case with the bricks, repositioning the detector may be of little value, since the surface of the bricks reflects the incident light in all directions.

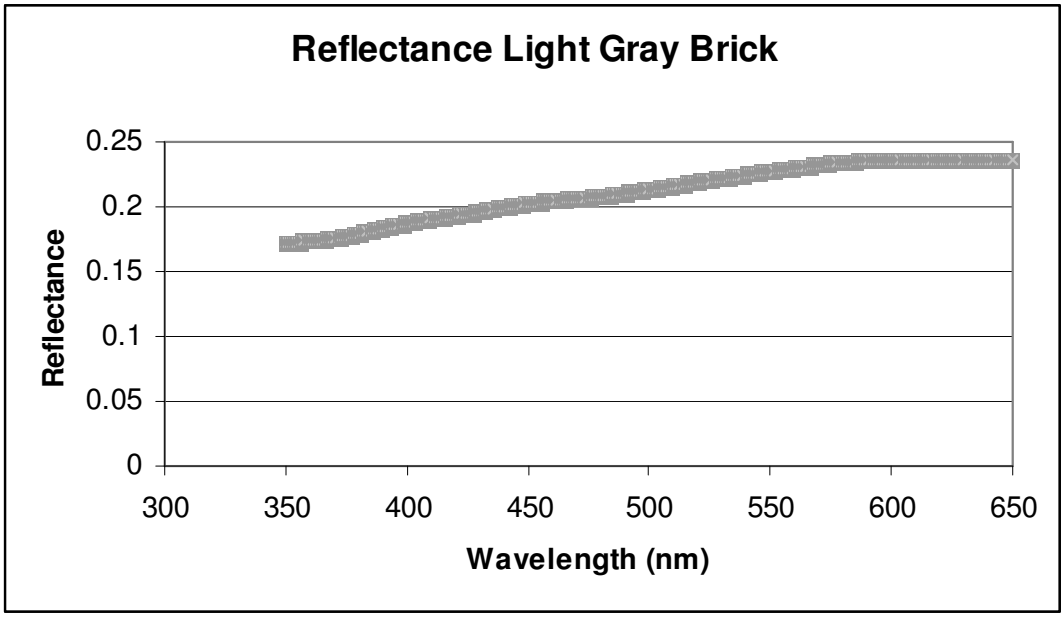

Figure 2.9: Reflectance of Light Gray Brick. Source: Data from Clark et al. 2007.

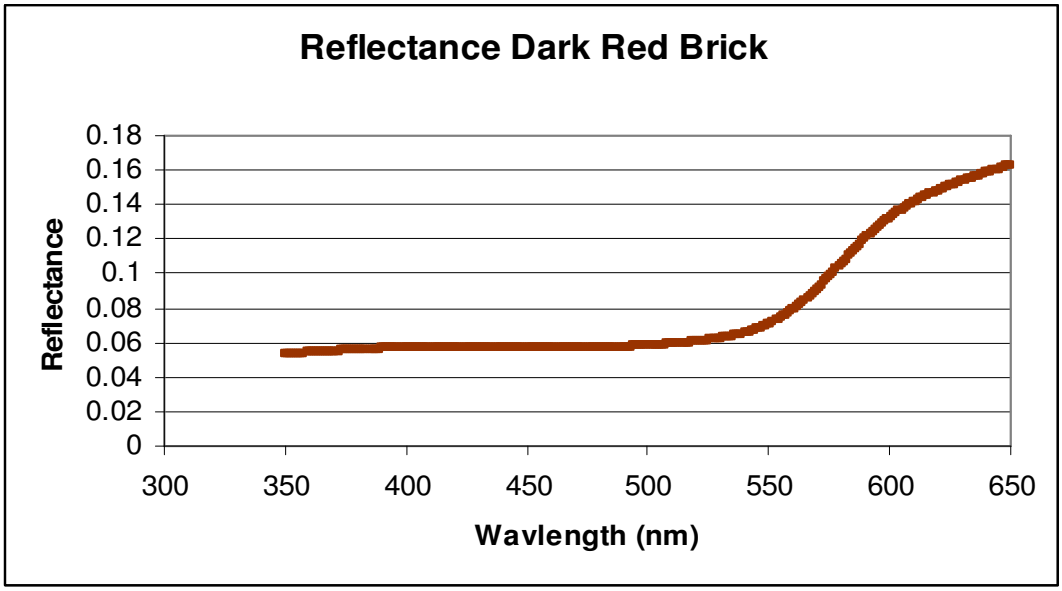

Figure 2.10: Reflectance of Dark Red Brick. Source: Data from Clark et al. 2007.

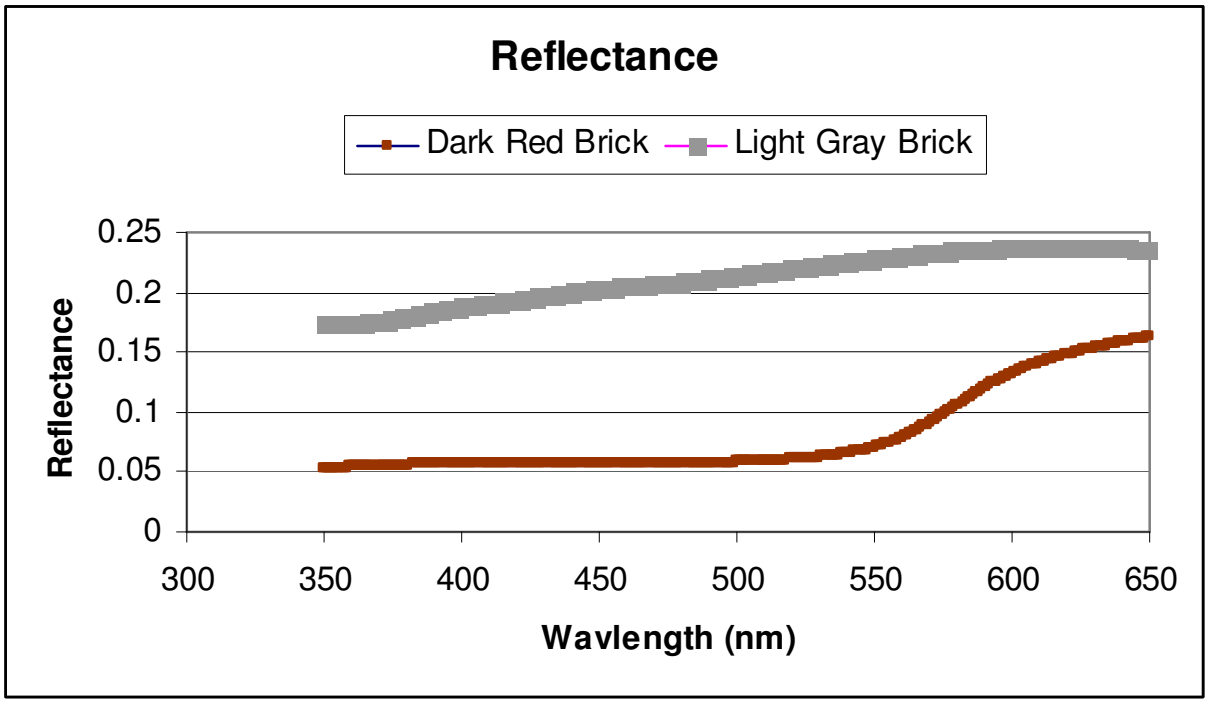

Figure 2.11: Reflectance of Gray and Red Brick. Source: Data from Clark et al. 2007.

2.3.4 Other UV Background

Other sources (sometimes called clutter) of UV background are electrical discharges, arcing, corona on utility lines, fires, welding, and insecticide lamps (Wilner and Ben-Yosef 1998). Using a photomultiplier based collector with solar blind filters, Wilner and Ben-Yesef (1998) stressed that the sun's radiation is negligible in the pass band 260-280 nm and can be completely filtered out leaving system noise as the major background noise, not considering clutter. Where clutter sources exists, some count rates (i.e., from high-voltage power lines, transformers, and welding) rise sharply in a "fluctuative" manner with temporal characteristics (Wilner and Ben-Yosef 1998). These same sources produce light in the 300 to 400 nm band and would be expected to show similar temporal characteristics. This is supported by Kozlowshi's (2001) research, discussing the impact of UV radiation at work stands, that shows substantial UV

radiation is produced from welding arcs in all regions of the UV (i.e., UA, UV-B, UV-C) in the 250 to 400 nm region.

2.4 Literature Search Summary

Ukrainian (Baschenko 2004) and French (Lamadie et al. 2004) studies validated the conclusion that optical detection methods can be used in the 300 to 400 nm wavelength portion of the UV spectrum under laboratory conditions that control the background UV light. This is further supported by Hannuksela (2010). However, these studies suffer from the limitation of only being able to detect radiation in total darkness. The possibility exists that improved detection efficiencies can be obtained. Using better filters, reducing the field of view, using scintillators, and/or repositioning the collector to reduce the direct and reflective effects of background light for a given wavelength, could yield such efficiencies. Additionally, collection schemes at wavelengths other than those with the highest fluorescence efficiencies may provide a better signal to noise ratio.

While earlier research efforts (Baschenko 2004 and Lamadie et al. 2004) stress the signal to noise ratio as an important factor, the research efforts focused on the fluorescence efficiencies at the four peaks (316, 337, 357, and 391nm) in the region between 300 to 400 nm shown in Figure 1.1. There have been no exhaustive studies of the background UV spectrum conducted to determine if one of these wavelengths offer more optimal conditions for the optical detection of radioactive sources under particular scenarios. This research is focused on determining if better signal to noise ratios can be obtained at 316, 337, 357, 380, 391 nm, or some other wavelengths, and which wavelength is better for a given expected scenario. The best wavelength for a particular application is dependent on the fluorescence efficiency, the magnitude of the

background UV noise and the fluctuations of that background noise. Using the lighting curves for general lighting lamps (Bergman et al. 1995), solar irradiance curves, and the reflectance, transmission, and scintillation properties of different materials, the possibility exists to better predict UV background conditions (magnitude and fluctuations) at a given wavelength. Armed with the predicted UV background conditions and the fluorescence efficiencies (Figure 1.1) at a particular wavelength, the collector's area, field of view, and position can be selected to obtain a SNR that provides the best chance for a definitive detection.

CHAPTER 3

SIGNAL DETECTION

3.1 Statistics of Signal Detection

UV photons are generated from solar flux, normal background radiation and man-made non-nuclear sources. These photons constitute the "noise" or "background". UV photons generated by the radiation source constitute the "source signal". In outside scenarios, the in-band background is random is always present and cannot be separated from the source signal due to the random nature of both signals. Thus, the total measured signal will be the "source signal plus the background signal." In order to use statistical signal detection methods, both signals (e.g., background and source signal plus background) have to be measured or estimated.

The probability of decay of atoms from a radioactive material follows a Poisson distribution, which approaches a Gaussian distribution where the average of the number of counts is more than 20 (Tsoulfanidis 1995). Thus, the Normal (Gaussian) distribution statistics can be used to analyze the probability of the presence of radioactive material. In doing this, the signal to noise ratio (SNR) of a random variable is defined as the mean squared ($\overline{X}^2$) divided by the variance (σ^2) (Saleh and Teich 1991).

$$SNR = \frac{\overline{X}^2}{\sigma^2} \tag{3.0}$$

There is some disagreement on what is the minimum detectable signal to qualify as a valid detection. Some (Ziock et al. 2004) have suggested when detecting small quantities of radioactive materials where there is little opportunity to determine the background (B) in advance and because the background can vary by an order of magnitude itself, the standard SNR expression (i.e., $SNR = \frac{Signal(S)}{\sqrt{Background}} = 1$) should be replaced by a more conservative expression (i.e., $SNR = \frac{Signal(B)}{Background} = 1$) (Ziock et al. 2004). Saleh and Teich (1991) define the minimum detectable signal as the mean squared signal that yields a SNR = 1 (i.e., $SNR = \frac{\bar{X}^2}{\sigma^2} = 1$).

The *International Union of Pure and Applied Chemistry (IUPAC)* defines the limit of detection of a concentration as the smallest measure (x_L) that can be detected with reasonable certainty by the following equation.

$$x_{Limit} = \bar{x}_{bi} + k\sigma_{bi} \tag{3.1}$$

where k is used to determine the confidence of the limit, with $k=2$ giving a 95% confidence that a desired signal has been detected, and $k=3$ giving a 99% confidence.

Prominent authors (Knoll 1999 and Tsoulfanidis 1995) on radiation detection and measurement identify two critical values. The first is a lower limit of detection, L_c (Knoll 1999) or critical limit of detection (*CDL*) (Tsoulfanidis 1995), defined as the lowest signal that is acceptable to report. The second is a Minimum Detectable Number of Counts (MDNC) or photons for the present research. The MDNC is the smallest number of counts that can be relied upon with some degree of confidence to reduce the chance of reporting a source is present when

none is actually present. When used to determine the presence of air fluorescence, the L_c is set low enough to reduce the chance that no air fluorescence from a radioactive source will be reported when there is in fact radioactivity present, a false negative (Knoll 1999). No background light (e.g., a dark test range) or instrument "fluctuations" yield a value of zero (Knoll 1999).

The net air fluorescence signal, N_s, is the total signal, N_T, minus the background signal, N_B. The background signal will include all background (i.e., natural and artificial background light and instrument fluctuations). Thus, the equation for the net signal would be (Knoll 1999)

$$Ns = N_T - N_B \tag{3.2}$$

with a variance defined as (Knoll 1999)

$$\sigma_{N_s}^2 = \sigma_{N_T}^2 + \sigma_{N_B}^2 \tag{3.3}$$

For no radioactivity signals present (i.e., there will be no radioactive induced air fluorescence), thus (Knoll 1999),

$$\sigma_{N_T} = \sigma_{N_B} = \sqrt{N_B} \tag{3.4}$$

and

$$\sigma_{N_s} = \sqrt{2\sigma_{N_B}^2} = \sqrt{2}\left(\sigma_{N_B}\right) \tag{3.5}$$

Thus (Tsoulfanidis 1995 and Knoll 1999),

$$L_C = CDL = k\sqrt{2}\left(\sigma_{N_B}\right) \tag{3.6}$$

where k is defined according to the level of confidence that one will not falsely report there is not radiation when there is radiation is present (Knoll 1999). Table 3.1 shows confidence limit values for different levels of confidence.

Table 3.1

Probability Values and Confidence Limits

Number of standard deviations (*k*)	P (*some x> some value, x_a*)	Confidence Limit in (%)
0	0.500	50
1.285	0.100	90
1.645	0.050	95
2.000	0.023	97.7
3.0	0.0013	99.87

Source: Data from Tsoulfanidis 1995.

When radioactivity is present, one looks for a Minimum Detectable Number of Counts, $N_{S_{\min}}$, that is the smallest number of counts that can be relied upon with some degree of confidence to reduce the chance of reporting a source is present when none is actually present. This would be L_C plus some number of counts, $k\sigma_{S_{\min}}$

$$N_{S_{\min}} = L_C + k\sigma_{S_{\min}} \text{ (Knoll 1999)} \tag{3.7}$$

Substituting the value for L_C

$$N_{S_{\min}} = k\sqrt{2}\left(\sigma_{N_B}\right) + k\sigma_{N_{S_{\min}}} \tag{3.8}$$

Where for no signal, $N_{S=0} = 0$ (Knoll 1999)

$$\sigma_{S_0} = \sigma_0 = \sqrt{N_S} = 0 \tag{3.9}$$

and

$$\sigma_0^2 = \sigma_{N_T}^2 + \sigma_{N_B}^2 = (\sigma_{N_S}^2 + \sigma_{N_B}^2) + \sigma_{N_B}^2 \quad \text{(Knoll 1999)} \tag{3.10}$$

$$\sigma_0 = \sqrt{0 + 2\sigma_{N_B}^2} = \sqrt{2}\sigma_B \text{ (Tsoulfanidis 1995)} \tag{3.11}$$

Using Table 3.1 for a 95% confidence limit, $k\alpha$ = 1.645 (Tsoulfanidis 1995)

$$MDNC = N_{s_{\min}} = k\alpha^2 + 2CDL \tag{3.12}$$

$$MDNC = N_{s_{\min}} = 2.71 + 4.653\sigma_B \quad \text{(Tsoulfanidis 1995)} \tag{3.13}$$

3.2 Solid Angle

The solid angle (Tsoulfanidis 1995) is defined as that number of particles per second emitted inside the space defined by the contours of the source and the collector aperture divided by the number of particles per second emitted by the source.

$$\Omega = \frac{Emitted\_Particles\_in\_Contours\_of\_Collector\_Aperture\_\&\_Source}{Total\_Particles\_Emitted\_from\_Source} \tag{3.14}$$

For a circular collector and a point source shown in Figure 3.1, the solid angle is

$$\cos\ \theta_0 = \frac{d}{\sqrt{d^2 + r^2}} \quad \text{(Tsoulfanidis 1995)} \tag{3.15}$$

$$\Omega = \frac{1}{2}\left(1 - \frac{d}{\sqrt{d^2 + r^2}}\right) \quad \text{(Tsoulfanidis 1995)} \tag{3.16}$$

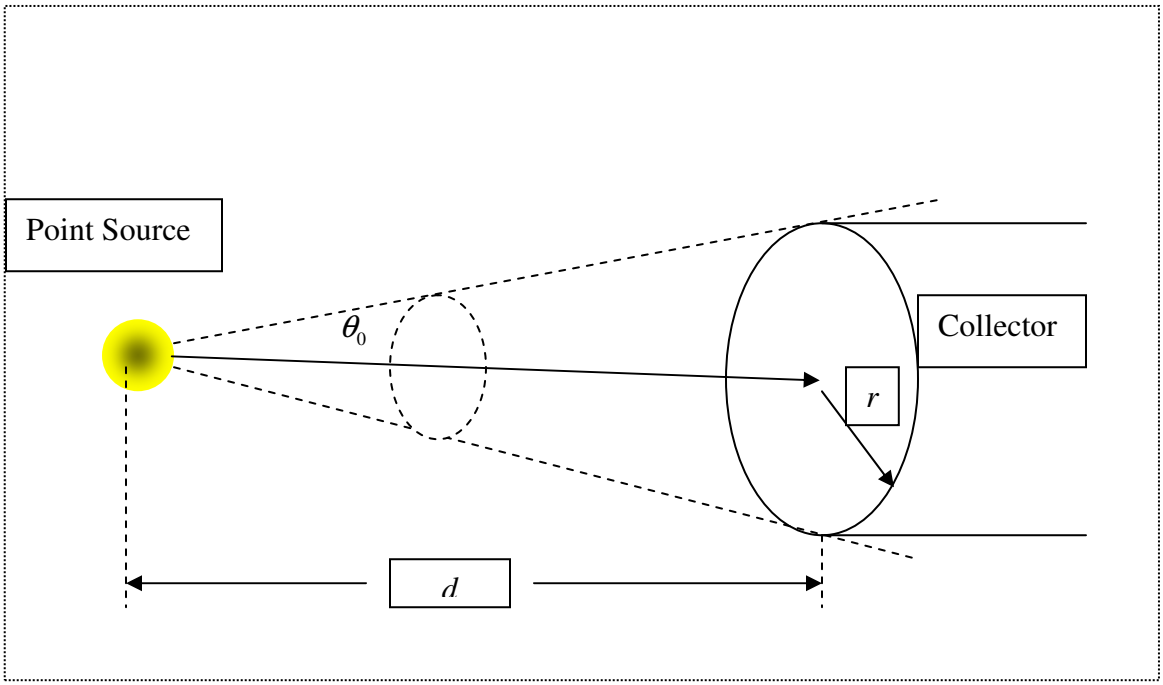

Figure 3.1: Point Source and Collector

Alternatively, the solid angle can be expressed as that area of the surface of the sphere which enters the collector aperture divided by the total area of the sphere. Where $d>>r$, the solid angle becomes

$$\Omega \cong \frac{Area_{collector\_aperture}}{4\pi d^2} = \frac{\pi r^2}{4\pi d^2} \quad \text{(Tsoulfanidis 1995)} \qquad (3.17)$$

Using the solid angle and efficiencies of the collector/detector one can determine the number of particles entering the collector from the point source, and thus determine the emission rate of the point source. For a point source mounted on a plane surface, half of the alpha particles would go into the surface and half out of the surface. This is called 2π geometry (Tsoulfanidis 1995). The goal is to maximize the collection area for the target signal, while

minimizing the collection of the background signal. As the field of view of the instrument becomes larger, more and more background is collected. At some point there is no longer a payoff in increasing the size of the collector. As the random background signal increases, the standard deviation of the background increases, requiring a proportionally larger share of minimum detectable number of signal counts as shown in Equation 3.13. If the background is only instrument noise, then theoretically, the background is independent of the field of view of the instrument and the collection area (e.g., increasing radius *r* for the collector of in Figure 3.1) can be increased without bound to collect as much signal as possible.

3.3 Collection Systems

The scintillation and air fluorescence tests and the imaging tests are performed using the collection systems shown in Figure 3.2 and Figure 3.3, respectively. A 100 mm diameter lens with a 200 mm focal length is used to focus the collected signal on the PMT and CCD. A filter wheel with 5 filters, each with a 10 nm band, centered on 313, 337, 355, 380 and 390 nm, is mounted between the PMT and lens. For imaging, the Cooler and PMT are replaced with a PIXIS 1024 cooled CCD camera, shown in Figure 3.3, supplied by Princeton Instruments. The camera provides a spatial picture of the air fluorescence and scintillation aura. The PMT and CCD camera are positioned 200 mm behind the lens, and the radioactive source is 1550 mm forward of the lens. A laser is used to align the PMT or CCD, the lens, and source on the optical axis. Care is taken to ensure any aura in the vicinity of the source is focused on the PMT/CCD.

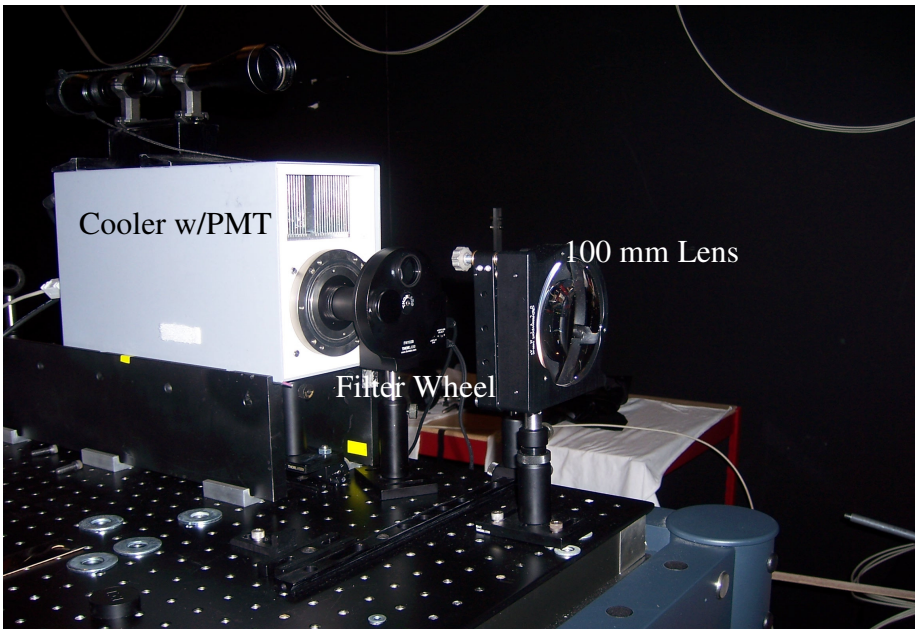

Figure 3.2: Cooler with PMT, Filter Wheel and 100 mm Lens

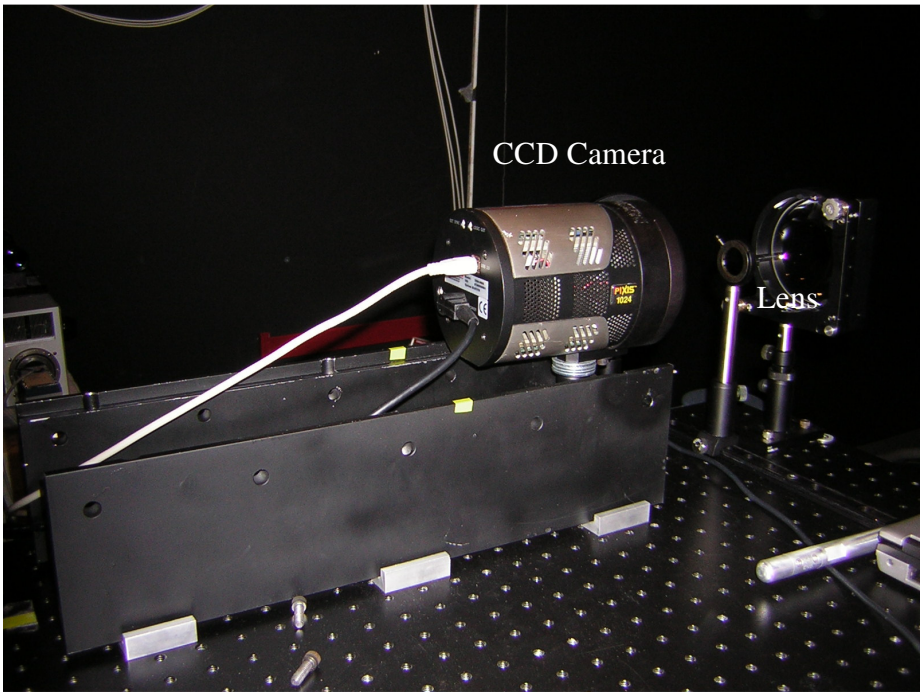

Figure 3.3: CCD Camera and 100 mm Lens

CHAPTER 4

SCINTILLATION OF STUDIED MATERIALS

Material scintillation is well known, and it is often integrated on the head assembly of many direct detection devices. In determining the actual intensity of the UV source, the scintillation of materials in the field of view resulting in a signal in the portion of the spectrum being studied are added to the UV light produced by air fluorescence from the targeted radioactive source, making an interpretation of the actual air fluorescence resulting from the radioactive emission difficult to ascertain. However, on the positive side, the same material scintillation characteristics that mask the actual intensity in one scenario can be used to enhance detections of small radioactive sources where contamination is known to exist in the targeted area, and the targeted area can be overlaid with a scintillator. Scintillation on the surface, caused by radioactive contamination on the surface, could also held in source location.

The scintillation characteristics of the studied materials are obtained by placing a layer of non-scintillating shield material behind the studied material, and obtaining the scintillation plus air fluorescence value. Then, placing the shield on the surface of the studied material nearest the collector, the fluorescence signal is obtained. By eliminating or masking certain emissions, simultaneous equations can be solved to determine photon counts due to scintillation.

Multiple photo-detectors (e.g., CCD camera and photomultiplier tubes) are used to determine the extent of the fluorescence region and measure the fluorescence. The sources are

placed in electromechanical irradiators, or source deployment devices, that allow for varying exposure times and to ensure an accurate monitoring of background conditions.

4.1 Source Deployment Devices

Two irradiators are used to provide for varying source exposure times while ensuring personnel safety. The source head is shielded when in the closed position to minimize the source's effect on measuring the background signal. Figure 4.1 shows Irradiator #1 with the source exposed. The black wheel rotates to shield the source. The source exposure period is capable of being controlled by a Windows-based computer system, allowing varying exposure times to be entered in the computer setup screen. The main disadvantage of Irradiator #1 is its size which limits the placement of the irradiator between the studied materials and the collector. Where the studied material is thin enough to allow the radiation to penetrate the material and reach the surface closest to the collector, the studied material can be mounted over the source. Back scatter of radiation and air fluorescence behind the test material are then confined in the closed volume behind the material and are not in the field of view of the signal collector. This simplifies the determination of air fluorescence and scintillation values. By masking or shielding the material surface, the air fluorescence plus background is recorded with the source exposed. Removing the shield will provide a value for scintillation plus air fluorescence plus background. Subtracting the air fluorescence plus background value obtained with the mask from the signal obtained without the mask will give the scintillation. The source shown in Figure 4.1 is a ^{90}Sr source. The location of the source, on the right side of the photo, should be kept in mind for future discussions on imaging material scintillation.

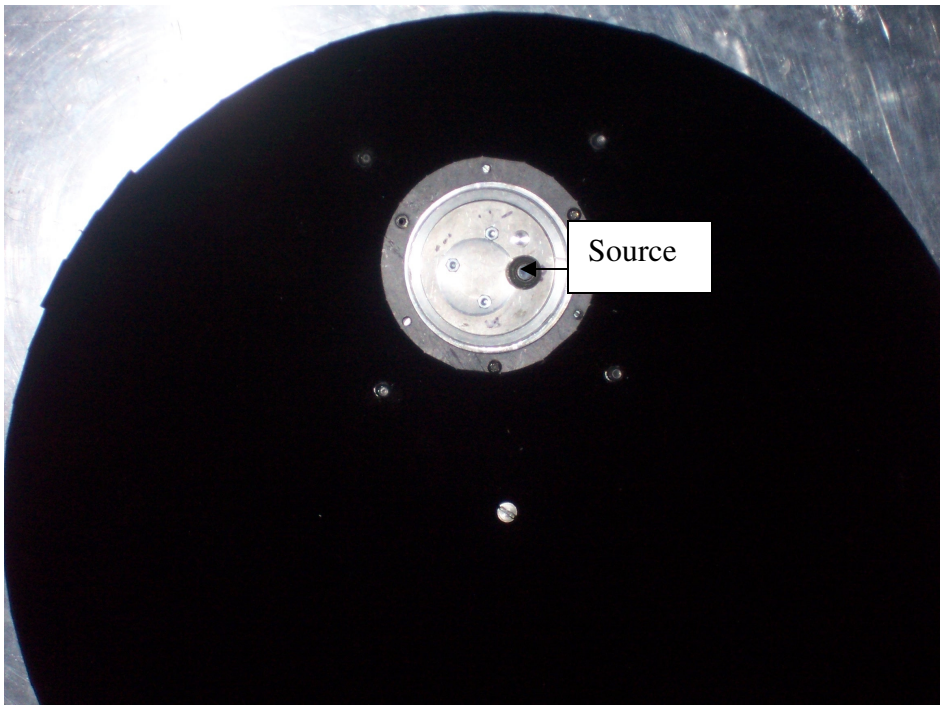

Figure 4.1: Irradiator #1 with source in the exposed position

Irradiator #2, shown in Figure 4.2, is designed for alpha and beta sources. Movement of the source head assembly is controlled by a garage door opener or a switch. This irradiator is designed for easy mounting of different source on the rod that snaps in a socket piston inside the tube. A top door opens when the source rod moves to the exposed position and closes when the rod descends in the tube. The source can be rotated in a horizontal plane allowing the source to be placed at varying angles to the scintillating surface. This enables the source to be positioned in front of the materials without obscuring the entire air fluorescence and scintillation signal going to the collector. A disadvantage of exposing the sources in front of the material is that one must deal with the scatter of the radiation off the surface. A mask, placed on the surface of the test material that is of a different composition than the test material, will scatter radiation differently than the test material making an easy determination of the exact contribution of air fluorescence and scintillation difficult, compared to scenarios where the source is placed behind

the material. However, this study is looking for scintillating materials with real value, materials that will provide scintillation to air fluorescence ratio greater than 10 in the 300 to 400 nm region. Scatter, at its maximum, will only double the scintillation plus air fluorescence signal.

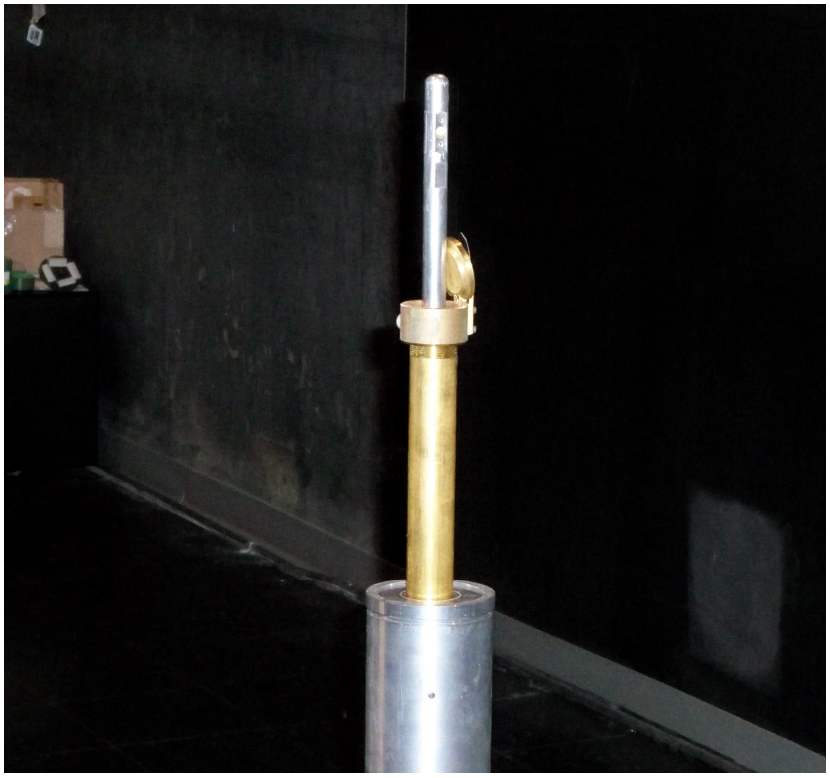

Figure 4.2: Irradiator #2 with source in unshielded position

Both electromechanical irradiators provide for varying source exposure times while ensuring personnel safety. The sources are mounted in heads capable of positioning the maximum radiation flux horizontally. The source head of each irradiator is shielded when in the closed position to minimize the source's effect on measuring the background signal. For alpha source scintillation measurements using Irradiator #1, the source stays in a fixed exposed position and the test materials are rotated away from the source.

4.2 Methodology of Scintillation Testing

For this study, the scintillation characteristics are determined for the 300 to 400 nm portion of the electromagnetic spectrum using two setup scenarios for the materials shown in Table 4.1. The materials are exposed to two sources, an alpha source, ^{241}Am, and a beta source, ^{90}Sr. The materials will be examined for the 10 nm bands centered on 313, 337, 355, 380 and 390 nm. These bands include the fluorescence peak efficiency bands of 316, 337, 354, 380, and 390 nm shown in Figure 1.1.

Table 4.1

Studied Materials

Number	Materials
1	Gray PVC
2	LDPE
3	HDPE
4	Polycarbonate
5	Plexiglas (extruded acrylic)
6	Polypropylene
7	TSA Plastic Bag
8	Red Brick
9	Light Brown Brick
10	Concrete (Smooth)
11	Concrete (Textured) cut face
12	Paper (White)
13	Paper (Black)
14	Plywood Luan
15	Aluminum

In the first scenario, Setup #1, shown in Figure 4.3, the source is placed in front of the studied material. In the second scenario, Setup #2, shown in Figure 4.4, the source is placed behind the studied material. For materials that completely attenuate the radiation signal, Setup #1 should be used. This includes alpha sources, which are easily attenuated by even thin

materials. For beta scintillation using ^{90}Sr, Setup #2 is used for a majority of the materials, but Setup #1 will be used for the red brick and the light brown brick, and the smooth and textured concrete.

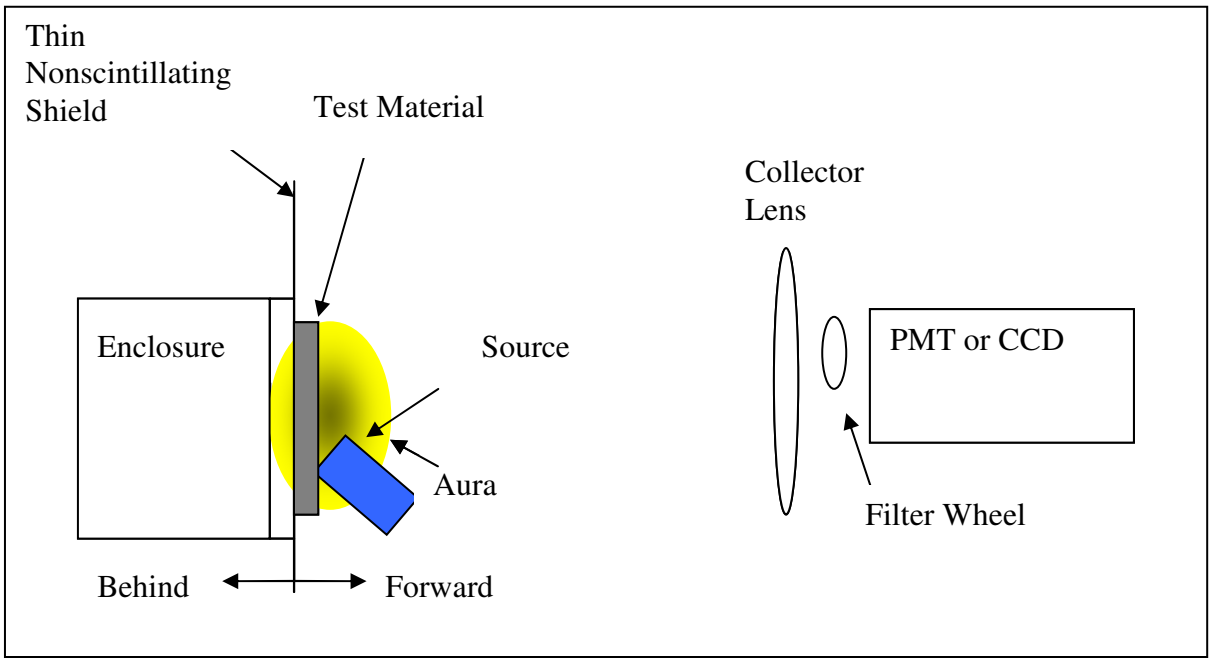

Figure 4.3: Source angled to the surface of the studied material, Setup #1

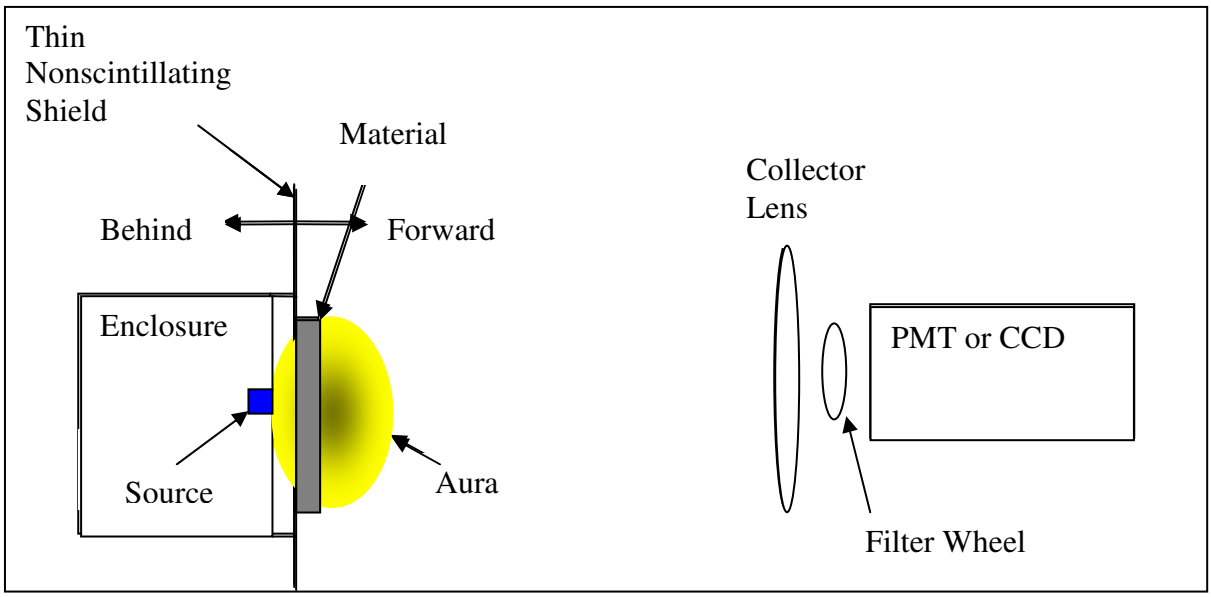

Figure 4.4: Source placed behind studied material, Setup #2

In Setup #1, when using the alpha source and Irradiator #1, the source is placed in a fixed position in front of the irradiator. In this scenario, the source touches the material to be scintillated, and is positioned at an angle of 55 degrees from the normal to the material. The studied material is then rotated out of the radiation's path and then returned to the path on alternate cycles. Placing the source holder at an angle to the surface of the studied material allows the collector to collect the signal without the source holder totally masking the scintillation signal. Since alpha radiation only travels a few centimeters, one must properly position the source to prevent a total obscuration of the signal.

In Setup #2, shown in Figure 4.4, the source is placed behind the side of the studied material farthest away from the collector. The studied materials are thin enough to allow the radiation to penetrate the material and reach the surface closest to the collector. Back scatter of radiation and air fluorescence behind the test material are contained in enclosed space behind the material, not in the field of view of the signal collector.

Any fluorescence photons, generated behind the material that might pass through a translucent material (S_{Fbt}), are contained in the enclosed volume by placing a thin, nonscintillating shield on the side of the test material furthest away from the collector. Thus, S_{Fbt} is zero. Additionally, any fluorescence outside of the material perimeter, resulting from radiation behind the studied material, S_{Fbop}, would be contained and be equal to zero. This simplifies the determination of air fluorescence and scintillation values. Upon moving one layer of the shield to the forward surface of the studied material, the air fluorescence in front of the material, S_{Ff}, plus background, S_B, is recorded. Removing the shield and returning it to a position behind the material, a value for scintillation, S_S, plus air fluorescence forward, S_{Ff}, plus S_B is obtained. Subtracting the signal obtained with the shield or mask in front, from the signal obtained with no

shield on the front surface will give the scintillation, S_S. This setup is more useful for beta sources, which are able to penetrate thin materials and scintillate the far surface. Generally, alpha sources cannot be placed behind the studied materials because the radiation is attenuated by the materials and fails to reach the far (i.e., forward) surface.

For a particular bandwidth, determined by optical filters on a collector, the total signal ($Signal_{SFbopFbtFfB}$) is the scintillation signal (S_S), plus the air fluorescence signal generated in back of the material from radiation behind the material, outside the material perimeter (S_{Fbop}), plus the air fluorescence in back of the material transmitted through the material (S_{Fbt}) to the collector, plus the signal for air fluorescence in front of the material (S_{Ff}), plus background noise (S_B) as indicated by Equation 4.1.

$$Signal_{SFbopFbtFfB} = S_S + S_{Fbop} + S_{Fbt} + S_{Ff} + S_B \tag{4.1}$$

To ensure there is no contribution of air fluorescence in back of the material that can be transmitted through the material (S_{Fbt}), a black non-scintillating shield is placed behind the studied material. Thus, S_{Fbt} is equal to zero, and the collected signal consists of S_S, S_{Fbop}, S_{Ff}, and S_B . The collected signal the for the scenarios shown in Figure 4.3 or Figure 4.4 is

$$S_{SFbopFfB} = S_S + S_{Fbop} + S_{Ff} + S_B \tag{4.2}$$

The next step is to remove one layer of nonscintillating shield behind the material and place the shield (or non-scintillating paper) between the studied material and the collector, shielding the effects of the scintillation and that portion of the air fluorescence generated behind the material which could be transmitted through it. This setup is shown in Figure 4.5 for Setup #2, with the same principles applying to Setup #1. The signal ($S_{FbopFfB}$) collected is the air

fluorescence behind the material outside the material perimeter (S_{Fbop}), plus the air fluorescence in front (S_{Ff}) of the material, plus the background noise (S_B), as indicated by Equation 4.3. The PMT dark count will be included in the background noise. For this study, the background noise (S_B) is essentially the PMT dark count since the experiments are conducted in a dark range.

$$S_{FbopFfB} = S_{Fbop} + S_{Ff} + S_B \tag{4.3}$$

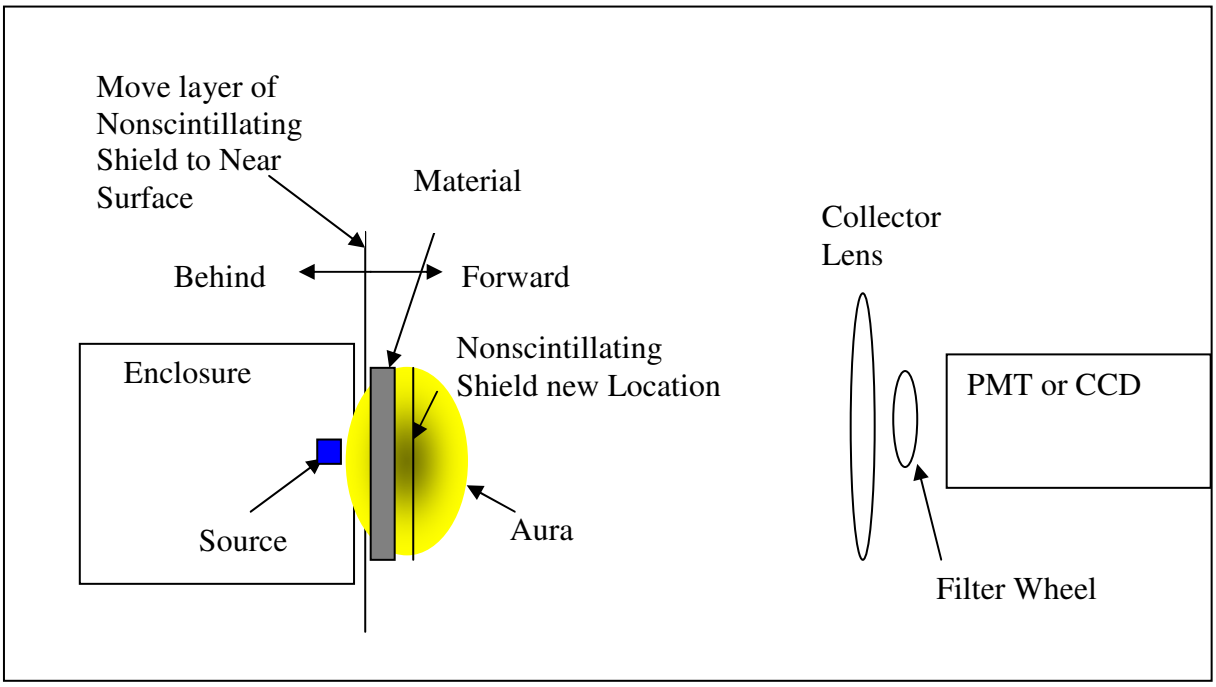

Figure 4.5: Signal with effects of scintillation shielded

The scintillation value (S_S) is then equal to the signal obtained with no shield in front of the studied material (i.e., Equation 4.2), minus the signal with the shield in front of the material (i.e., Equation 4.3)

$$S_S = \text{Signal}_{\text{Scintillation}} = \text{Equation 4.2} - \text{Equation 4.3} = S_{SFbopFfB} - S_{FbopFfB} \tag{4.4}$$

4.3 Air Fluorescence Images of ^{241}Am

Using the Test Setup #1, illustrated in Figure 4.3, the PMT is replaced by a PIXIS 1024 cooled CCD camera supplied by Princeton Instruments. A 100 mm diameter lens with a 200 mm focal length is used to focus the image on the CCD. The CCD is 20 cm from the lens and the source is 155 cm from the lens. The source is 0.107 mCi of ^{241}Am, mounted in Irradiator #2, and exposed for a period of 20 minutes facing the lens and CCD. First, the air fluorescence, plus background, plus dark count image is taken. Next, the source is lowered to a shielded position in the irradiator. A background plus dark count image is taken for 20 minutes. The second image is subtracted, pixel by pixel, from the first to get the air fluorescence image. The image is shown in Figure 4.6. The source is raised second time and a visible image taken. The raw image, collected first, is then overlaid on the visible image to get the image in Figure 4.7. Color is then added to those pixels around the source to show the aura of the air fluorescence, as shown in Figure 4.8. Looking at the ruler in Figure 4.7 and the color enhanced aura in Figure 4.8, the aura is shown to be approximately 4 to 5 centimeters in diameter.

Attempts were made using Setup #1 to collect scintillation images of all the materials in Table 4.1 exposed to the 0.107 mCi ^{241}Am source. However, no scintillation was observed using the CCD camera despite long exposure times of 40 minutes using the 0.107 mCi ^{241}Am source.

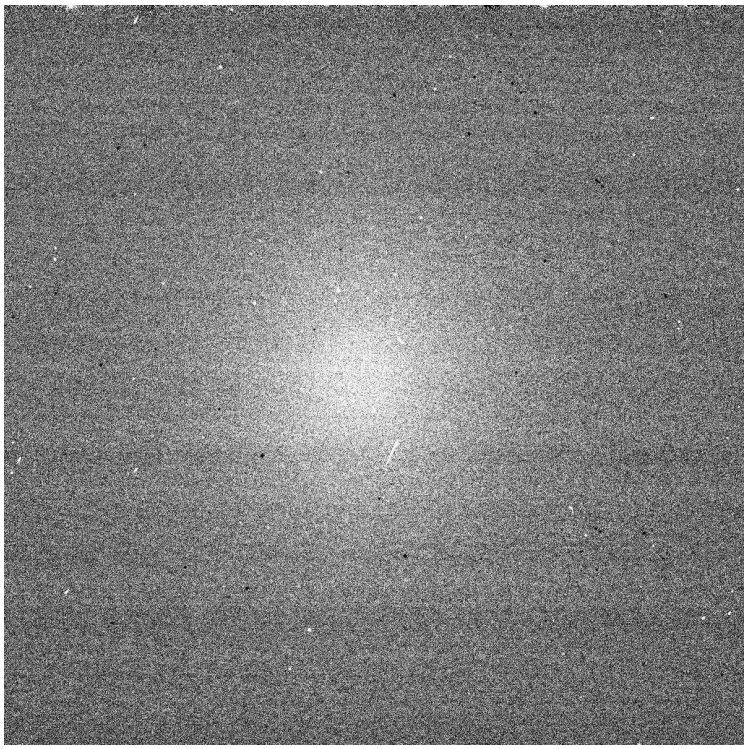

Figure 4.6: Air fluorescence image collected by CCD

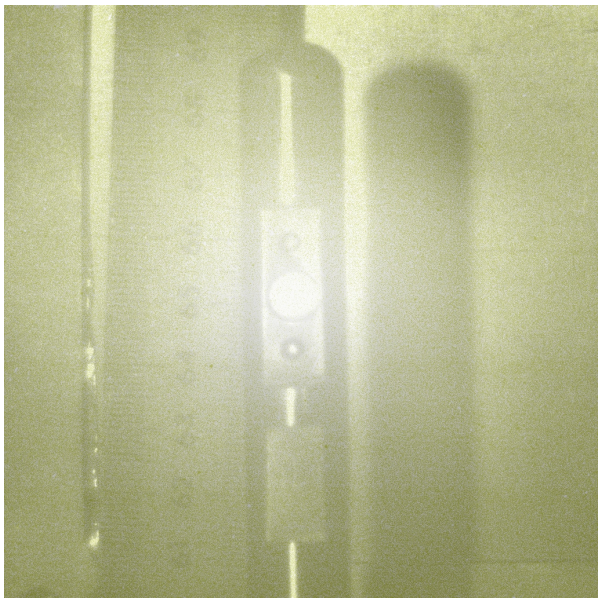

Figure 4.7: Air fluorescence image overlaid on source holder

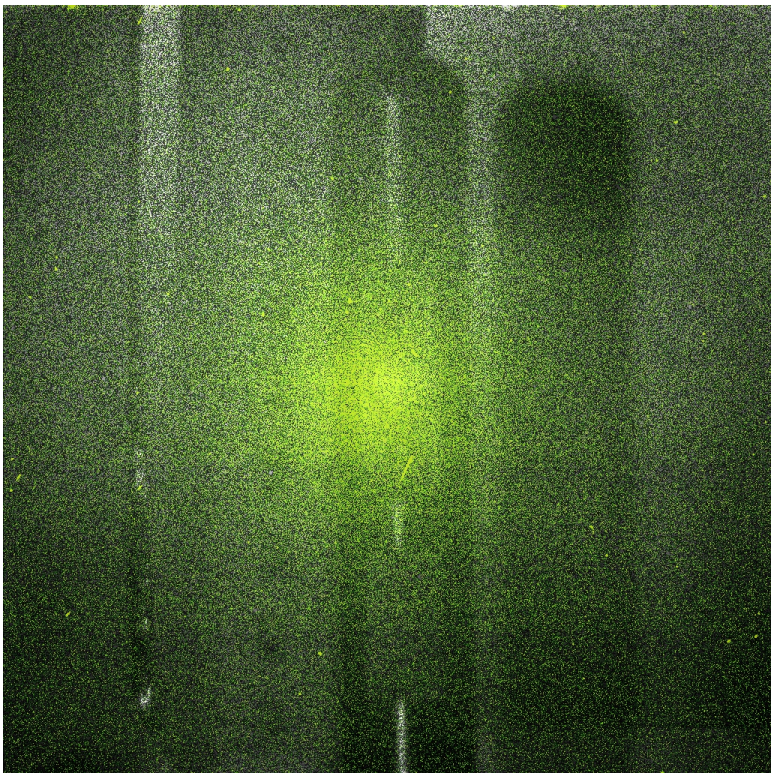

Figure 4.8: Air fluorescence aura around ^{241}Am

4.4 Air Fluorescence Images of ^{90}Sr

Attempts were made to collect images of 1 mCi of ^{90}Sr using Setup #2. The setup is illustrated in Figure 4.4. The shields are removed and the source placed in Irradiator #1 as shown on Figure 4.1. However, little air fluorescence was observed using the CCD camera, despite exposure times of 80 minutes. Because the air fluorescence volume for the ^{90}Sr beta source is much larger than alpha sources, either a larger field of view collector is required, or the radiation flux in the volume must be increased. To demonstrate the possibility of imaging the aura of beta source, an image is collected using an available lower energy 14.7 mCi ^{63}Ni source on a foil, rolled up inside a tube, and placed in a 3 inch diameter can. All electrons from the foil are directed toward the center of the rolled foil, increasing the flux in center of the pipe. Using

the setup shown in Figure 4.4, a 20 minute exposure is collected and overlaid on visual image of the source holder. Figure 4.9 is a raw picture of the air fluorescence, color enhanced to show the air fluorescence. The air fluorescence image in Figure 4.9 is overlaid on a visual image of the can in Figure 4.10. The air fluorescence is easily seen, looking down the tube in the center of the can.

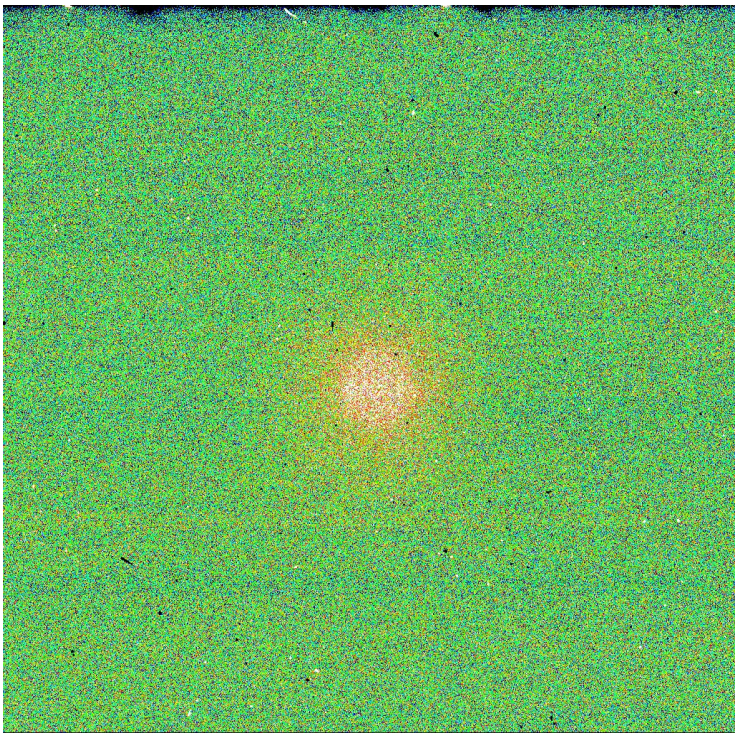

Figure 4.9: ^{63}Ni air fluorescence image color

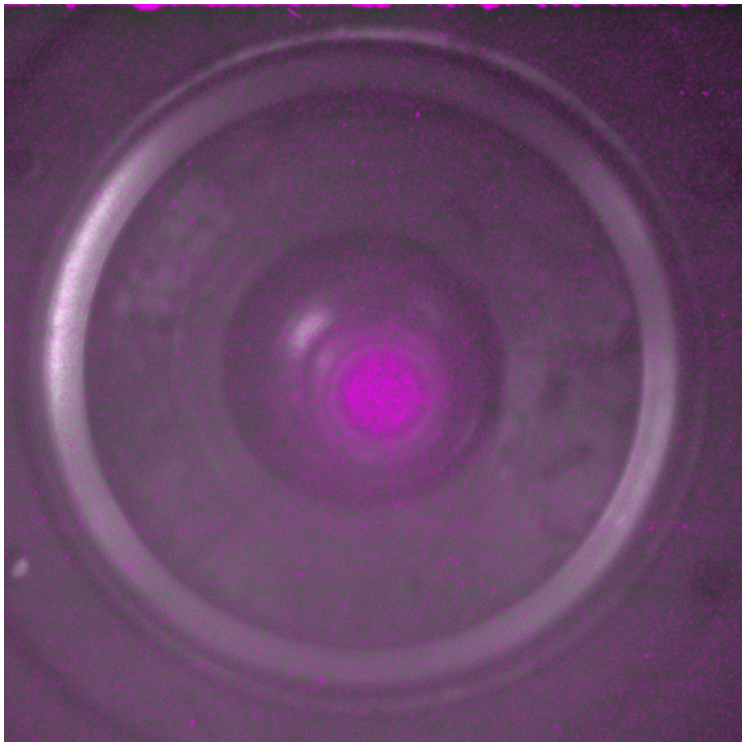

Figure 4.10: ^{63}Ni air fluorescence image color enhanced overlaid on image of holder

4.5 Scintillation of Materials by ^{241}Am

Alpha source radiation only travels a few centimeters. Thus, a source must be almost next to the material for the alpha particles to reach the surface. The particles are easily stopped by very thin materials, and fail to reach the alternate surface. Thus, Setup # 1, using a PMT based collector system, is used to collect scintillation counts for the materials in Table 4.1. Attempts were also made to collect scintillation images of the materials in Table 4.1. However, no scintillation image was observed using the CCD camera despite long exposure times of 40 minutes.

4.5.1 Test Setup

Setup #1, shown in Figure 4.3, is used to study the scintillation of the material in Table 4.1 when exposed to ^{241}Am. Because alpha particles can only travel a few centimeters, the source is placed in front of the material at angle of 55 degrees to the normal to the material surface as shown in Figure 4.11, to measure the scintillation signal (S_S), plus the air fluorescence signal generated in back of the material from radiation behind the material, outside the material perimeter (S_{Fbop}), plus the signal for air fluorescence in front of the material (S_{Ff}), plus background noise (S_B). The wheel holding the material is then rotated away from the source to place the material in the unexposed position. Five cycles with 1 minute of exposure time are conducted for each material. Equation 4.2 shows the collected signal.

$$S_{SFbopFfB} = S_S + S_{Fbop} + S_{Ff} + S_B \tag{4.2}$$

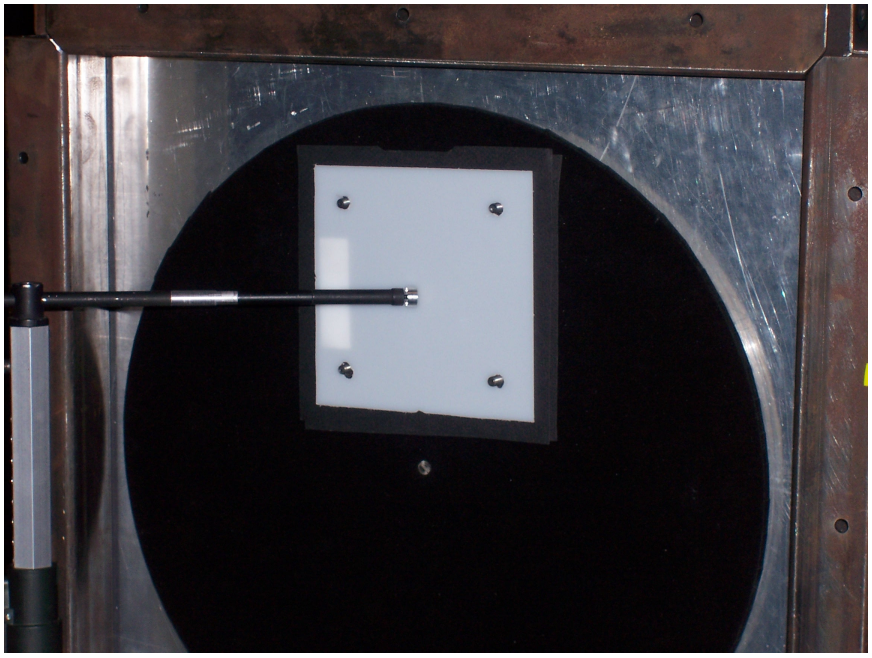

Figure 4.11: ^{241}Am on material surface used to determine $S_{SFbopFfB}$

Figure 4.12 shows the studied materials covered with a nonscintillating material. The total signal collected with the materials covered is the fluorescence behind the material outside material perimeter (S_{Fbop}), plus the air fluorescence in front (S_{Ff}) of the material, plus the background noise (S_B), as shown in Equation 4.3. The procedure is repeated for 10 nm bands centered on 313, 337, 355, 380 and 390 nm.

$$S_{FbopFfB} = S_{Fbop} + S_{Ff} + S_B \tag{4.3}$$

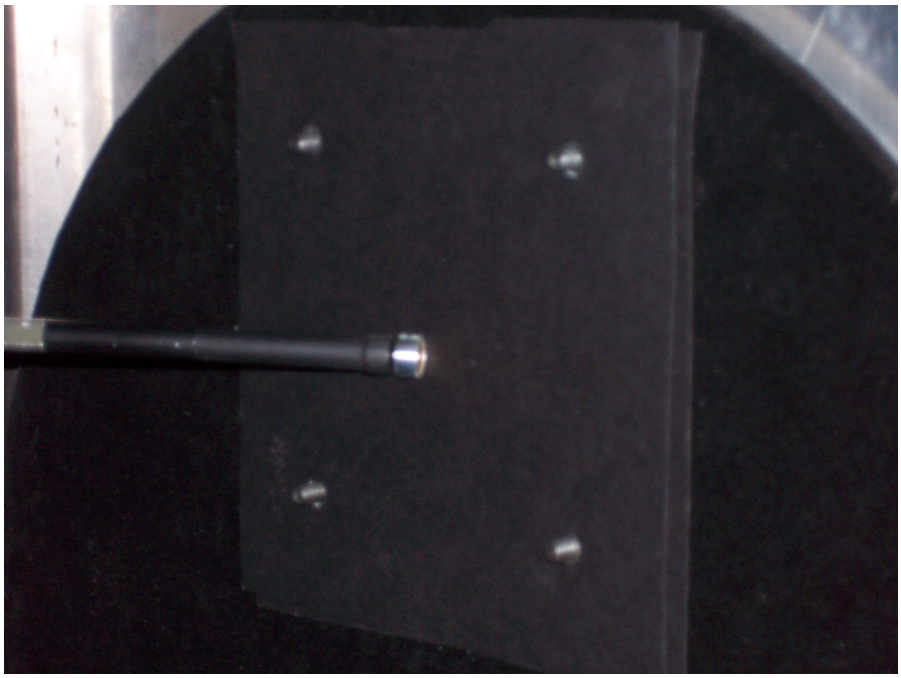

Figure 4.12 : ^{241}Am with material shield to measure $S_{FbopFfB}$

4.5.2 Tests Results

The results of the ^{241}Am scintillation tests are depicted on three graphs. Figure 4.13 is a comparison of the scintillation values. Figure 4.14 shows the air fluorescence seen by the collector, and Figure 4.15 shows the scintillation to air fluorescence ratio. The scintillation ratios

are generally poor for all wavelengths (i.e., 313, 337, 355, 380, and 390). The Plexiglas showed the highest values at 313 nm yielding a ratio close to one. However, small values are suspect. A small variation (i.e., 2 mm) in the distance from the source to the material surface was observed to change the air fluorescence counts by over 20%. Additionally, alpha particles striking the material surface can scatter, increasing the particle flux in the volume of air next to the studied material. During the collection of air fluorescence plus scintillation this would increase that portion of counts due to the increased air fluorescence. Also, the shield is less dense than the studied material, and except for the paper products, the radiation will scatter less, giving a lower value for air fluorescence than the contribution when the material is uncovered. If there is little or no scintillation, small deviations in the air fluorescence counts could result in the negative scintillation values shown in Figure 4.13.

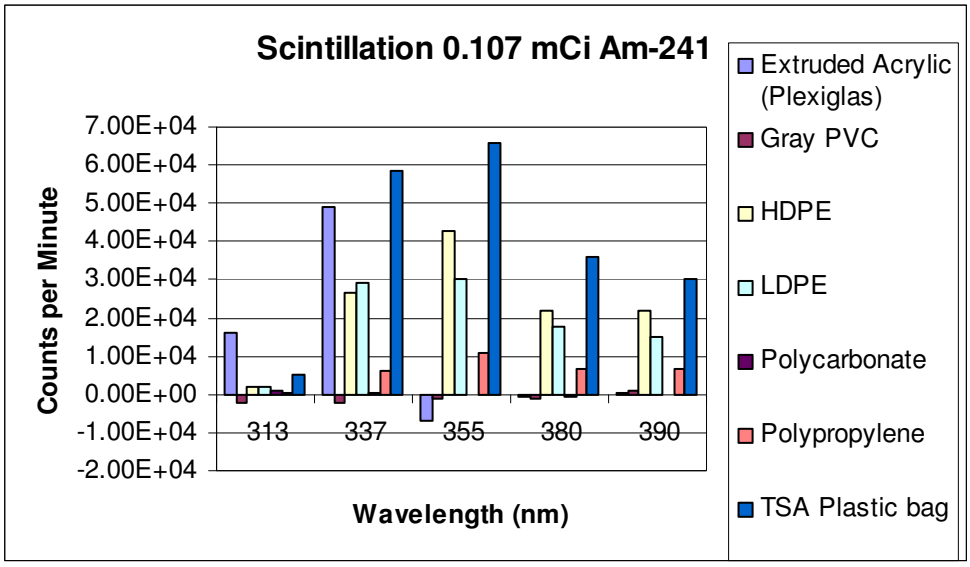

Figure 4.13: Scintillation of Studied Materials with ^{241}Am

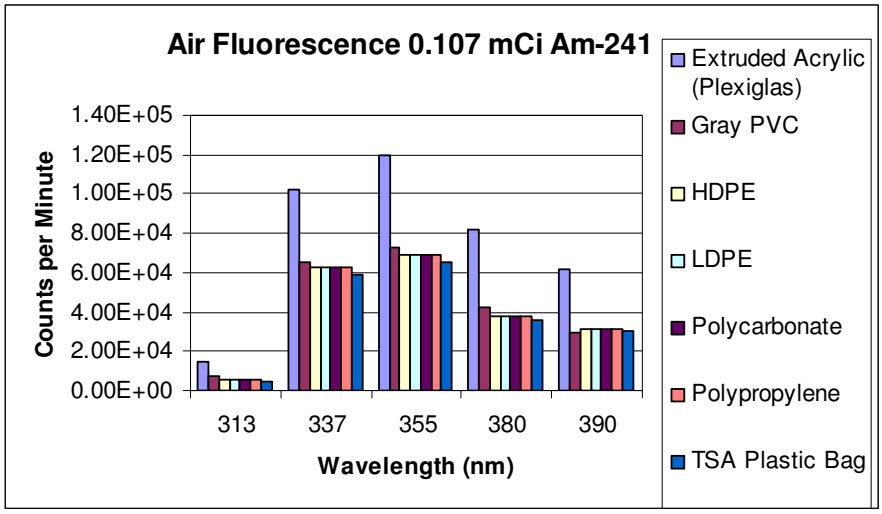

Figure 4.14 Air Fluorescence of ^{241}Am

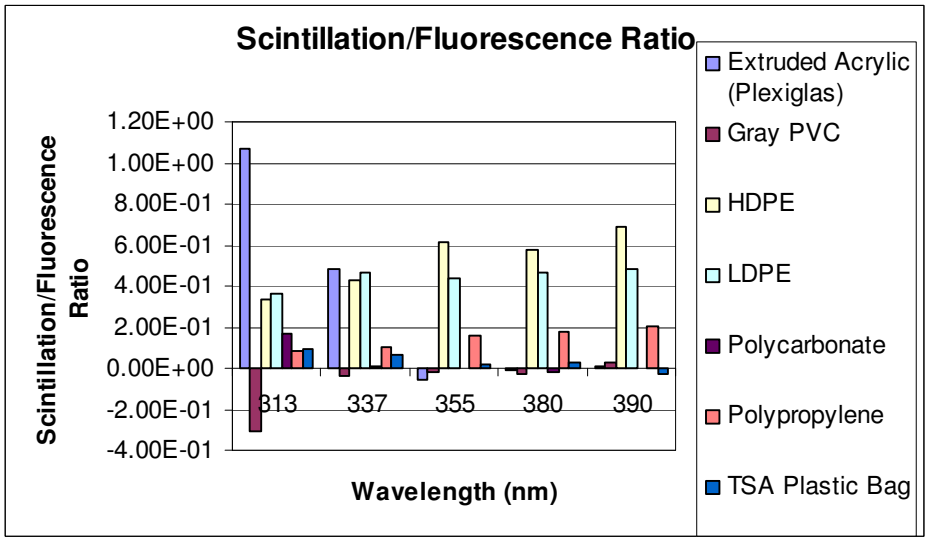

Figure 4.15: Scintillation – Air Fluorescence Ratio

4.5.3 Tests Conclusions

Figure 4.15 shows that all the studied materials in Table 4.2 are very poor scintillators in the presence of ^{241}Am. The Plexiglas showed the best results at 313 nm. However, these results are suspicious. The ratios at 313 is still small, but significantly larger than the values at the 337,

355, 380 nm. The increase at 313 nm could be due to some small difference in the thickness of the shield. For example, moving a surface around 2 mm from the alpha source increases the air fluorescence count by around 10,000 counts or 1/5 of the total counts. Since alpha only travel a few centimeters, a small decrease in the distance from the source to the surface of the material will reduce the air fluorescence in the volume. Also, when the surface is unshielded, alpha particles can scatter back off the surface increasing the flux of alpha particles in a given volume capable of creating fluorescence. This would apply during the collection of air fluorescence plus scintillation, providing a larger contribution due to air fluorescence. When the material is covered by the shield to determine the air fluorescence plus background, and the shield composition is different (i.e., less dense) than that of the test material, it will absorb more alpha particles, and the associated air fluorescence value will be less. Thus, the ratio in Figure 4.15 would be higher than expected. Although all the mechanisms are not understood, the value of scintillation is so small as to be insignificant for the purposes of this study. These same mechanisms likely effected the testing of Materials 7-15, which also provided little scintillation value and will not be discussed further.

4.6 Scintillation of Materials by ^{90}Sr

Where the studied materials are thin enough to allow the radiation to penetrate the material and reach the surface closest to the collector Setup #2 is used. Back scatter of radiation and air fluorescence behind the test material are contained in enclosed space behind the material, not in the field of view of the signal collector. This is the preferred setup for tests using ^{90}Sr, where the beta particles are not totally attenuated and can reach the far surface closest to the collector. Setup #2 is used in all cases except when testing the brick and concrete. For these

materials, Setup #1 is used. Five cycles, with 1 minute of exposure time per cycle, are conducted for each material.

4.6.1 Test Setup

In Setup #2, shown in Figure 4.4, the source is placed behind the studied material, away from the collector. The studied materials are thin enough to allow the radiation to penetrate the material and reach the surface closest to the collector. Back scatter of radiation and air fluorescence behind the test material are contained in the enclosed space behind the material, not in the field of view of the signal collector. This is the preferred setup for tests using ^{90}Sr, where the beta particles are not totally attenuated and can reach the far surface closest to the collector. However, the brick and concrete attenuate the beta particles and Setup #1 is used when testing these materials.

Using Setup #2, shown in Figure 4.16, materials are placed over the source in Figure 4.1.

Figure 4.16: Test material over ^{90}Sr source

With the material uncovered by the scintillation shield, scintillation signal (S_S), plus the air fluorescence signal generated in back of the material from radiation behind the material, outside the material perimeter (S_{Fbop}), plus the signal for air fluorescence in front of the material (S_{Ff}), plus background noise (S_B) is collected. The wheel holding the material is then rotated away from the source to place the material in the unexposed position. Five cycles with 1 minute of exposure time are conducted for each material. The collected signal is shown in Equation 4.2.

$$S_{SFbopFfB} = S_S + S_{Fbop} + S_{Ff} + S_B \tag{4.2}$$

The total signal collected with the materials covered is the fluorescence behind the material outside material perimeter (S_{Fbop}), plus the air fluorescence in front (S_{Ff}) of the material, plus the background noise (S_B), as shown in Equation 4.3.

$$S_{FbopFfB} = S_{Fbop} + S_{Ff} + S_B \tag{4.3}$$

Subtracting the results of Equation 4.3 from Equation 4.2 yields the scintillation value as shown in Equation 4.4.

$$S_S = \text{Signal}_{\text{Scintillation}} = \text{Equation 4.2} - \text{Equation 4.3} = S_{SFbopFfB} - S_{FbopFfB} \tag{4.4}$$

The procedure is repeated for 10 nm bands centered on 313, 337, 355, 380 and 390 nm for materials 1-6 in Table 4.1. For materials 7, 12,13, 14 and 15 the procedure is repeated for

the 40 nm band around 320 nm, the 44 nm band centered on 357 nm and the 23 nm band centered on 386 nm.

Setup #1 is used for materials 8, 9, 10 and 11 in Table 4.1 at 313, 337, 355, 380 and 390 nm. The concrete and brick samples are too thick to allow radiation to penetrate the surface sufficient amounts to effectively radiate the surface closest to the collector. Thus, Irradiator #2 and Setup #1 are used to expose the materials to the beta particles. For ease of testing, a 2 mCi ^{90}Sr is used instead of the 1 mCi used on materials 1 though 7, and 12 through 15 in Table 4.1. The techniques and governing equation remain the same for determining the scintillation value and the air fluorescence. Scintillation tests are performed using Setup #2 shown in Figure 4.4. However, only three materials are imaged. The remaining materials do not scintillate enough to gather an image.

4.6.2 Test results

The results of the ^{90}Sr scintillation tests are depicted on three graphs. Figure 4.17 is a comparison of the scintillation values. Figure 4.18 shows the air fluorescence seen by the collector, and Figure 4.19 shows the scintillation to air fluorescence ratio. The scintillation ratios are generally very good for all tested wavelengths (i.e., 313, 337, 355, 380, and 390 nm) for HDPE, LDPE and Polypropylene with a 35 or better gain at all tested wavelengths. All three have gains of over 100 at 313, 380 and 390 nm. Consequently, the scintillation of these materials is easily imaged. Polycarbonate and extruded acrylic are very poor at all wave lengths with the extruded acrylic showing some promise at 380 and 390 nm with gains of above 50 and 80, respectively. The remaining materials, 7-15 in Table 4.1 are generally poor scintillators compared to HDPE, LDPE and Polypropylene. There total scintillation-air fluorescence ratios

are shown in Figure 4.20. Looking at Figure 4.20, because of their low total scintillation to air fluorescence ratios, these materials are not examined with the exception of the TSA bag, the white poster board, and the concrete cut face, whose scintillation, air fluorescence, and scintillation ratios are shown in Figures 4.17, 4.18. and 4.19, respectively, at individual wavelengths.

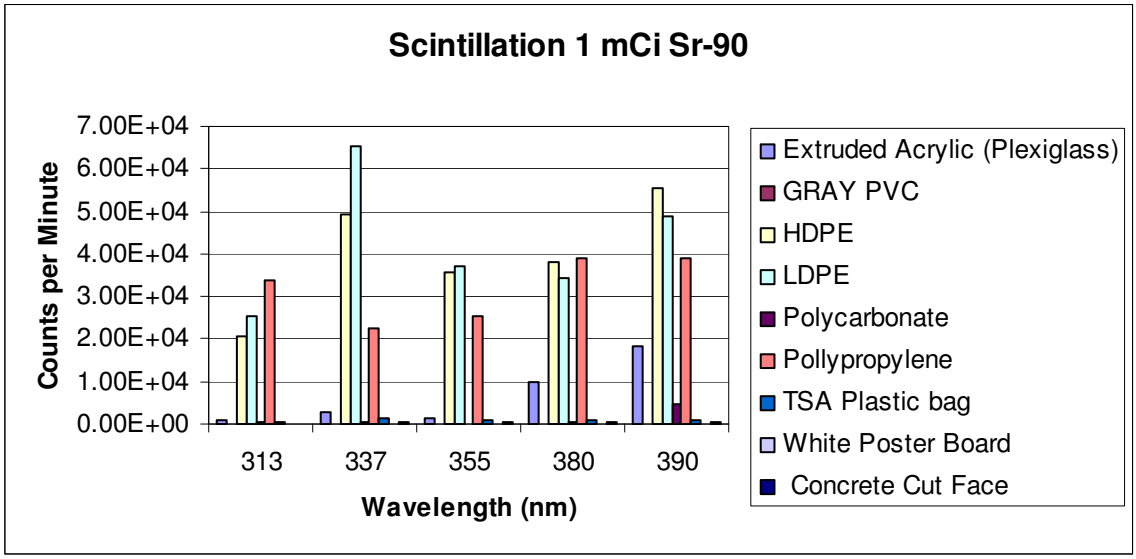

Figure 4.17: Scintillation of Studied Materials with ^{90}Sr

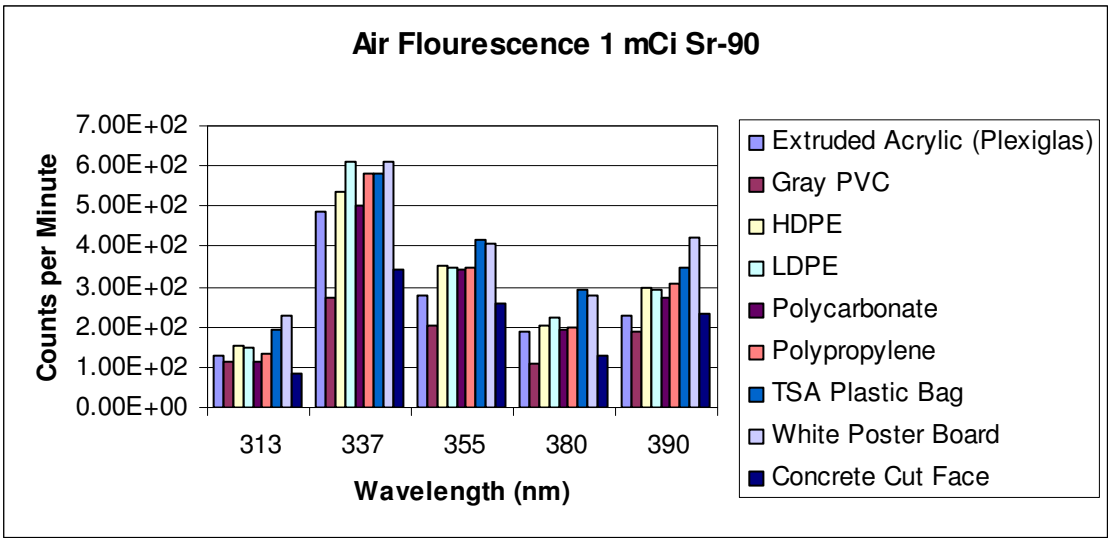

Figure 4.18: Air Fluorescence of ^{90}Sr

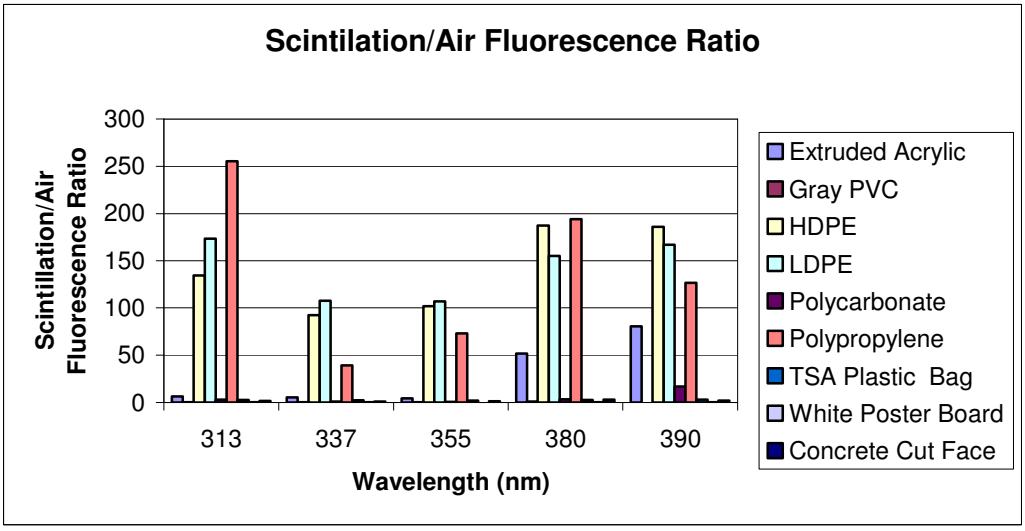

Figure 4.19: Scintillation – Air Fluorescence Ratio

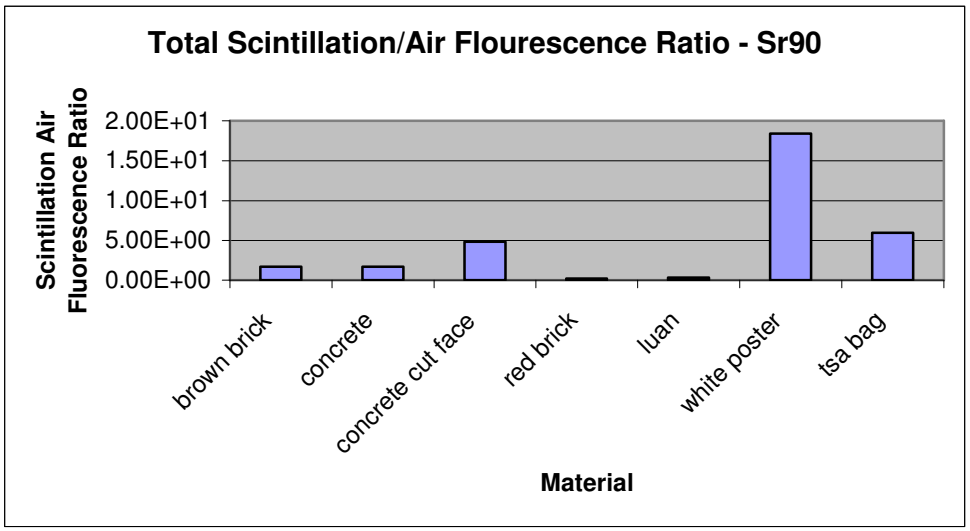

Figure 4.20: Total Scintillation – Air Fluorescence Ratio

4.6.3 CCD Image of Scintillation by ^{90}Sr

Using Setup #2, shown in Figure 4.4, with the PMT replaced by the CCD, sample test materials in Table 4.1 are placed over the source as shown in Figure 4.11. With the source in the exposed position, an image is collected with the material present and then one collected without the material. The second image is then subtracted from the first, pixel by pixel, to determine the scintillation image. With the source in the exposed position for 5 minutes, only 3 materials showed scintillation value, HDPE, polypropylene, and LDPE. Color enhanced images of these materials are shown in Figure 21, Figure 22, and Figure 23, respectively. The source, positioned on the right side facing the material, and shown in Figure 4.1, is clearly depicted by the outlined white area on the right side of all three images. The scintillation ratios in Figure 4.19 validate that these three tests materials have sufficient scintillation values from which an image is possible with minimum exposure times.

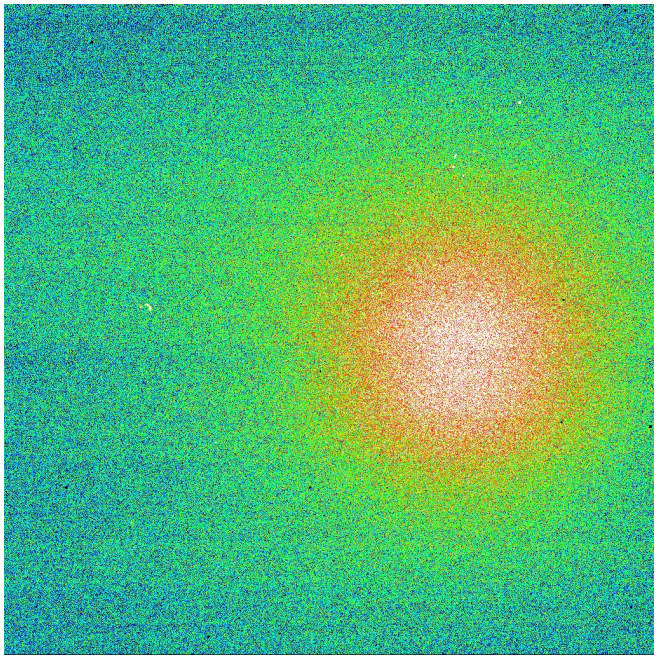

Figure 4.21: HDPE Scintillation 5 Minute Exposure

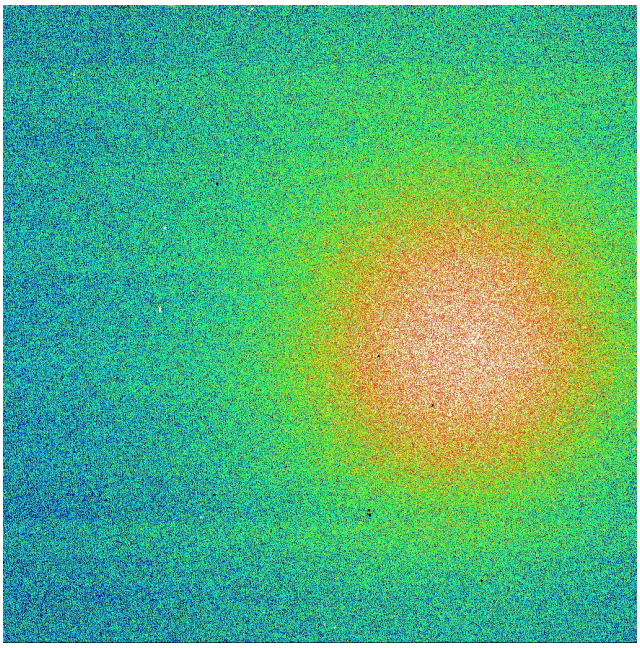

Figure 4.22: Polypropylene Scintillation 5 Minute Exposure

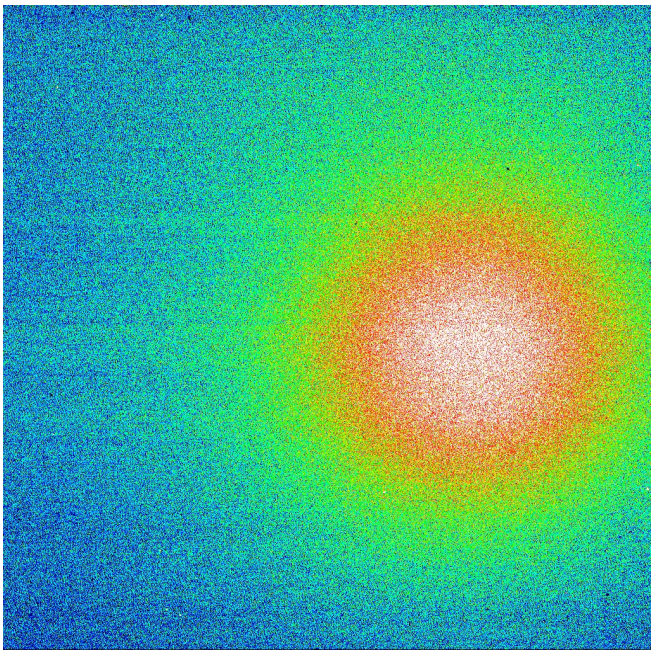

Figure 4:23 LDPE Scintillation 5 Minute Exposure

4.6.4 Tests Conclusions

High Density Polyethylene (HDPE), Low Density Polyethylene (LDPE), and Polyethylene were reasonably good scintillators when exposed to ^{90}Sr. The 1 mCi source easily penetrated the 1.56 mm thick material, achieving scintillation to air fluorescence ratios or 35 or above at all tested wavelengths (i.e., 313, 316, 337, 355, 380, and 390 nm). Especially promising are the results achieved in the 10 nm band centered at 313 nm. The HDPE, LDPE, and polypropylene achieved scintillation to air fluorescence ratios above 125, 160 and 250, respectively, and produce scintillation images with 5 min exposure times. Also of interest is the plastic bag which showed scintillation/air fluorescence ratio values of over 2 at 313, 337, 355, and 380, and a 3.81 ratio at 390. This would indicate the material could be of value in the detections of ^{90}Sr radioactive material at airport security checkpoints.

None of the tested materials in Table 4.2 showed promise as a scintillator when exposed to the 0.107 mCi ^{241}Am alpha source. The distance alpha particles (i.e., a few centimeters) travel dictates that the material is in almost direct contact with the source. Additionally, the source is easily attenuated by the material, and unable to penetrate even materials a few millimeters thick.

CHAPTER 5

REFLECTIVE CHARACTERISTICS OF STUDIED MATERIALS

Two types of reflective properties will be studied, specular and back reflectance at 45 degrees. Back reflectance at 45 degrees is a fraction of diffuse reflectance. Diffuse reflectance is light scattered from the incident ray, scattered in random directions by the surface contour. The incident light ray is reflected in many different rays, in all directions, at many different angles from the normal to the surface (Knight, Jones, and Field 2006). Specular reflectance is the mirror like reflectance observed when light is reflected from a surface at an angle between the normal to the surface and the reflected ray equal to the angle between the normal to the surface and the incident ray (Knight, Jones, and Field 2006).

5.1 Back Reflective Characteristics of Studied Materials

The back reflectance at a particular angle is that part of the diffuse reflectance reflected back from the surface contour at the same angle as the incident ray. Using a deuterium lamp and spectrometer, both coupled by a fiber optical "Y" cable to a probe as shown in Figure 5.1, back reflectance values are measured for the material shown in Table 5.1. The probe is inserted into a rectangular test block, shown in Figure 5.1, at 45 degrees from the horizontal plane and that portion of the light reflected back compared to that portion of light projected on a standardized sample and reflected back.

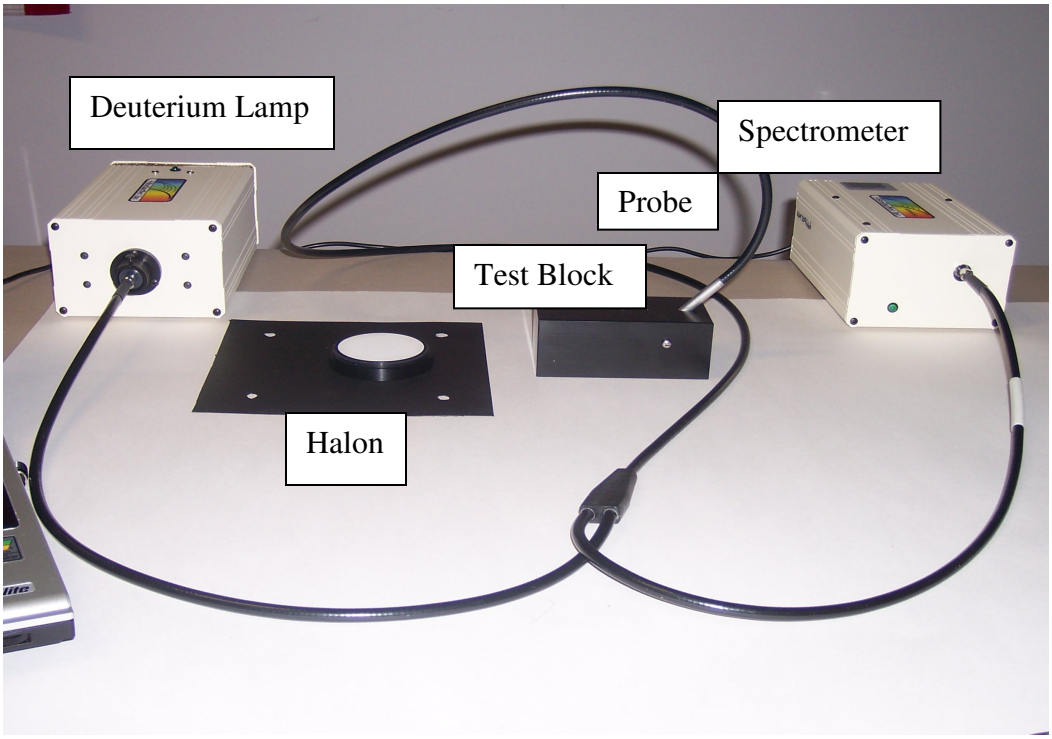

Figure 5.1: Spectrometer, Deuterium Lamp, Probe, and Test Block

The rectangular test block with the probe inserted (Figure 5.1) is placed on top of the studied material and the reading taken is compared to the reading taken when the test block is placed on top of the reflectivity standard, Halon (RS50), shown in Figure 5.1 and 5.2. The data for determining the back reflective properties for UV light hitting as surface at 45 degrees of the materials was gathered using the setup shown in Figure 5.1 and Figure 5.3. Using a deuterium lamp and a probe, an incident light beam is projected at an angle of incidence ($\theta_{incidence}$) of 45 degrees to the material surface of varying common materials. The probe then collects the light reflected back at 135 degrees (see Figure 5.3) to the surface or 45 degrees to normal, and compares that to the amount of light originally projected to determine the percent of light back reflected. Results of the diffuse back reflectivity curves are shown in Figures 5.4 through 5.6, for the materials listed in Table 5.1.

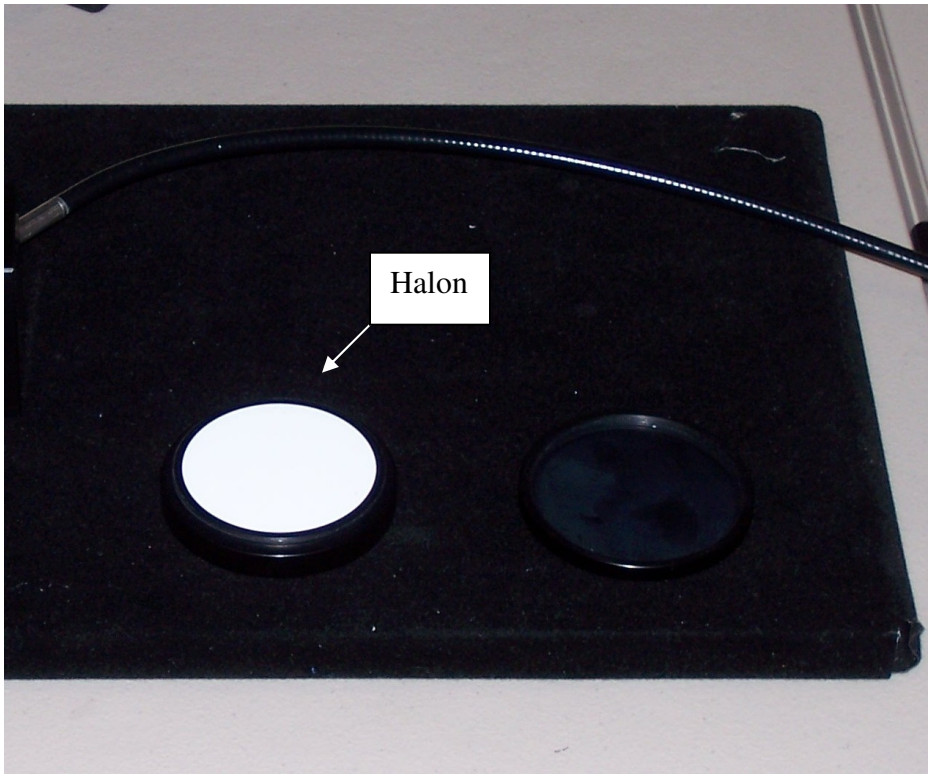

Figure 5.2: Reflectivity Standard (RS50) Halon

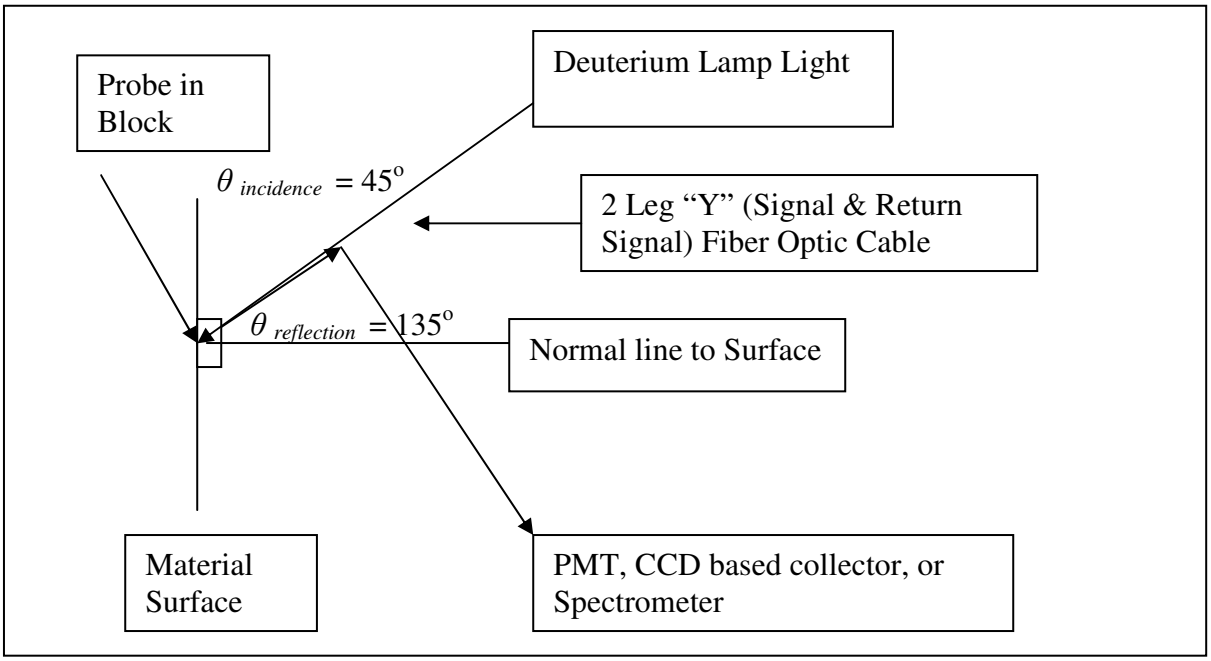

Figure 5.3: Back Reflectivity Setup

Table 5.1

Reflectance Tests Materials

Materials
Gray PVC
LDPE
HDPE
Polycarbonate PVC
Plexiglas (extruded acrylic)
Polypropylene
TSA Plastic Bag
Light Red Brick
Gray Brick
Concrete (Smooth)
Concrete (Textured)
Paper (White)
Paper (Black)
Plywood
Aluminum

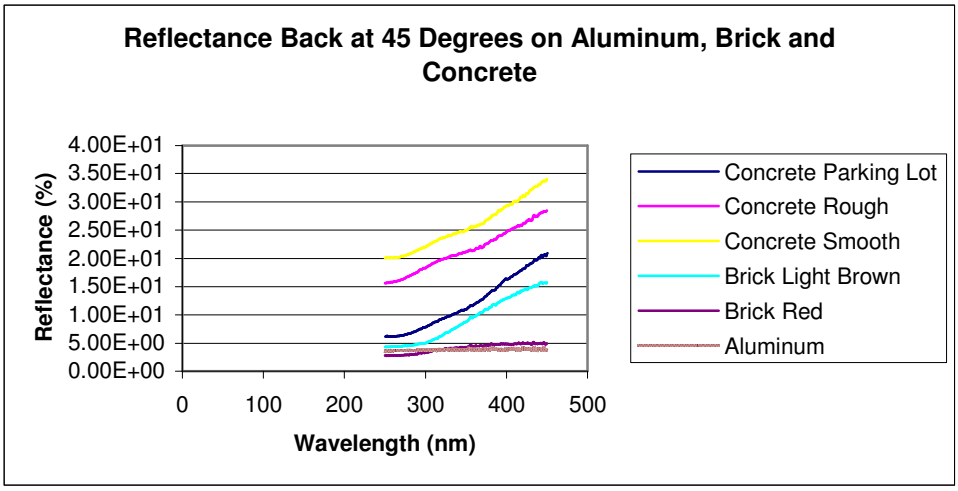

Figure 5.4: Reflectance Back at 45 Degrees on Aluminum, Brick and Concrete

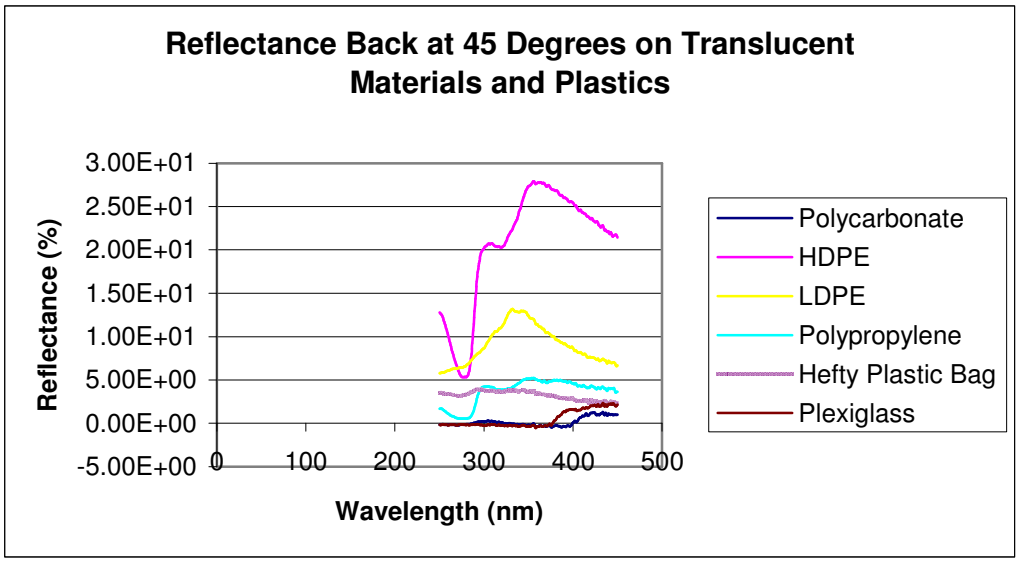

Figure 5.5: Reflectance Back at 45 Degrees on Translucent Materials and Plastics

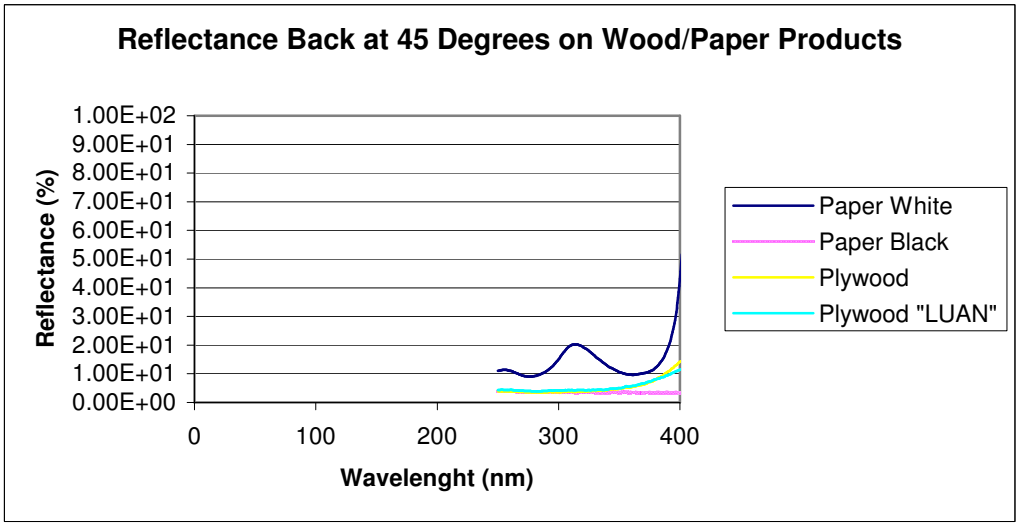

Figure 5.6: Reflectance Back at 45 Degrees on Wood/Paper Products

5.2 Specular Reflective Characteristics of Studied Materials

The data for determining the specular reflective properties of the materials is gathered using the setup shown in Figure 5.7 and in Figure 5.8. Using a deuterium lamp and a probe, an

incident light beam is projected at an angle of incidence ($\theta_{incidence}$) on a surface of varying common materials. The spectrometer and the same probe are used to collect the light reflected from the surface. The probe is positioned vertically giving a $\theta_{incidence}$ of 0^o from normal or 90^o from the material surface. The reflected light is then collected using a same probe meaning the angle of reflection ($\theta_{reflection}$) equals the angle of incidence ($\theta_{incidence}$). The data taken when the rectangular block is placed on top of the studied material is compared to the data taken when the test block is placed on top of the an aluminum coated UV coated mirror provided by Edmund Optics shown in Figure 5.7. The reflectivity relative to the mirror is reported in Table 5.3 and displayed in the reflectance curves in Figures 5.9 through 5.11.

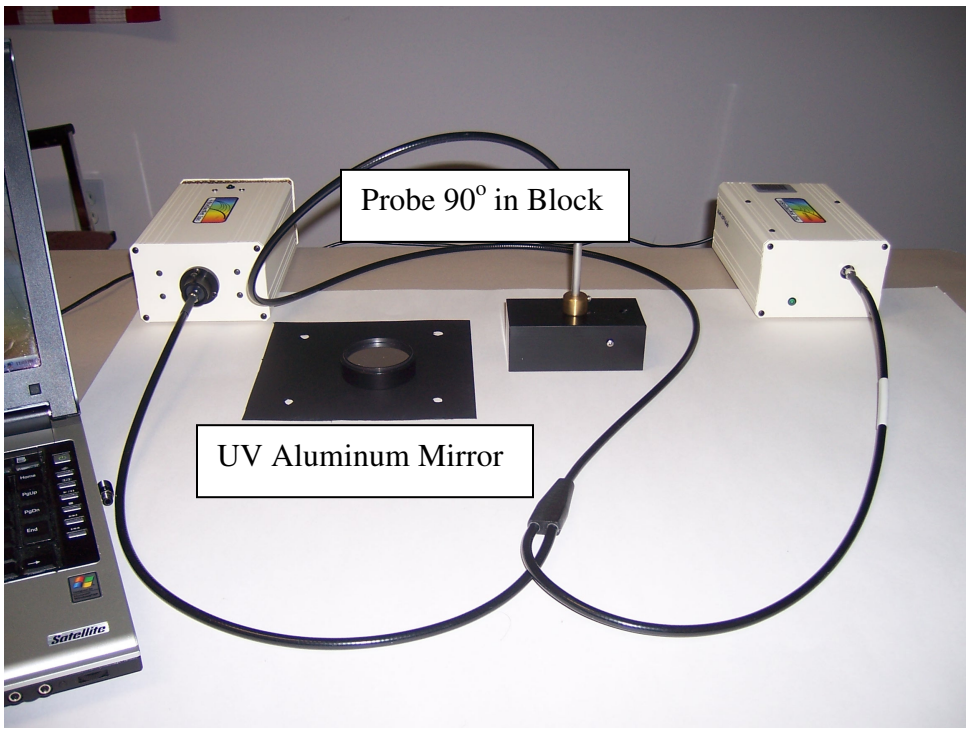

Figure 5.7: Test Block with Probe Mounted on Top at 90 degrees

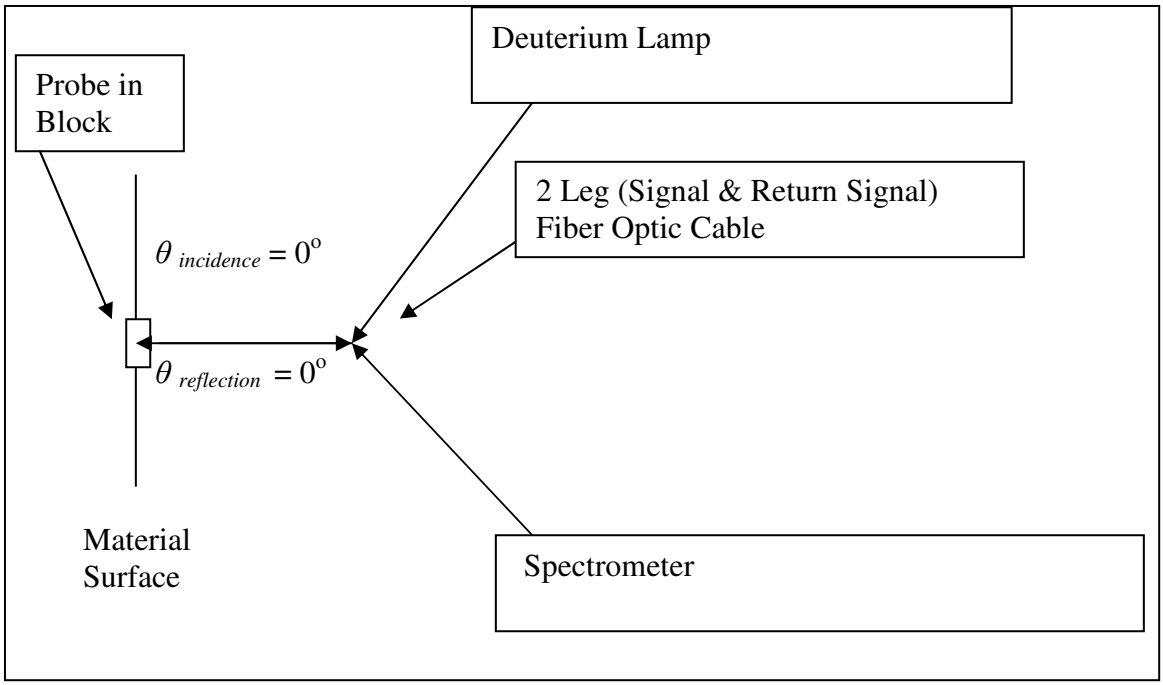

Figure 5.8: Specular Reflective Characteristics Setup

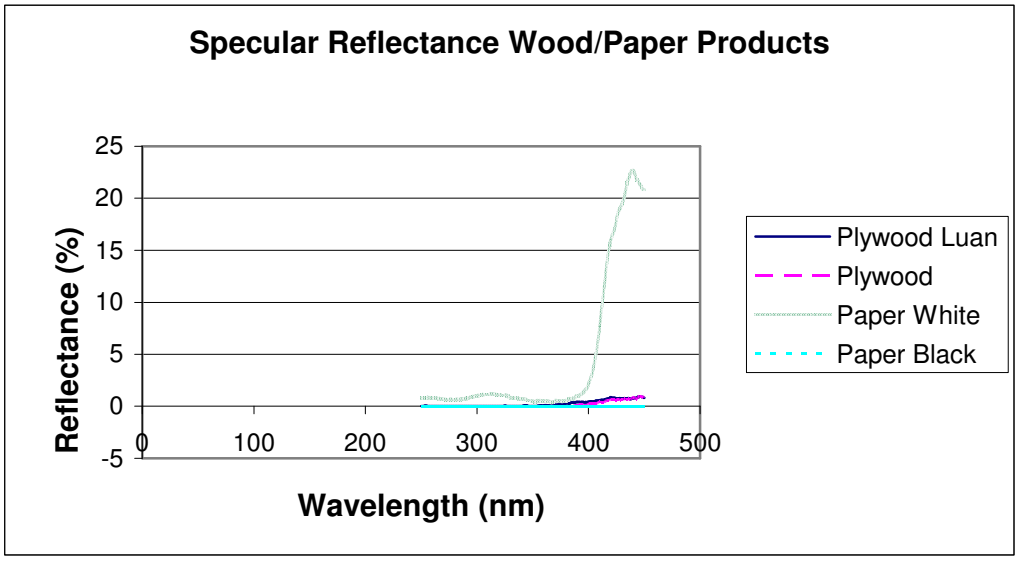

Figure 5.9: Specular Reflectance Wood/Paper Products

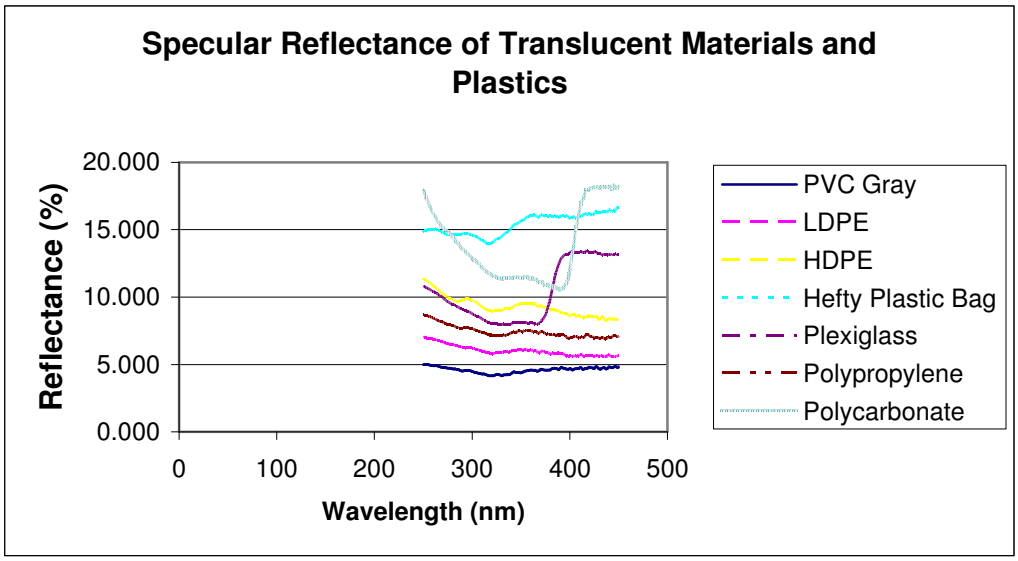

Figure 5.10: Specular Reflectance of Translucent Materials and Plastics

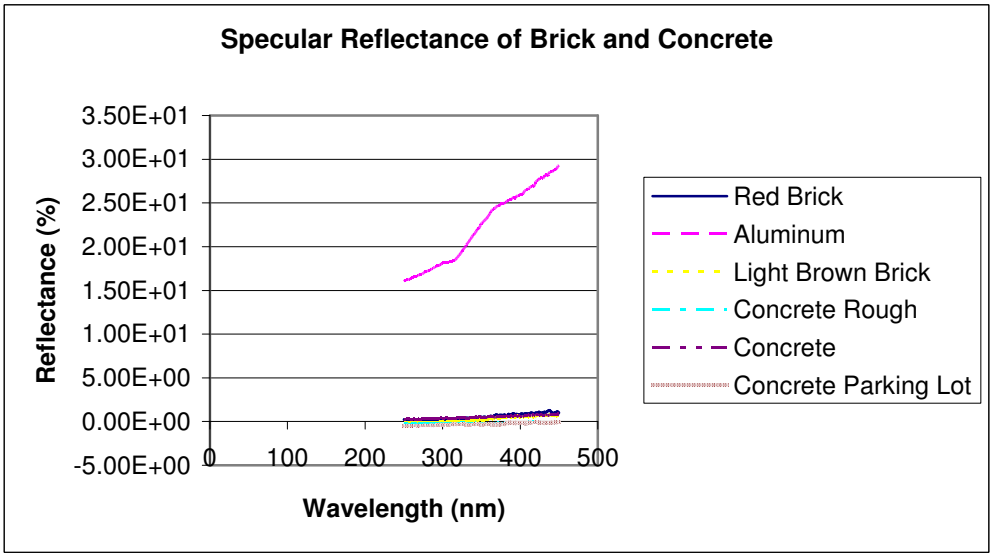

Figure 5.11: Specular Reflectance of Brick and Concrete

5.3 Conclusion

The back reflectance at 45 degrees to the normal along the same path as the incident light bundle is just an approximate technique to provide an estimate of the diffuse reflectance. Where

possible, the observed values are compared to similar material reflectance values in the USGS Digital Spectral Library (Clark 2007). The percentages in Figure 5.4 are the percent of the incident bundle of rays reflected back. For the aluminum, brick and concrete, shown in Figure 5.4, the aluminum plate reflected the smallest portion of incident light back, around 4 percent from 300 to 400 nm. This is reasonable, since the aluminum surface was smooth and somewhat shinny, indicating a higher specular reflectance value. The medium red brick had a smooth, dull surface and reflected back 4% of the incident ray at 300 nm, 4% at 350 and about 5% at 400 nm. These percentages appear reasonable when compared to the medium brick in the USGS Spectral Library, which show a value of 8.3% at 350 and 7.8% at 400 nm. The light brown brick start approximately 5% at 300 nm, 10% at 350 nm and 13% at 400 nm. This compares reasonably well with the light gray brick in Figure 2.9 that shows a gradual increase from 17% at 350 nm to 18% showing a gradual increase. The USGS data table indicates light gray concrete has diffuse reflectance values of 15.2% at 350 nm and 18.4% at 400 nm. The smooth surface concrete tested in Figure 5.9 reflected more light (i.e., 22% at 300 nm, 15% at 350 nm, and 28% at 400 nm) than the USGS values, and the rough and parking lot samples tested. This seems reasonable since the sample had many small contours on the surface and was lighter in color than the rough concrete and the parking lot sample. The rough concrete is darker than the other samples had many large deep contours and its curve was in between the smooth and parking lot values. The parking lot concrete was around 12% at 350 nm and 17% at 400 nm, which is close to the USGS values stated previously. All samples increase around 3.5 % per 50 nm from 300 to 400 nm. This is consistent with the USGS slope 3.2% per 50 nm over the same range.

The USGS tables show translucent HDPE has a diffuse reflectance value of 10.2% at 350 and then moves up to 45% at 400 nm. Looking at Figure 5.5, the HDPE sample has reflectance

values of 22% at 350 nm and 26% at 400 nm. These are less than the USGS library value at 400 nm and greater than the USGS value at 350 nm. One reason may be the surface of the test material was very smooth and glossy. The test LDPE sample rose from 8% at 300 nm to a peak of 12% at 340 and them dropped off to 8% at 400 nm. The USGS library shows a steady increase from 4.3% at 350 nm and then a consistent rise to a value of 39% at 400 nm. As with the HDPE, the surface of our sample is glossy which may explain the lower values. The polycarbonate, extruded acrylic (i.e., Plexiglas), and the plastic bag all have glossy surfaces and have back reflectance values below 5% across the 300 to 400 nm spectrum.

The USGS table indicates paper white bond has a diffuse reflectance 13.7% at 350 and then moves up to 37.5% at 400 nm. Looking at Figure 5.6, the white paper sample is close in color to the white bond paper but showed negligible back reflectance from 300 to 400 nm, as did the black paper sample and the plywood sample the one plywood and the "Luan" plywood. The white paper sample shows a steep rise at 400 nm approaching over 40% around 400 nm.

As previously discussed, specular reflectance is a "mirror like" reflectance. The brick and concrete products in Figure 5.11, and the wood and paper products in Figure 5.9 have dull surfaces with many contours, and there specular reflectance values are negligible. The Gray PVC, LDPE, HDPE, and polypropylene, have glossy surfaces and exhibited some specular reflectance. All have generally consistent values across the 300 to 400 nm with never varying by more than 2% across the region and generally having specular values between 5% and 10%. The polycarbonate sample has reflectance values between 12.5% at 300 nm and drops across the region to 11% at 400 nm and then rises sharply. The extruded acrylic (Plexiglas) curve resembles the polycarbonate specular reflectance curve except the reflectance values are lower below 370 nm, and the rise above polycarbonate at 390 nm approaching 13% at 400 nm. The

plastic bag is the second best specular reflector; generally have reflectance value of 15% across the region. As expected, the best specular reflector was the aluminum plate, increasing across the 300 to 400 nm band from 18% at 300 nm to over 25% at 400 nm. The “mirror like” surface is the superior specular reflector.

The results of the reflectance tests indicate care must be taken when working in areas which have highly reflective materials. High reflectance values can increase the background levels from UV source outside of the area of operations. The effects from specular surfaces can sometimes be avoided by relocating the instrument. However, the effects from diffuse surfaces are hard to avoid, and must be considered when determining the possibility of using optical detection methods.

CHAPTER 6

TRANSMISSIVE CHARACTERISTICS OF STUDIED MATERIALS

The transmission properties of the selected tests materials compared to those of air are determined using two procedures. The first procedure, with the source exposed, records the number of counts with the test material between a 4 inch lens and a PMT, and then, divides that number by the counts recorded when only air is present between the PMT and the 4 inch lens. The second technique requires the measurement of the transmission properties by placing the test materials between a deuterium lamp and a small spectrometer. Fiber optic cables attached to collimating lenses and special computer software, provided by Stellarnet, Inc., compares spectrometer readings when the test material is in the path between the spectrometer and the deuterium lamp, and a reading when the material is removed and only air is between the lamp and the spectrometer.

Six of the test materials were purchased from McMaster-Carr (McM) and the seventh, a "Hefty" plastic bag, was purchased from a local supermarket. The bag is similar to those used by the Transportation Security Agency at airport security stations for the screening personal items. The test materials are shown in Table 6.1.

Table 6.1

Tests Materials

Material	Vendor Item Number	Thickness (inches(mm))
Clear Extruded Acrylic Sheet Plexiglas	McM #8589K11	0.0600 (1.5240)
Polypropylene Translucent Sheet White	McM 8742K131	0.0625 (1.5875)
Polycarbonate Sheet	McM 8574K24	0.0625 (1.5875)
Polyethylene (LDPE)	McM 8657K111	0.0625 (1.5875)
Polyethylene (HDPE)	McM 8619K421	0.0625 (1.5875
Gray PVC (type I)	McM 8747K111	0.0625 (1.5875)
Hefty Plastic Bag	Pactiv Corporation	0.0020 (0.0500)

6.1 First Transmission Technique.

With the source exposed, the number of counts is recorded with the test material between the 4 inch lens and the PMT with filter. Next, the material is removed and a reading taken with just air between the lens and the PMT and filter. Then, divide that number of counts with the test material between the lens and PMT by the number of counts when there is no test material (i.e., air) present. The fractions at different wavelengths obtained times 100% are the transmissive values of the sample material. This procedure is repeated for the 10 nm bands centered on 313, 337, 355, 380 and 390 nm. The setup for the first technique is shown in Figure 6.1, and the transmissive values obtained are shown in Table 6.2 for a 0.107 mCi ^{241}Am source.

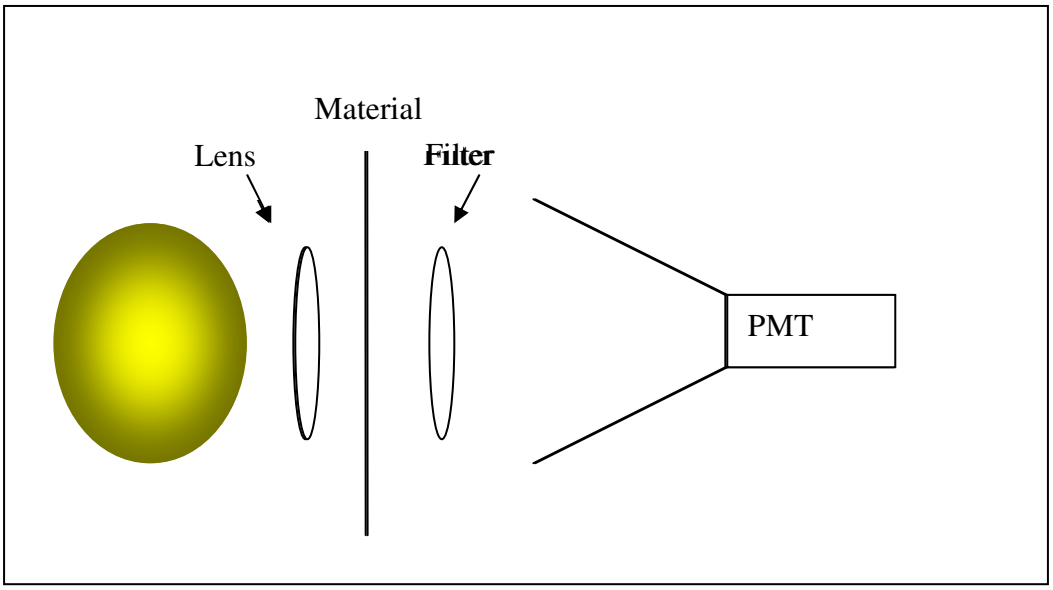

Figure 6.1: Test Sample between the PMT and the 4 inch Lens

Table 6.2

Percent Transmission Compared to Air

Materials	313 nm	337 nm	355 nm	380 nm	390 nm
Air	1.00E+02	1.00E+02	1.00E+02	1.00E+02	1.00E+02
Gray PVC	6.70E-01	0.00E+00	6.13E-03	0.00E+00	0.00E+00
LDPE	5.61E+00	7.54E+00	9.16E+00	1.10E+01	1.11E+01
HDPE	3.39E-01	9.08E-01	1.52E+00	2.20E-01	1.87E+00
Polycarbonate	0.00E+00	1.76E-01	0.00E+00	4.86E-01	3.56E+00
Plexiglas (extruded acrylic)	6.11E-01	0.00E+00	1.86E+00	5.24E+01	8.66E+01
Polypropylene	4.85E+00	6.37E+00	7.57E+00	8.50E+00	9.48E+00
TSA "Hefty" Plastic Bag	7.49E+01	7.71E+01	7.87E+01	7.81E+01	7.96E+01

6.2 Second Transmission Technique Using a Spectrometer

Next, the transmission of light through the studied material is assessed by placing the deuterium lamp in the back of the material, and measuring the percent of transmitted light through the material. This procedure should yield more accurate results than the previous technique because of the large signal by the lamp compared with the small air fluorescence signal used in the previous technique. The procedure is illustrated in Figure 6.2 with S_B representing the background signal. A picture of the transmission test stand is shown in Figure 6.3.

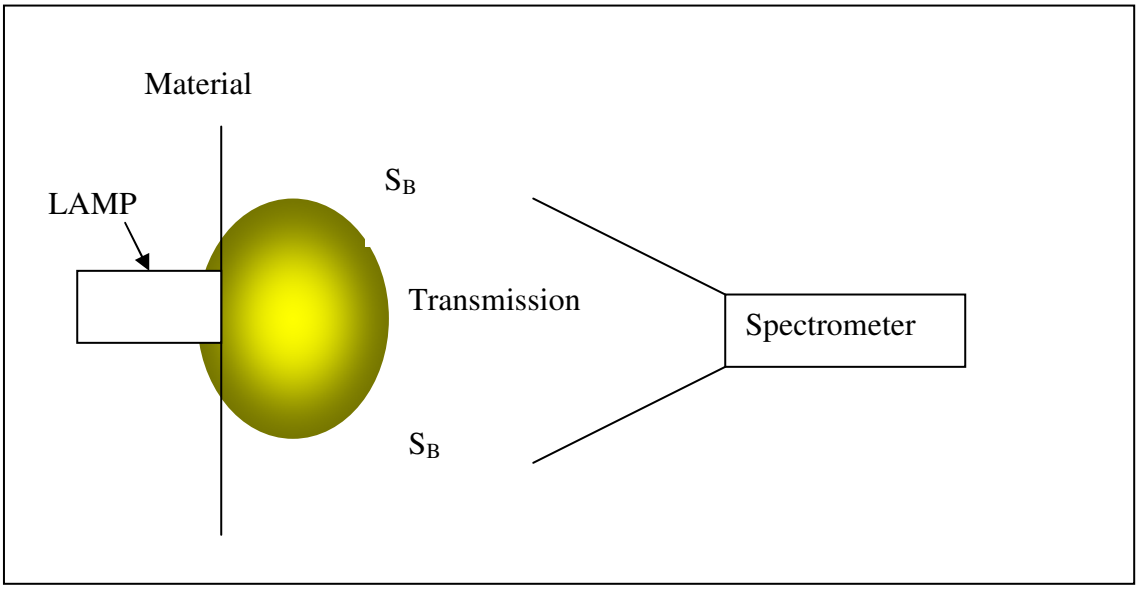

Figure 6.2: Test Material between Deuterium Lamp and the Spectrometer

The mini-spectrometer, deuterium lamp and a transmission test stand, provided by Stellarnet, Inc., are shown in Figure 6.3. A small focusing lens is positioned at the test stand end of the cable running from the deuterium lamp to the test stand to focus the light on the material. Another focusing optic is used to divert light that has passed through the material into the fiber optic cable running to the spectrometer.

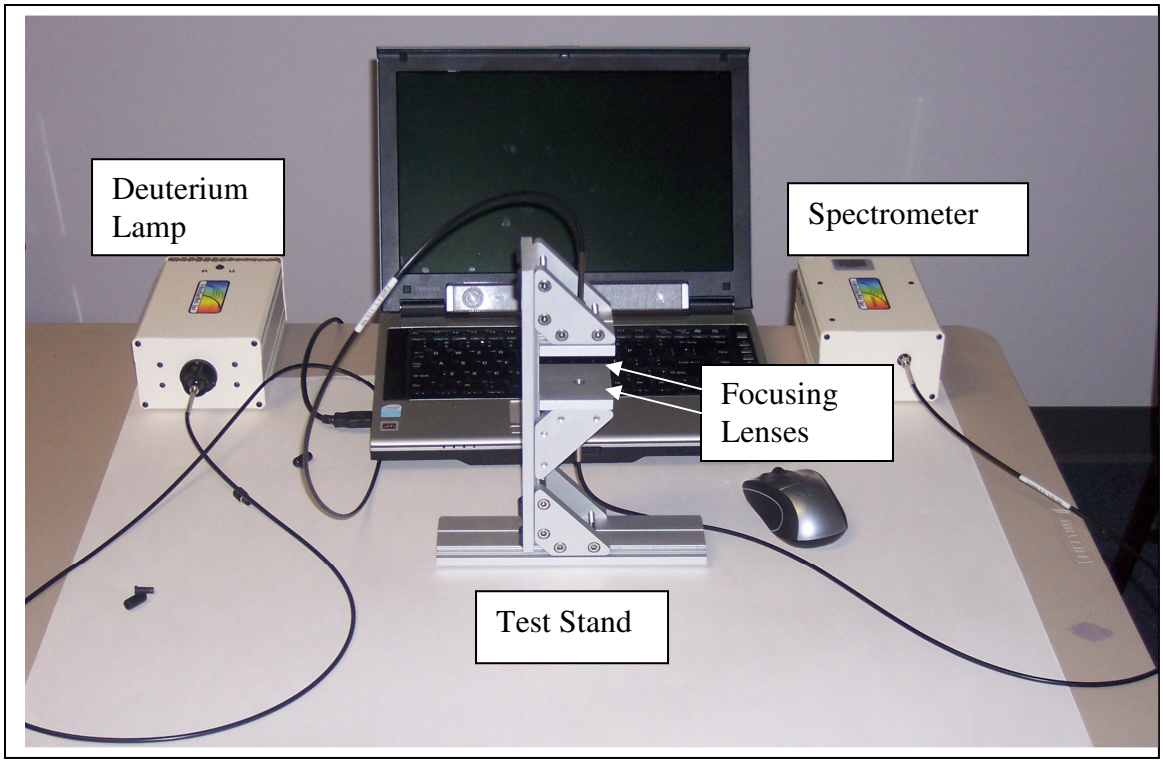

Figure 6.3 – Transmission Test Stand

Transmission curves, using the setup shown in Figure 6.3, are presented in Figure 6.4 for the materials shown in Table 6.1.

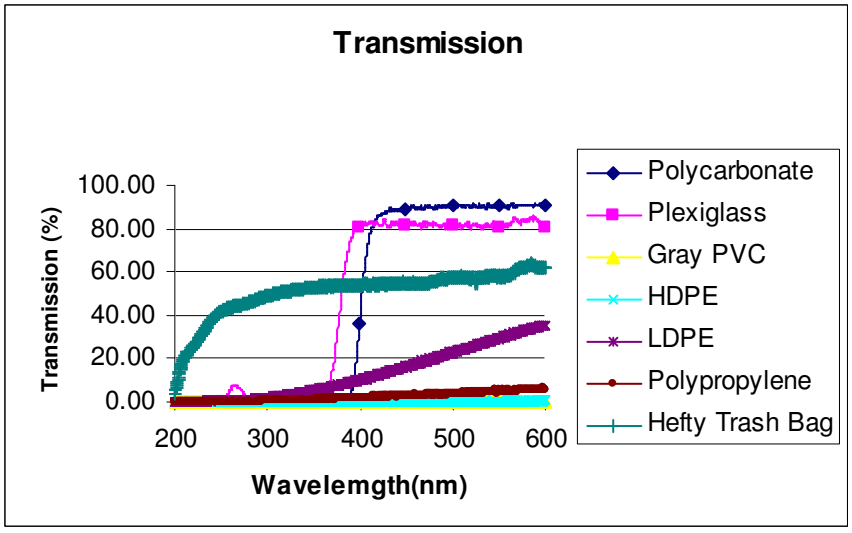

Figure 6.4 Transmission Curves for Materials in Table 6.1

Table 6.3

Percent Transmission Compared to Air Using a Spectrometer

	Wavelengths				
Materials	313 nm	337 nm	355 nm	380 nm	390 nm
Gray PVC	1.12E-02	1.58E-01	0.00E+00	2.37E-01	4.61E-02
LDPE	2.75E+00	4.29E+00	5.71E+00	7.98E+00	9.01E+00
HDPE	0.00E+00	4.38E-02	1.61E-01	1.60E-01	1.15E-01
Polycarbonate	1.58E-02	9.33E-02	5.13E-02	4.73E-01	3.11E+00
Plexiglas (Extruded Acrylic)	0.00E+00	3.65E-01	1.23E+00	4.92E+01	7.50E+01
Polypropylene	7.81E-01	1.08E+00	1.21E+00	1.52E+00	1.58E+00
TSA "HEFTY" Plastic Bag	5.04E+01	5.22E+01	5.31E+01	5.36E+01	5.37E+01

6.3 Conclusions

The transmission values in Table 6.3 were obtained using the spectrometer and a deuterium lamp. Those are generally lower than the values in Table 6.2, which were obtained measuring the direct air fluorescence of the materials. One would expect the spectrometer reading to be more accurate due to the large number or photons by the deuterium lamp directed at the materials. Lamadie et al. (2004) indicated that 1 mm of Polycarbonate and Plexiglas (i.e., extruded acrylic) had values of 92% and 97%, respectively, when compared to air. The transmission values of Polycarbonate and Plexiglas depend on the coating. Generally, polycarbonates have low transmission values in the UV. The polycarbonate transmission curve in Figure 6.4 shows a steep cutoff around 400 nm with very little transmission observed between 300-400 nm. This agrees with most published literature. The Extruded Acrylic (i.e., Plexiglas) transmission curve is similar to the published curve for UV-G by Altuglas International and Rideout Plastics (www.eplastics.com and www.plexiglas.com 2010). This particular extruded acrylic tested does not transmit well in the UV. Many extruded acrylic surfaces are coated to

prevent transmission in the UV. However, UV-T Plexiglas does transmit well in the 300- 400 nm band approaching the values in the 90 percentile range for thin sheets similar to the 1 mm sheet tested by Lamadie et al. (2004). Several manufacturers (i.e., www.eplastics.com and www.plexiglas.com 2010) put the value for UV-T Plexiglas around 90 to 92%. The "Hefty" plastic bag, similar to those used in airports by TSA, transmitted approximately 50% of the UV light between 300 and 400 nm using the spectrometer, and over 70% using the first technique. The plastic bag, thin HDPE, due its crystallite structure, scatters the direct light instead of transmitting it directly (Sigmore 1968). Thus, a portion of the transmitted light is more likely collected by the PMT with a larger collection area, than the small optical lens in the tests stand used in the second technique, which only collects a portion of the scattered light. The fact that the bag transmits UV will allow for the optical detection of radioactive materials placed next to, or in such bags, at airport security passenger checkpoints.

The HDPE, Polypropylene, and Gray PVC have very low transmissive values in the UV. Placing the materials between an optical detector and the radioactive air fluorescence blocks the transmission of UV light through the material. However, as discussed in Chapter 4, when the ^{90}SR source is in close proximity (i.e., a few centimeters) to the HDPE and Polypropylene, scintillation of the surface area will enhance the detection. The LDPE transmitted 2.75% of the UV light at 313 nm, and rose gradually to around 9% at 390 nm. However, as with the HDPE and Polypropylene, the high scintillation surface values of the LDPE enhances the detection of radioactive materials placed close to the LDPE.

CHAPTER 7

OPTICAL BACKGROUND LEVELS

Threshold background detection levels are determined for radioactive sources using published data and laboratory systems. Outdoor background levels are observed using a mini-spectrometer during the evening hours to determine the magnitude of the background UV and background fluctuations. Using the measured outdoor background UV data and estimating the solar contribution from published data, a determination is made concerning which wavelength and associated outside scenarios offer the best possibility for the optical detection of radioactive materials. Bunner's (1964) efficiency factor is used to determine the UV air fluorescence for ^{241}Am at the selected band in the UV. This UV fluorescence is used to predict definitive detections of the radioactive materials in given scenarios with a 95% confidence.

7.1 Solar Background

To determine the effects of the solar background, one must appreciate the number of photons represented by a watt of optical power. A watt of optical power at 300 nm is equal to 1.5×10^9 photons per nanosecond, or 1.5×10^{18} photons per second (Saleh and Teich 1991). Outdoor background light levels of only a micro-watt between 300 and 400 nm prevent the optical detection of air fluorescence signatures except where the radioactive source is extremely large (i.e., many curies). ASTM G173-03 provides useful reference solar spectral irradiance

data for the sun's contribution to background radiation at sea level. Based on a south facing surface titled 37 degrees from the horizontal, the reference value is the spectral radiation from the solar disk plus the sky diffuse light and the diffuse light reflected from the ground. Figure 7.1 shows a graph of the ASTM G173-03 "Global Tilt" data plotted from 200 to 900 nm. Shown in Table 7.1, for selected wavelengths, are the ASTM G173-03 data in watts/m^2 per nm converted to the number of photons per second that would fall on a one cm^2 collector for wavelengths of interest.

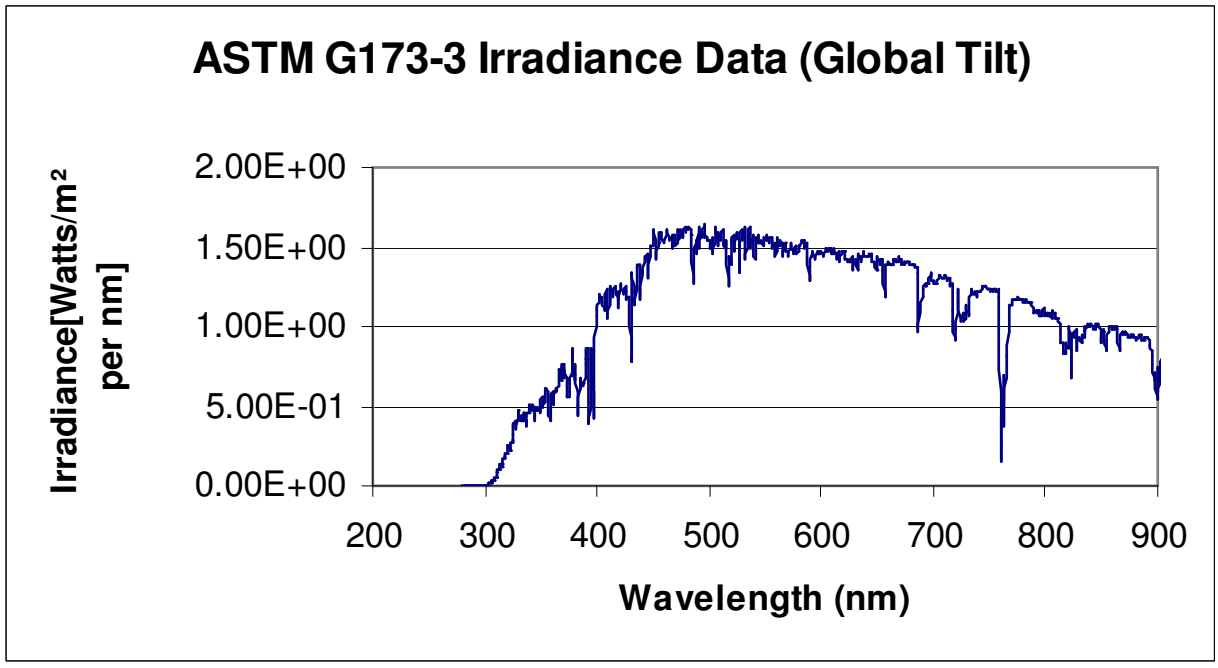

Figure 7.1 ASTM G173-3 Irradiance Data (Global Tilt)

Table 7.1

Selected Reference Solar Spectral Irradiance Data
at Sea Level from ASTM G173-3

Wavelength (nm)	**Global Tilt ($W*m^{-2}nm^{-1)}$**	**Photon Flux Density ($Photons*s^{-1}cm^{-2)}$**
280.0000	4.7309E-23	6.6233E-09
290.0000	6.0168E-09	8.7244E+05
297.5000	1.8608E-04	2.7679E+10
300.0000	1.0205E-03	1.5308E+11
313.0000	1.0733E-01	1.6797E+13
316.0000	1.2348E-01	1.9510E+13
337.0000	3.7380E-01	6.2985E+13
358.0000	4.3006E-01	7.6981E+13
380.0000	7.0077E-01	1.3315E+14
391.0000	8.5138E-01	1.6644E+14
400.0000	1.1141E+00	2.2282E+14
500.0000	1.5451E+00	3.8628E+14
600.0000	1.4753E+00	4.4259E+14
700.0000	1.2823E+00	4.4881E+14
800.0000	1.0725E+00	4.2900E+14

Looking at Table 7.1, the solar photon flux density is around 10^{14} above 380 nm, and starts to drop off under 380 nm, approaching 10^{11} at 300 nm, and then falls rapidly to 10^{-9} at 280 nm. Above 380 nm, the photon flux density remains around 10^{14} photons per cm^2 per nm. Typical values for the mean photon flux density are 10^{14} for sunlight, 10^{10} for twilight, 10^{8} for moonlight, and 10^{12} for indoor light (Saleh and Teich 1991). The difference in sunlight and moonlight is a 10^{-6} factor. Approximate values for moonlight at a given wavelength are obtained by multiplying the sunlight photon flux density values in Table 7.1 by the 10^{-6} factor. Table 7.2 gives the photon flux density for a sunlight and moonlight.

Table 7.2

Photon Flux Density

Wavelength(nm)	Global Tilt w/m^2-nm	Photons/s-cm^2-nm Sunlight	Photons/s-cm^2-nm Moonlight
280.0000	4.7309E-23	6.6233E-09	6.6233E-15
290.0000	6.0168E-09	8.7244E+05	8.7244E-01
297.5000	1.8608E-04	2.7679E+10	2.7679E+04
300.0000	1.0205E-03	1.5308E+11	1.5308E+05
313.0000	1.0733E-01	1.6797E+13	1.6797E+07
316.0000	1.2348E-01	1.9510E+13	1.9510E+07
337.0000	3.7380E-01	6.2985E+13	6.2985E+07
358.0000	4.3006E-01	7.6981E+13	7.6981E+07
380.0000	7.0077E-01	1.3315E+14	1.3315E+08
391.0000	8.5138E-01	1.6644E+14	1.6644E+08
400.0000	1.1141E+00	2.2282E+14	2.2282E+08

For a collection period of 1 minute, using the photon flux values during daylight and moonlight in Table 7.2, a Critical Detection Limit (CDL) and a Minimum Detectable Number of Photons (MDNP) or Minimum Detectable Number Counts (MDNC) can be calculated using Equation 3.6 and Equation 3.13, respectively, for a 95% confidence of a detection. Where the optical background level is large (i.e., values larger than 10^4 counts a minute for purposes of this study), PMT dark counts (i.e., 250 or less) are neglected. For example, referring to Table 7.2, for 280 nm during daylight, and 280 and 290 nm at night, there is such a small natural background that only the PMT dark count (e.g., 36 counts per minute) is used to calculate CDL and MDNP values. Table 7.3 and Table 7.4 show Critical Detection Limits (CDLs) and a Minimum Detectable Number of Photons (MDNP) for certain values between 280 nm and 400 nm during daylight conditions and nighttime conditions, respectively.

Table 7.3

CDL and MDNP for Daylight Operations

Wavelength (nm)	Background Daylight (Photons/ min-cm^{-2})	CDL Sunlight (Photons/ min-cm^{-2})	MDNP Sunlight (Photons/ min-cm^{-2})
280.0000	6.6233E-09 + PMT	1.8933E-04	2.7064E+00
290.0000	8.7244E+05	2.1729E+03	4.3486E+03
297.5000	2.7679E+10	3.8704E+05	7.7409E+05
300.0000	1.5308E+11	9.1019E+05	1.8204E+06
313.0000	1.6797E+13	9.5345E+06	1.9069E+07
316.0000	1.9510E+13	1.0276E+07	2.0551E+07
337.0000	6.2985E+13	1.8463E+07	3.6926E+07
358.0000	7.6981E+13	2.0411E+07	4.0823E+07
380.0000	1.3315E+14	2.6844E+07	5.3688E+07
391.0000	1.6644E+14	3.0013E+07	6.0027E+07
400.0000	2.2282E+14	3.4726E+07	6.9453E+07

Table 7.4

CDLs and MDNPs for Nighttime Operations

Wavelength (nm)	Background Night ((Photons/ min-cm^{-2}) with $PMT_{dark\ count} = 36$	CDL Moonlight (Photons/ min-cm^{-2})	MDNP Moonlight (Photons/min-cm^{-2})
280.0000	6.6233E-15 + PMT	8.46	30.62
290.0000	8.7244E-01 + PMT	8.58	30.96
297.5000	2.7679E+04	3.8704E+02	7.7679E+02
300.0000	1.5308E+05	9.1019E+02	1.8231E+03
313.0000	1.6797E+07	9.5345E+03	1.9072E+04
316.0000	1.9510E+07	1.0276E+04	2.0554E+04
337.0000	6.2985E+07	1.8463E+04	3.6929E+04
358.0000	7.6981E+07	2.0411E+04	4.0825E+04
380.0000	1.3315E+08	2.6844E+04	5.3690E+04
391.0000	1.6644E+08	3.0013E+04	6.0030E+04
400.0000	2.2282E+08	3.4726E+04	6.9455E+04

For a 1 minute collection period, and a 95% certainly (i.e., $k\alpha$ = 1.645), neglecting collection instrument background and any artificial light, the natural background at 300 nm and

400 nm during nighttime hours requires MDNPs of 1.8231E+03 and 6.9455E+04 fluorescence photons/min per cm^2, respectively. During daylight one would have to collect 1,000 times or 3 orders of magnitude more photons at 300 nm and 400 nm than at night. Referring to Table 7.4, at 290 nm, the night time natural background is 0.87 photons per minute and the PMT dark count can no longer be ignored. The PMT dark count is approximately equal to or greater than natural background. The dark count (e.g., 36) of the PMT must be combined with the natural background count. One would only have to collect an MDNP of 30.96 photons/minute on a one cm^2 collector. At 280 nm the background due to artificial light and the instrument background become the only major obstacles that must be overcome. For a collection time of 1 minute, a PMT with a dark count around 36 counts/minute, zero artificial light, and k_α =1.645, for a 95% confidence of a detection

$$MDNP = k_\alpha^2 + 2CDL = 2.71 + 4.653\sigma_B = 30.62 \quad (7.1)$$

The above values are based on a 1 cm^2 collector. A 1 cm^2 collector collects few photons unless the collector is very close to the source. For the extended range detection scenario shown in Figure 7.2, increasing the collection area (i.e., increasing *r* for a circular detector) increases that portion of the photon aura intersecting the collector aperture. Since the distance, *d*, from the source to the detector/collector is much greater than the collector radius, the solid angle (i.e., that portion of photons emitted that are received by the collector), calculated using Equation 3.15, is shown in Equation 7.2.

$$\Omega \cong \frac{Area_{collector\_aperture}}{4\pi d^2} = \frac{\pi r^2}{4\pi d^2} \quad \text{(Tsoulfanidis 1995)} \quad (7.2)$$

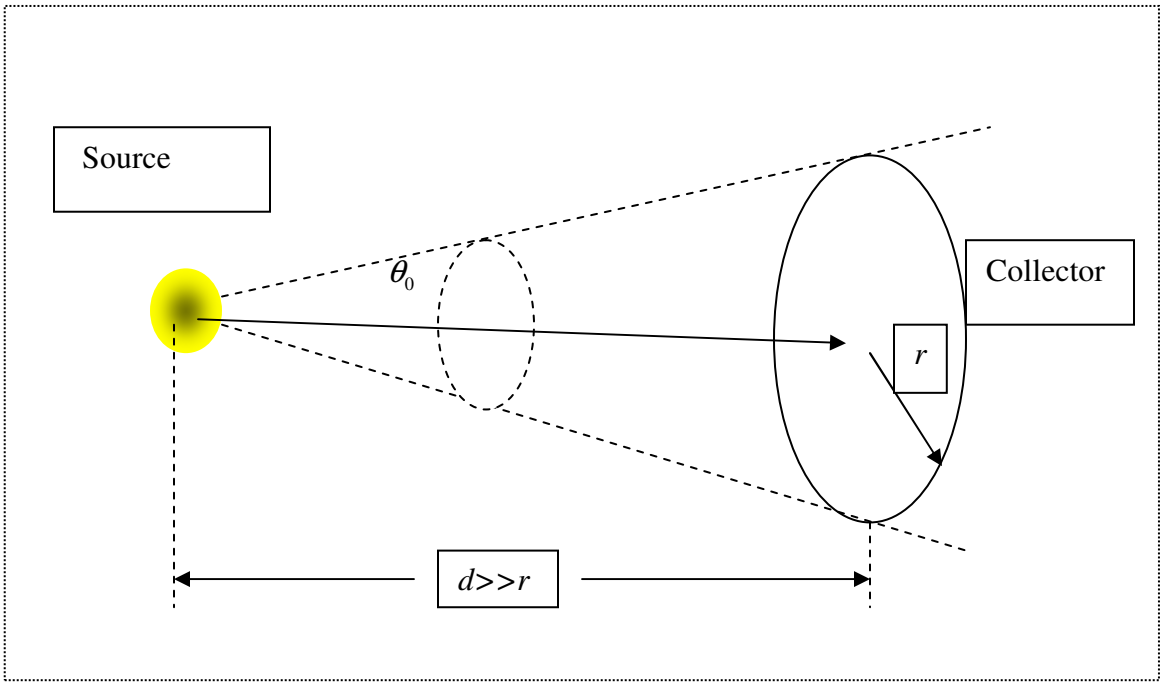

Figure 7.2: Extended Range Detection where $d >> r$

7.2 Nighttime Background Levels of Potential Targets

To effectively show the value of the optical detection of radiation, the optical background must be overcome. There is some minimal detectable number of photons that one must collect above background to determine a detection with some certainty. To determine that minimal number for various outdoor locations, background lighting surveys were taken of banks, drug stores, supermarkets, convenience stores, strip malls, fast food establishments, restaurants, hotels, car dealerships, etc. Surveys are taken in three cities (i.e., Hattiesburg, Mississippi; Tuscaloosa, Alabama; and Houston, Texas) to determine if lighting in the UV varies greatly geographically and to determine if there are similarities among like establishments.

7.2.1 Test Setup for the Nighttime Optical Background

The optical background surveys are performed using a fiber optic mini-spectrometer (i.e., Avantes AvaSpec-ULS2048-USB2). The instrument had a 25 um slit, a CCD detector with 2048 pixel array, and was calibrated for a range of 200 to 1100 nm. Attached to the fiber optic cable was cosine receptor with a 180 degree field of view. To determine the number of watts per square meter of background that would be meaningful to report using the mini-spectrometer, the dark count of the spectrometer is used to determine a lower critical detection limit using Equation 3.6. This limit is based on a 95% probability (i.e., a *k* value of 1.645 from Table 3.1), that the collected number of counts will lie between the mean of the instrument dark count and $1.645\,\sigma_{instrument\_dark\_count}$. Using Equation 3.6, a lower critical detection limit (CDL) is established. This lower critical detection limit (CDL) ensures that the false positive probability (i.e., reporting background was present when there was only instrument noise) was no larger that 5%. Selecting the 95% confidence *k* value from Table 3.1, the average CDL, using Equation 3.6, over the 300 to 400 nm band was 0.01037 microwatts. Using Equation 3.13, and discarding the 2.71 factor due to the high photon background, a minimal detectable number of microwatts is calculated to ensure a false negative rate (i.e., reporting that there is no background light when there is background) no larger than 5%. The average minimal detectable number of microwatts is determined to be 0.0207 microwatts per square centimeter. Readings of 0.0207 microwatts per square centimeter or above, for a particular wavelength, provides evidence of background light at that wavelength with a 95% confidence. Values below 0.0207 microwatts per square centimeter indicate that an accurate quantification of the background light is not achieved.

7.2.2 Background Surveys of Potential Targets

Optical background measurements are collected from establishments in Hattiesburg, Mississippi; Tuscaloosa, Alabama; and Houston, Texas. These measurements indicate that establishments with similar commercial activities have similar outside lighting. The results in spectral lighting patterns vary mainly in intensity with the peaks occurring at the same wavelengths.

Outside lighting levels are presented in Figure 7.3 - Figure 7.43 for a number of commercial establishments and outdoor lights.

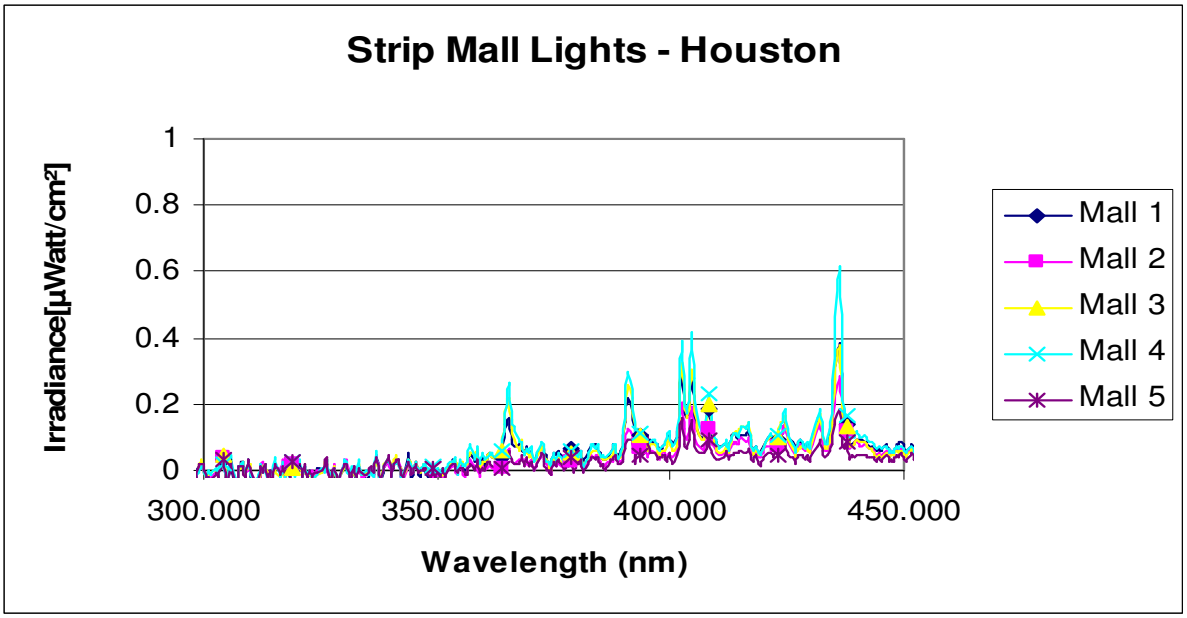

Figure 7.3: Strip Mall Lights - Houston

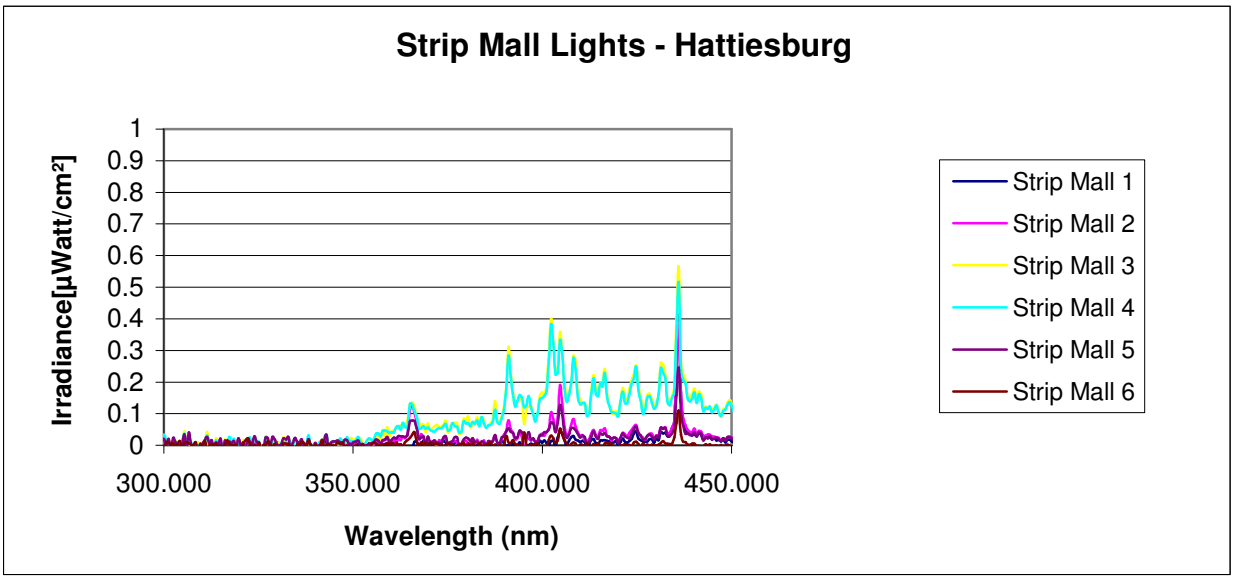

Figure 7.4: Strip Mall Lights - Hattiesburg

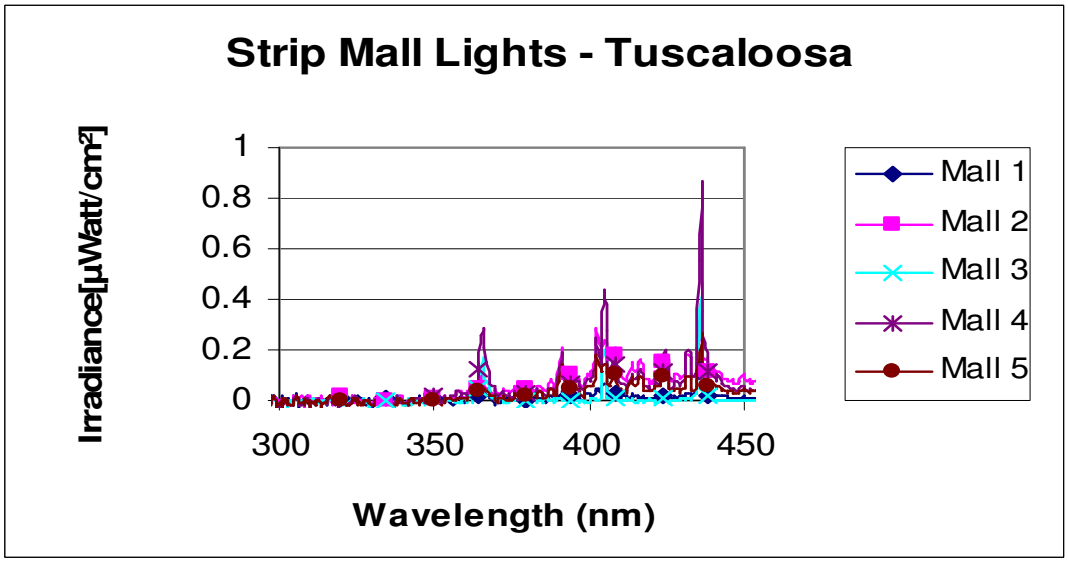

Figure 7.5: Strip Mall Lights - Tuscaloosa

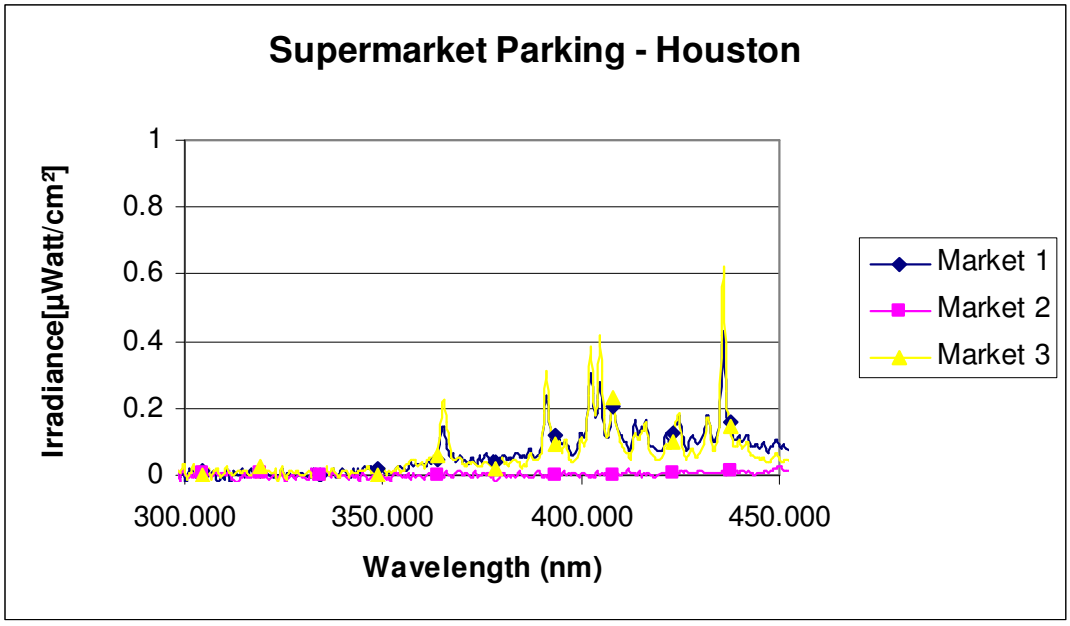

Figure 7.6: Supermarket Parking Lights - Houston

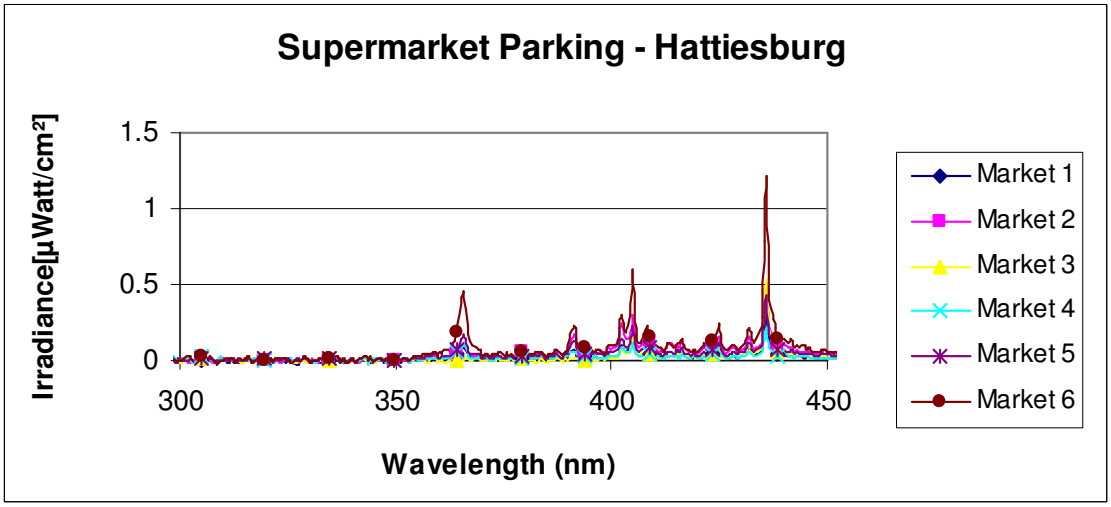

Figure 7.7: Supermarket Parking Lights - Hattiesburg

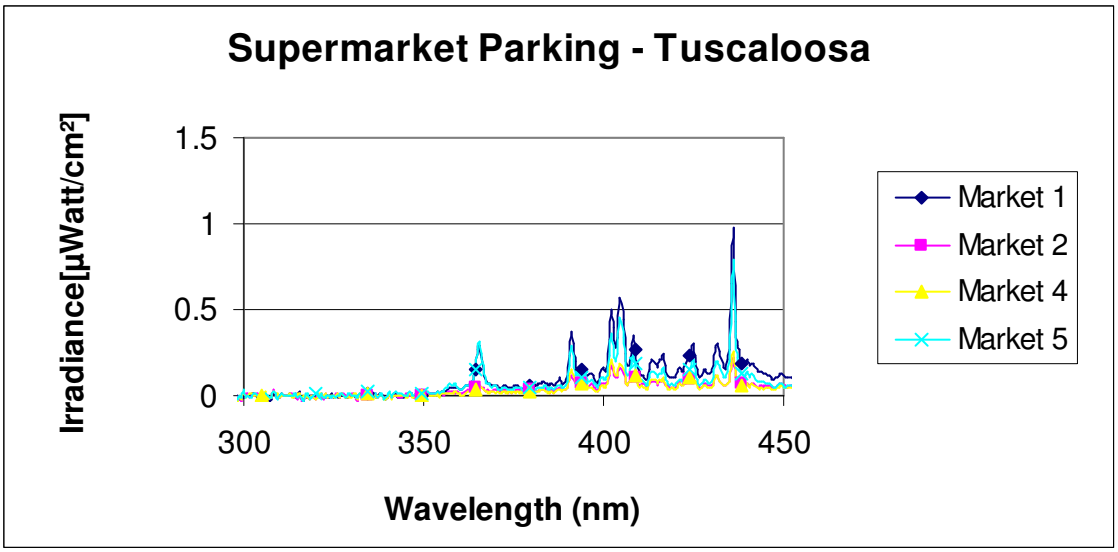

Figure 7.8: Supermarket Parking Lights - Tuscaloosa

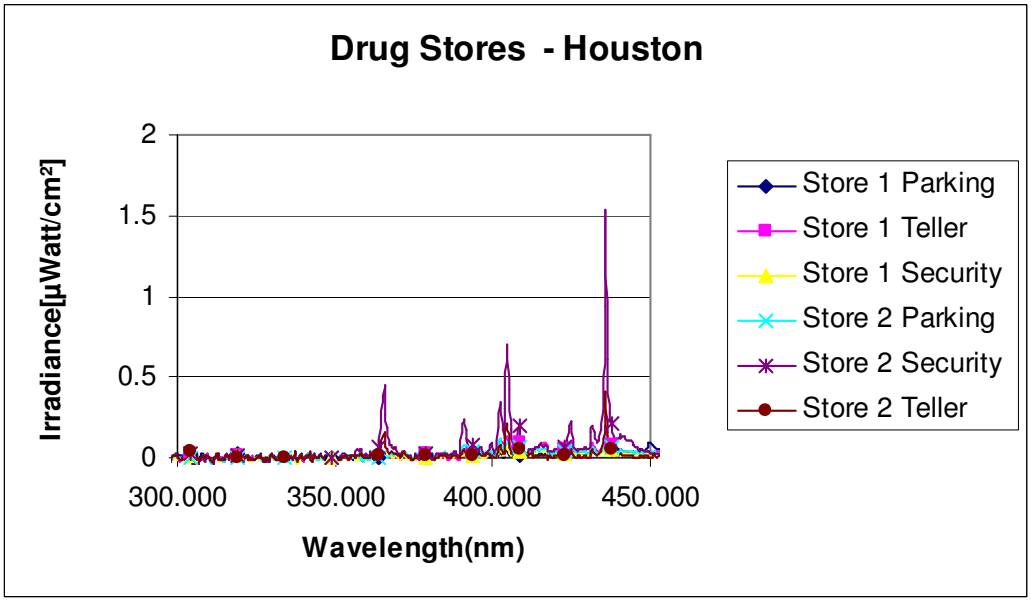

Figure 7.9: Drug Stores - Houston

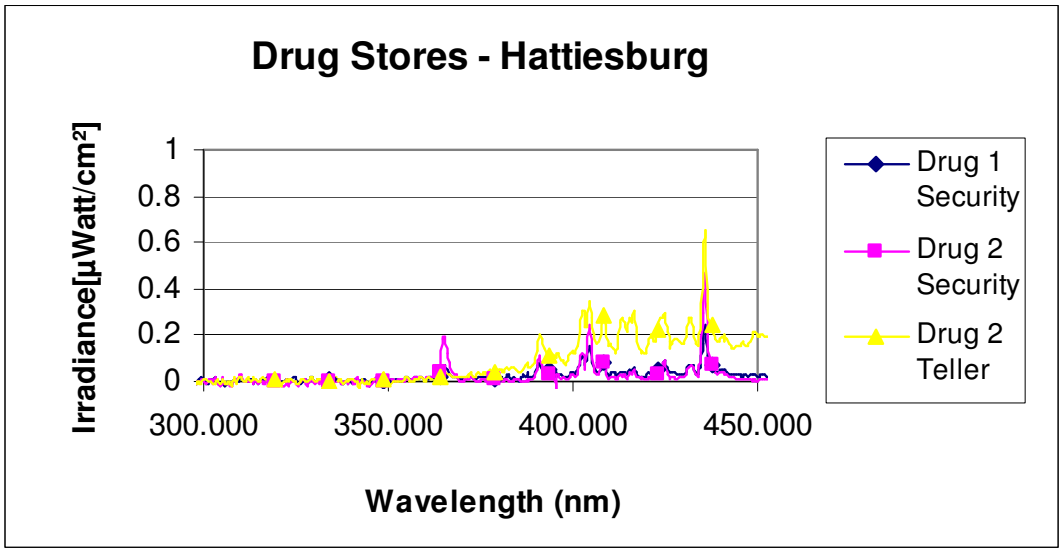

Figure 7.10: Drug Stores - Hattiesburg

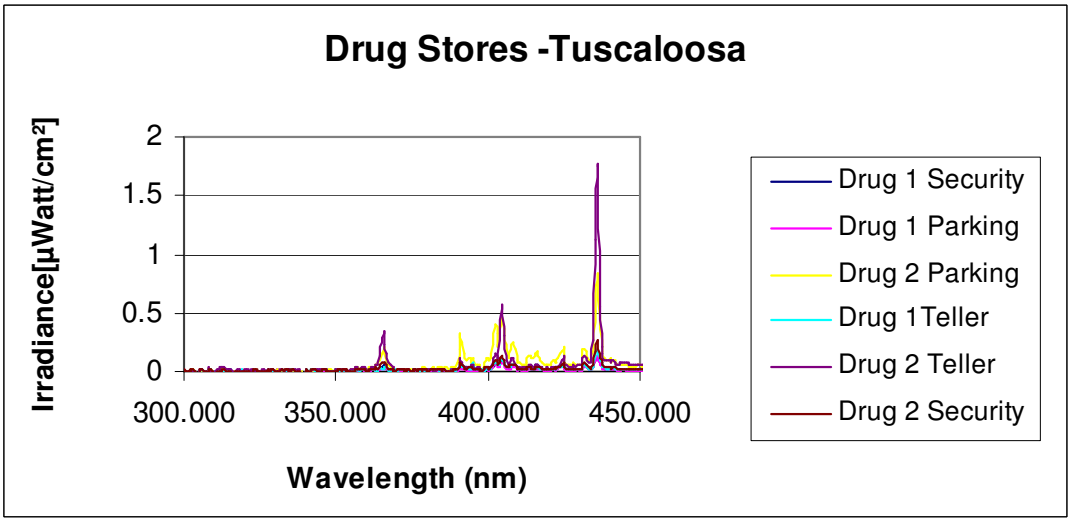

Figure 7.11: Drug Stores - Tuscaloosa

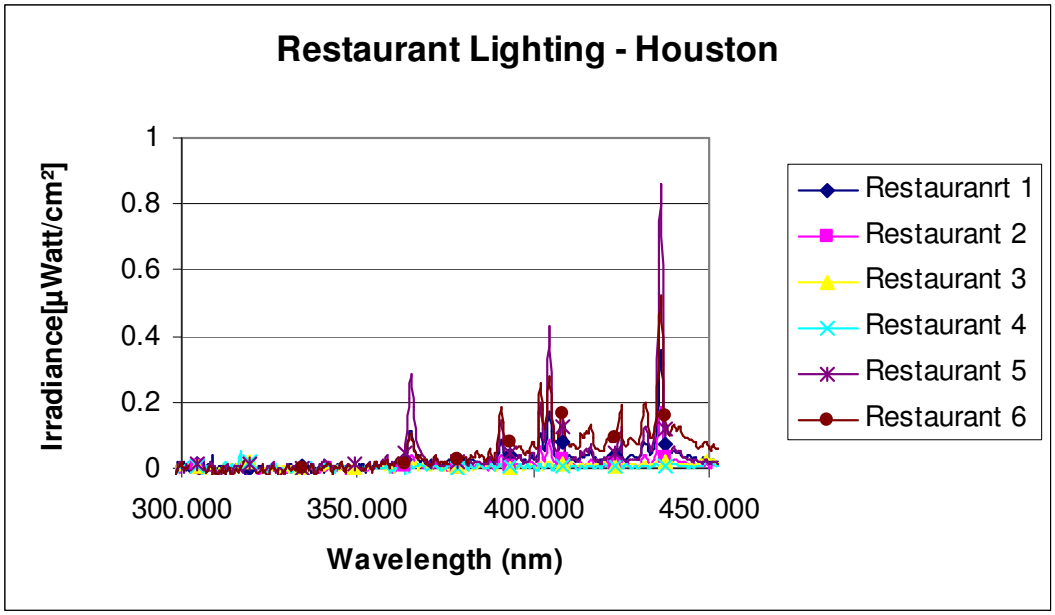

Figure 7.12: Restaurant Lighting - Houston

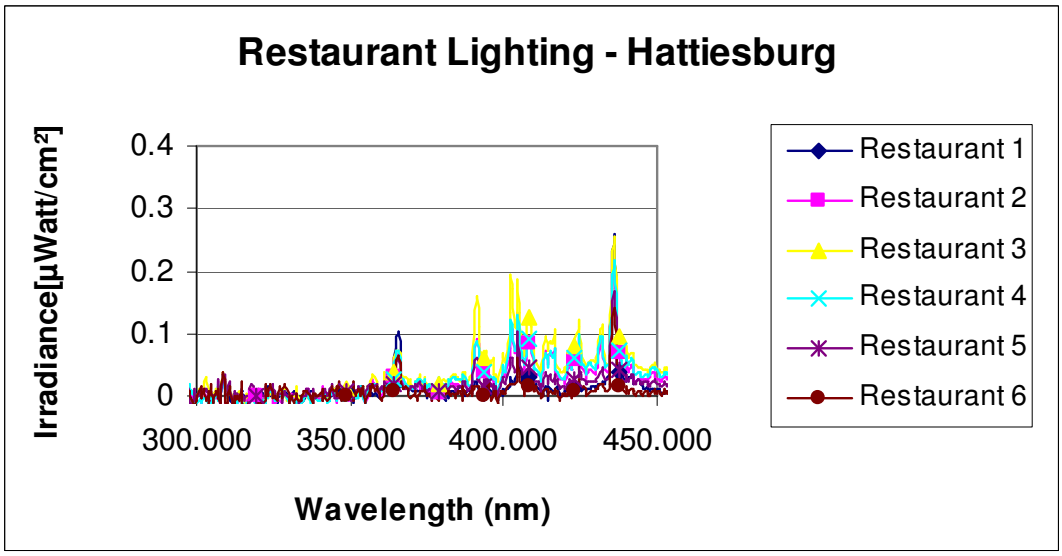

Figure 7.13: Restaurant Lighting - Hattiesburg

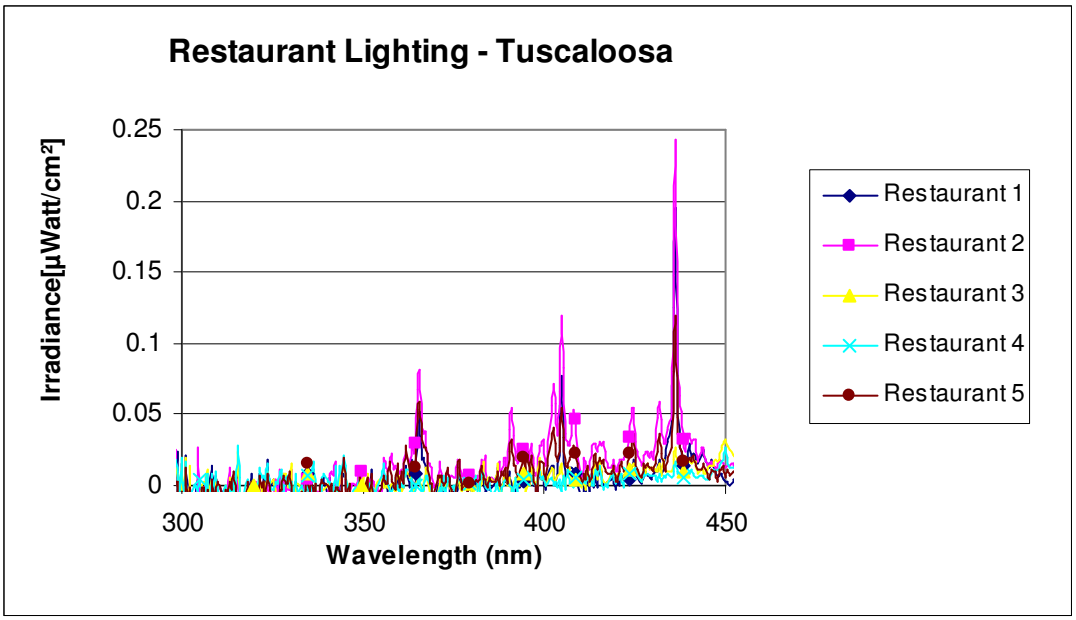

Figure 7.14: Restaurant Lighting - Tuscaloosa

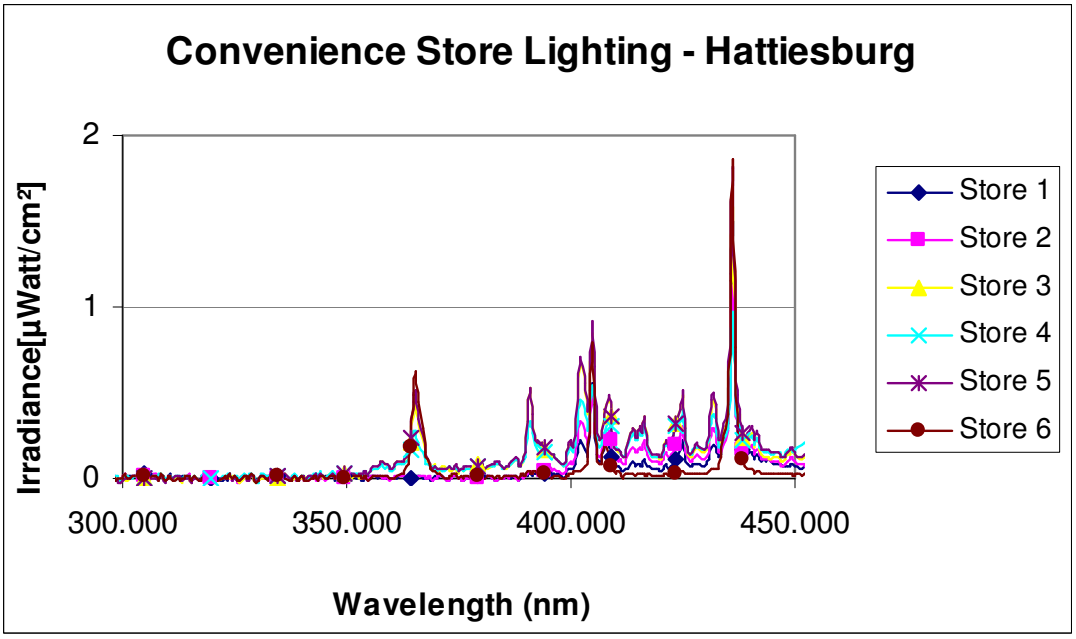

Figure 7.15: Convenience Store Lighting - Hattiesburg

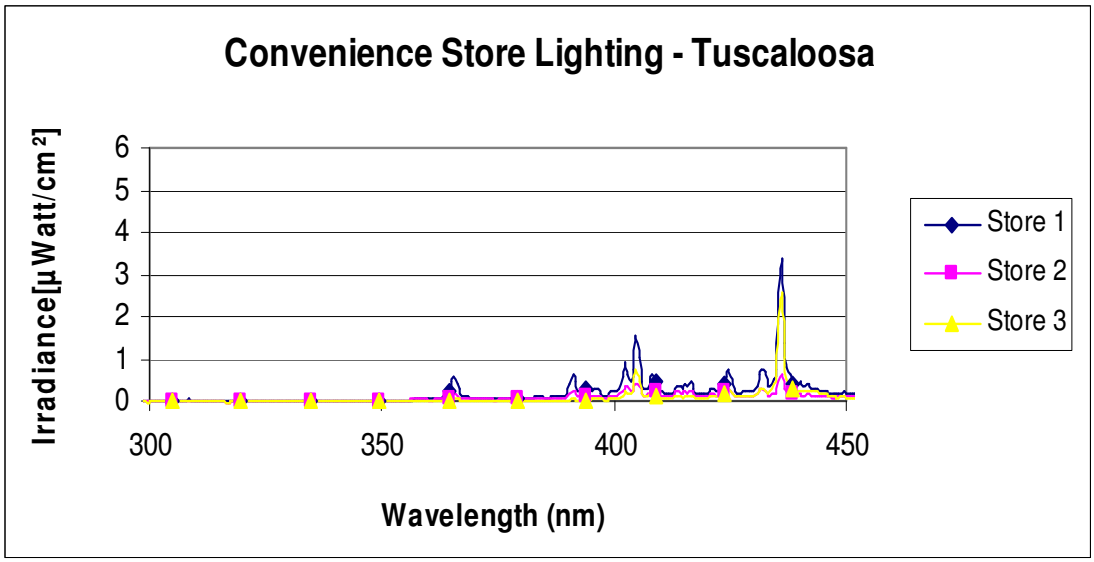

Figure 7.16: Convenience Store Lighting - Tuscaloosa

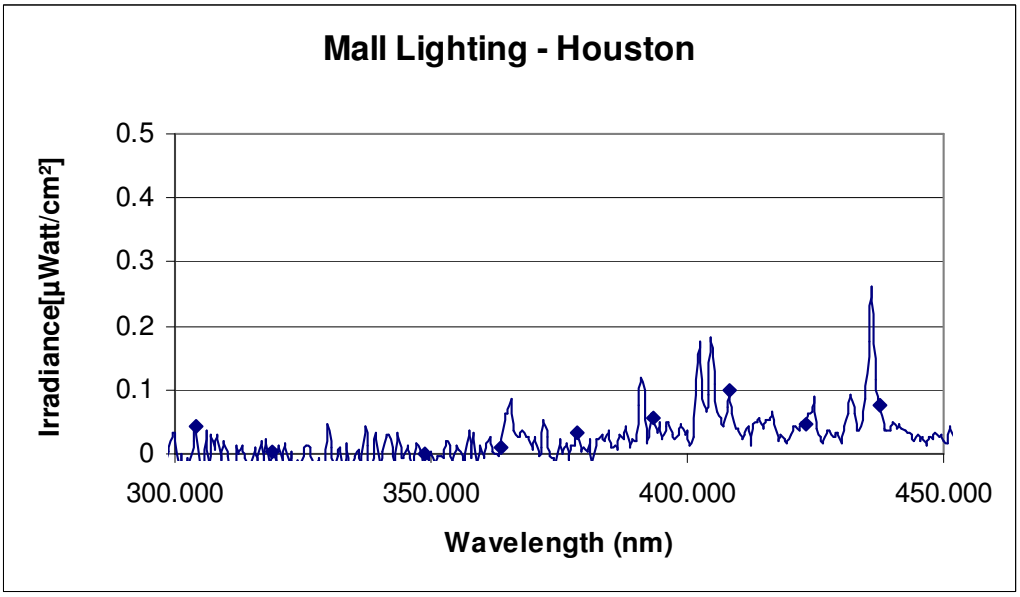

Figure 7.17: Mall Lighting - Houston

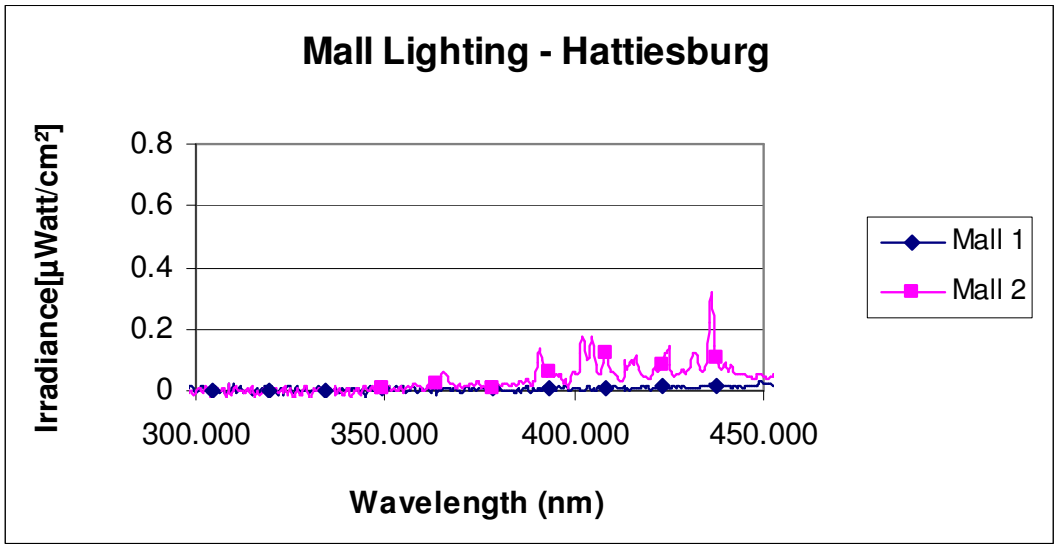

Figure 7.18: Mall Lighting – Hattiesburg

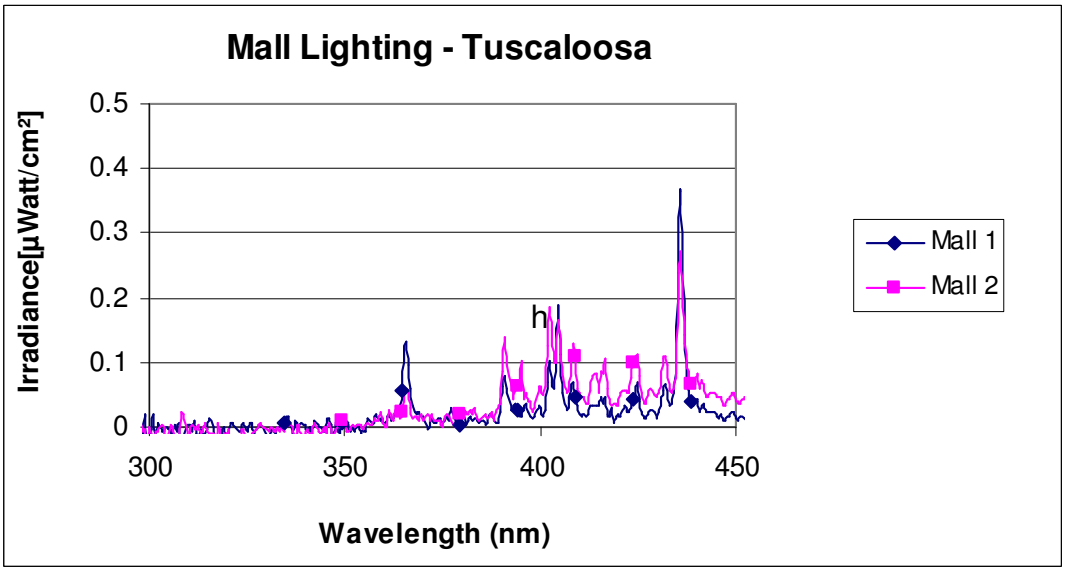

Figure 7.19: Mall lighting - Tuscaloosa

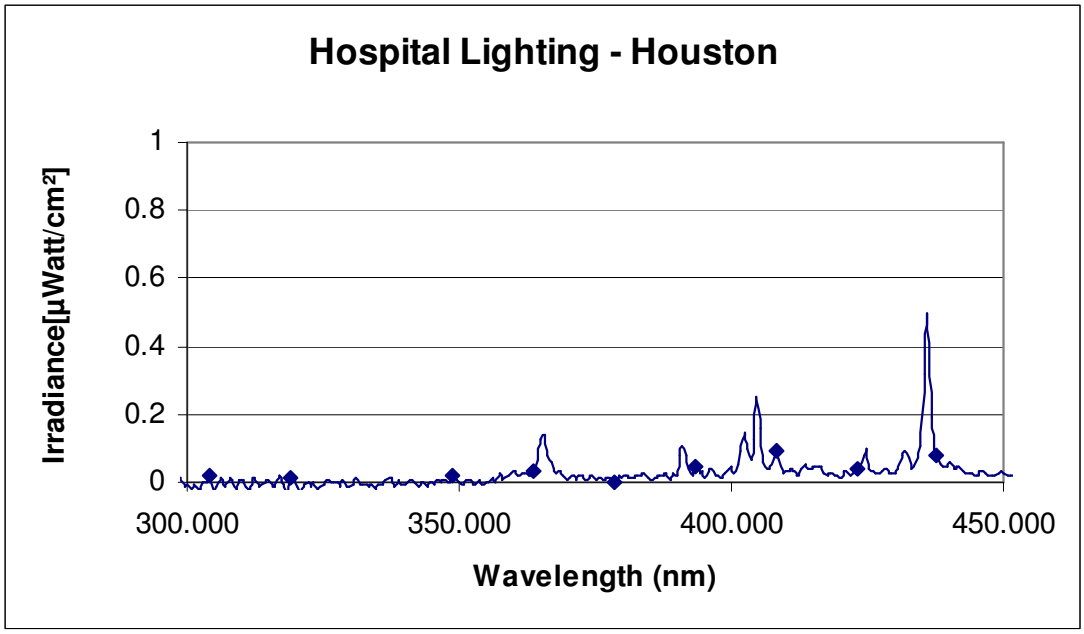

Figure 7.20: Hospital Lighting – Houston

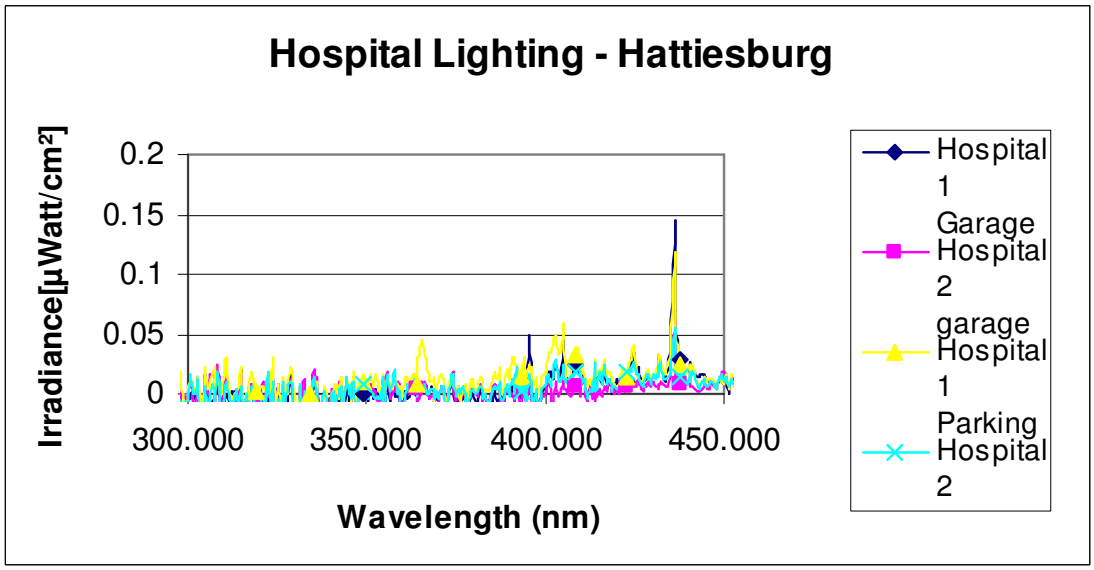

Figure 7.21: Hospital Lighting - Hattiesburg

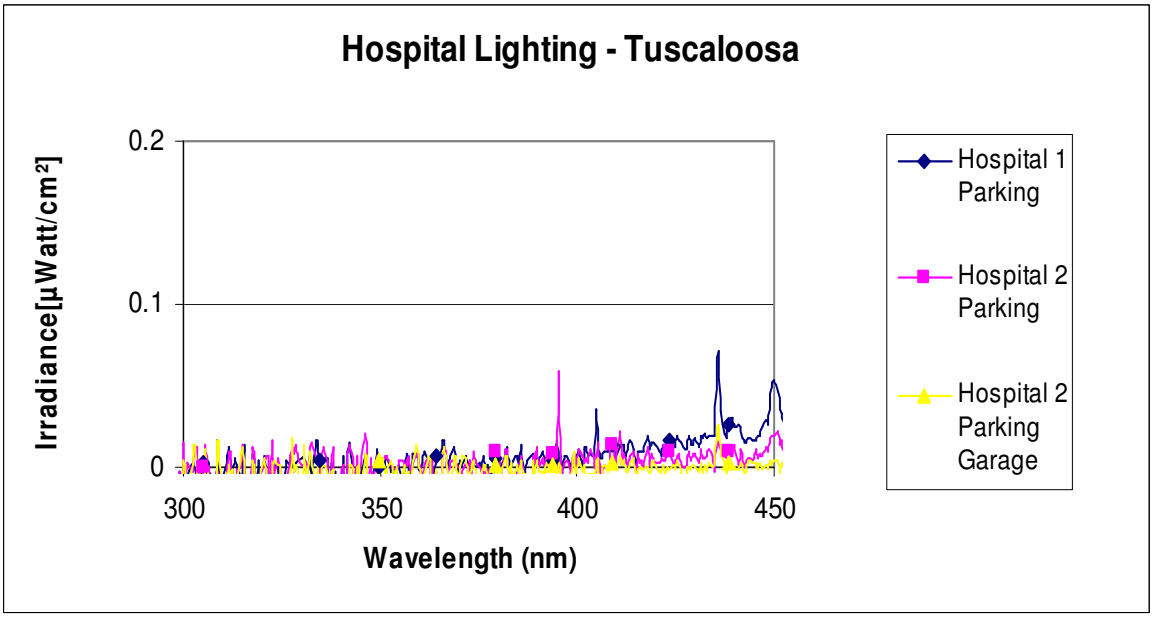

Figure 7.22: Hospital Lighting – Tuscaloosa

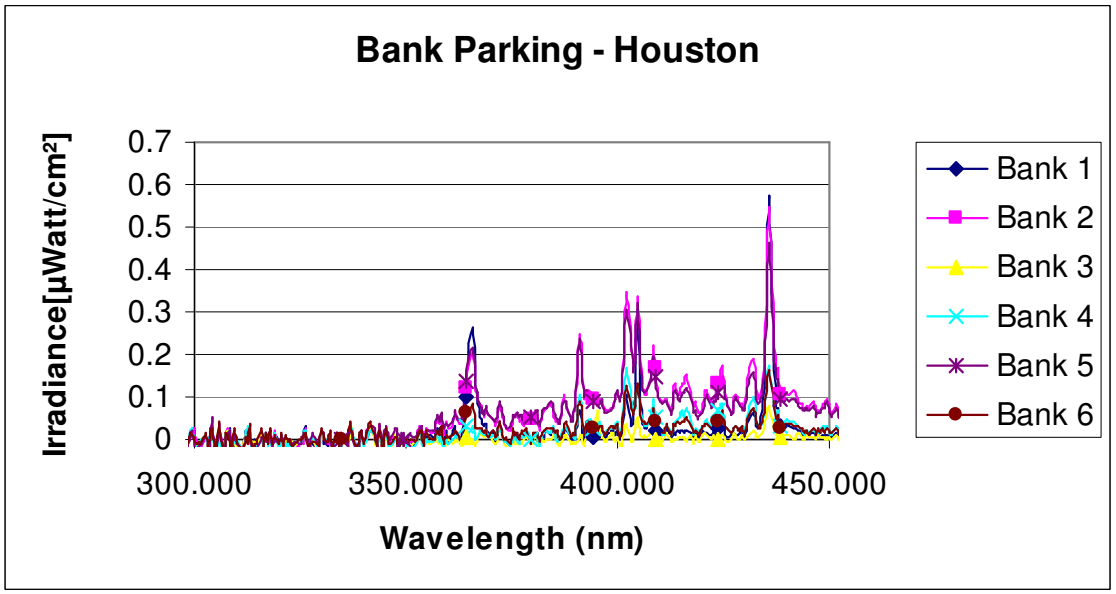

Figure: 7.23: Bank Parking - Houston

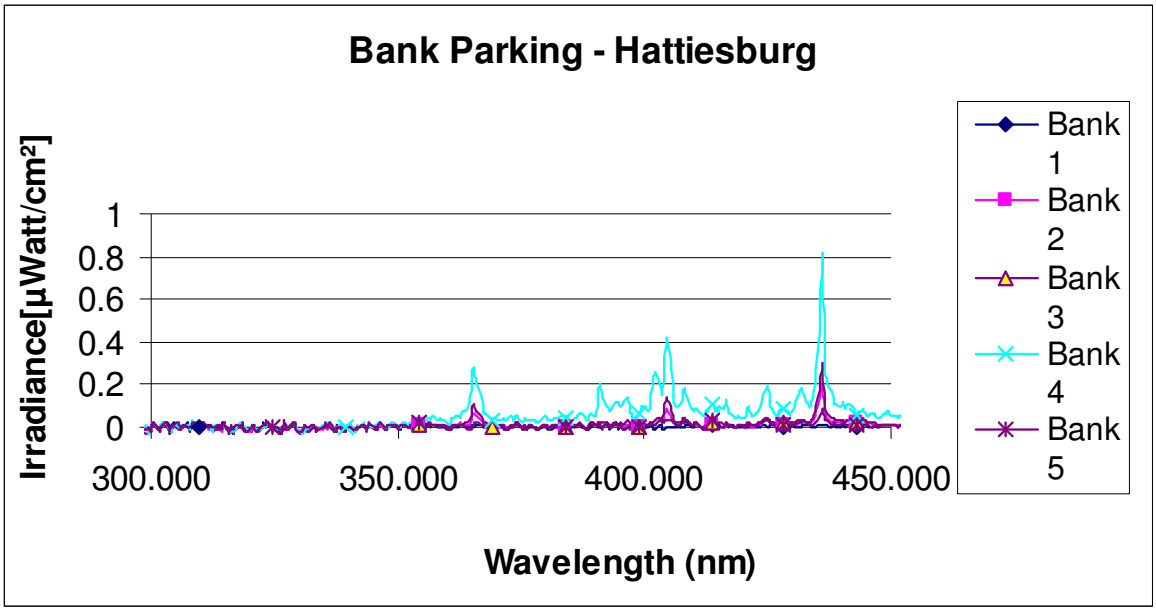

Figure 7.24: Bank Parking - Hattiesburg

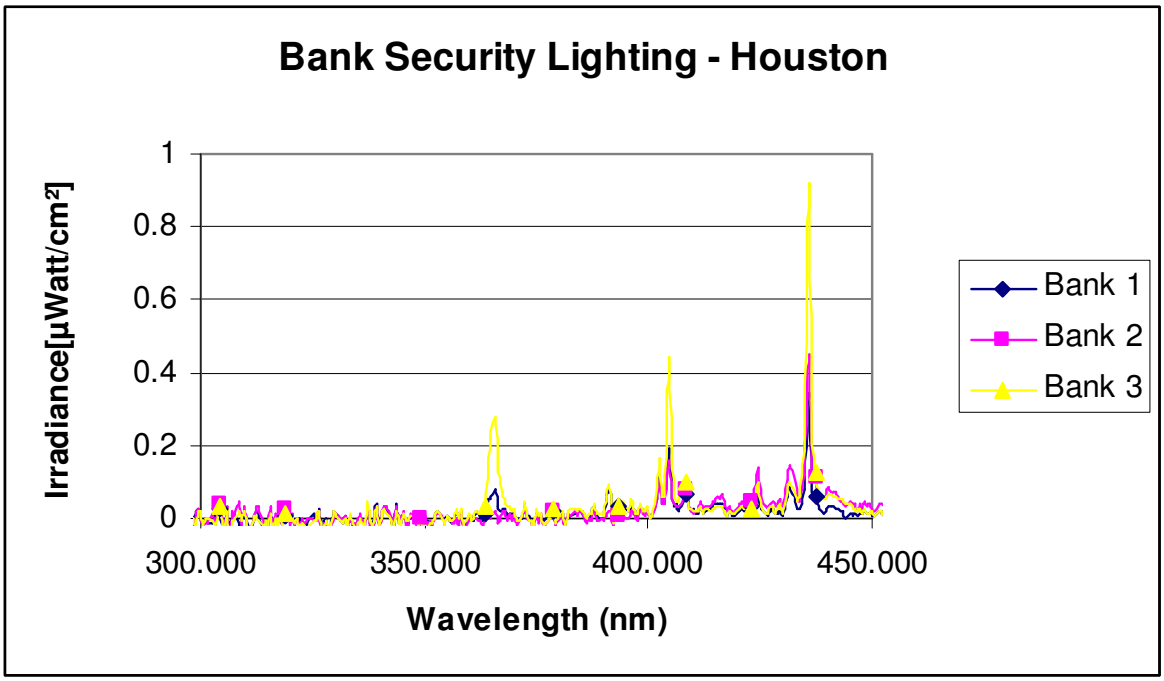

Figure 7.25: Bank Security Lighting - Houston

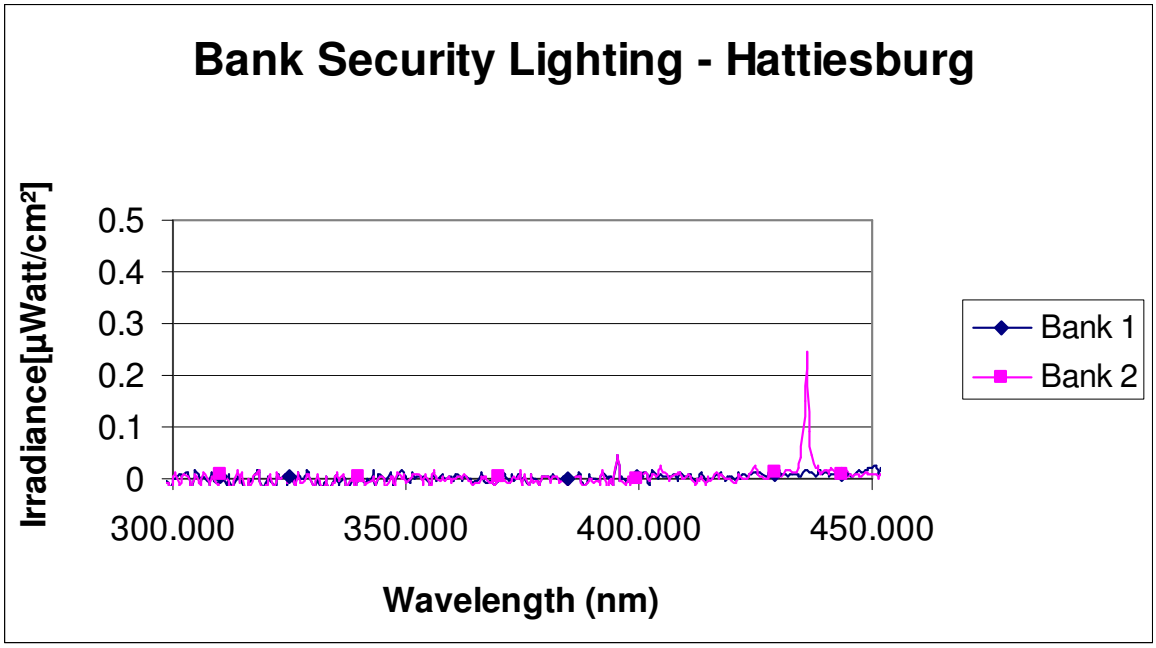

Figure 7.26: Bank Security Lighting - Hattiesburg

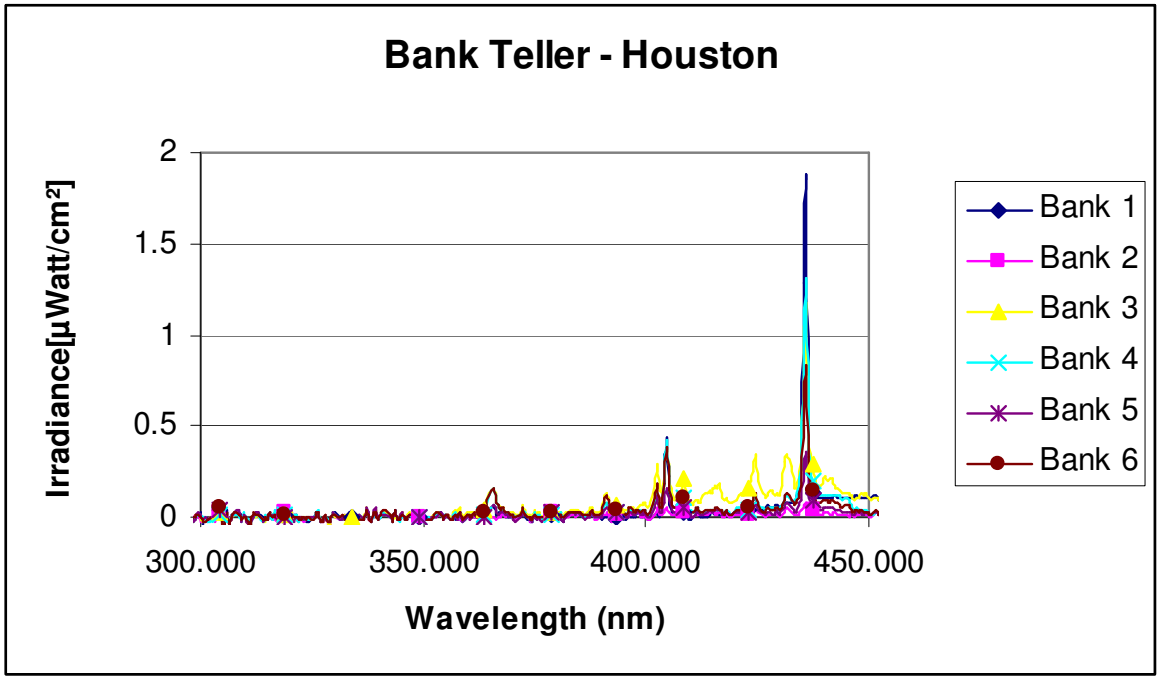

Figure 7.27: Bank Teller - Houston

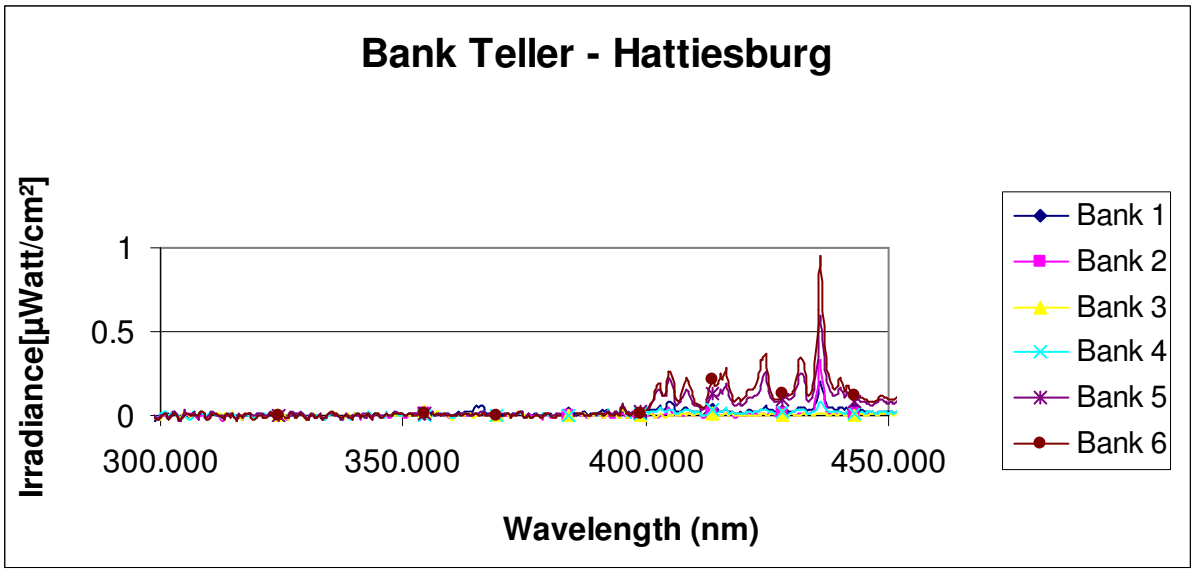

Figure 7.28: Bank Teller - Hattiesburg

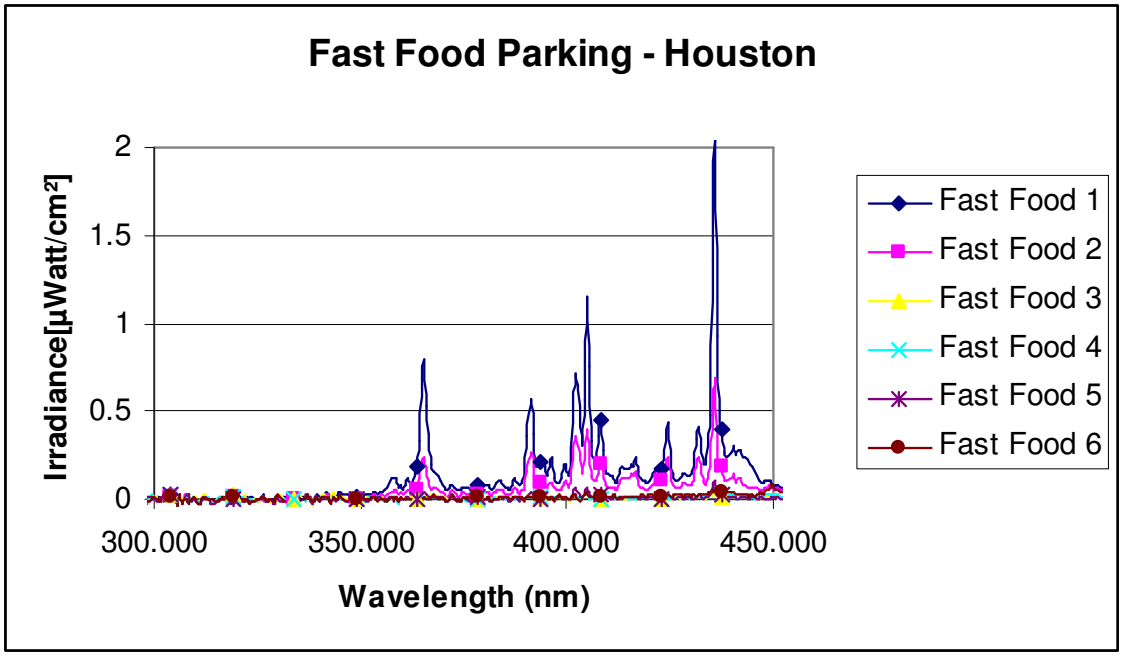

Figure 7.29: Fast Food Parking - Houston

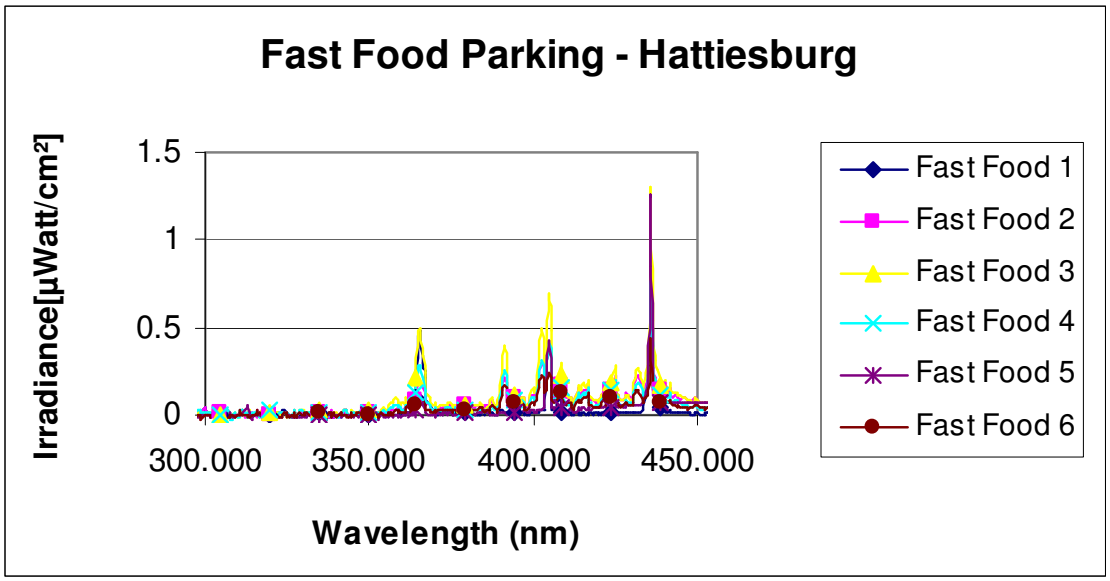

Figure 7:30: Fast Food Parking – Hattiesburg

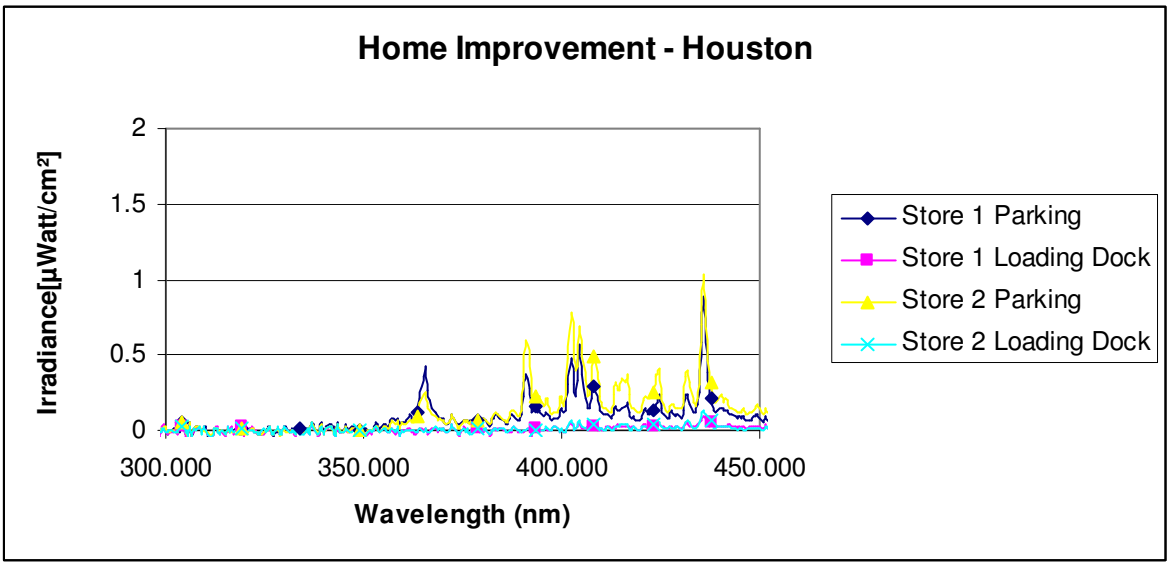

Figure 7.31: Home Improvement Lighting – Houston

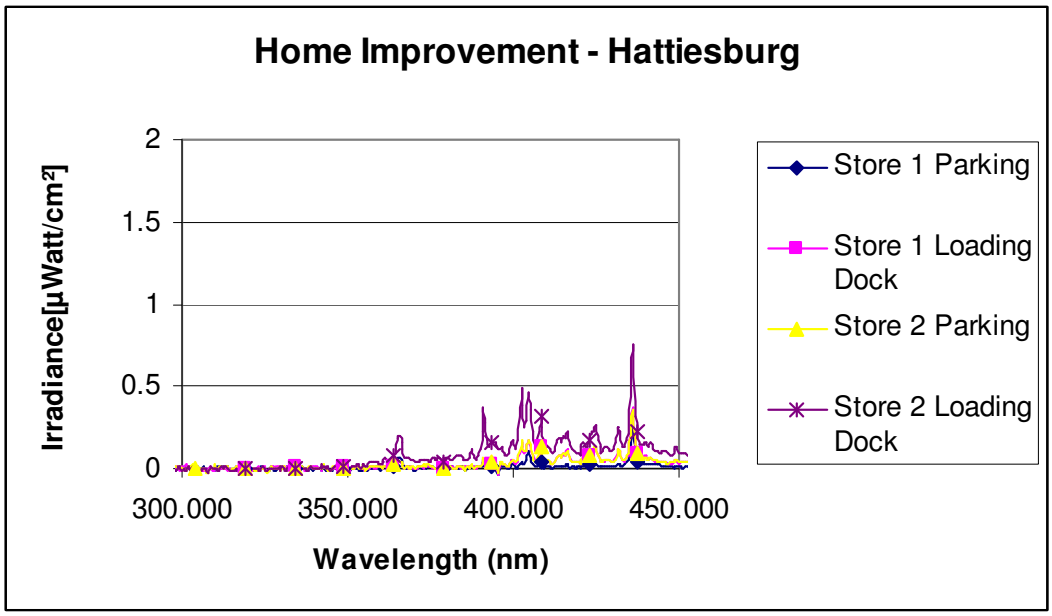

Figure 7.32: Home Improvement Lighting – Hattiesburg

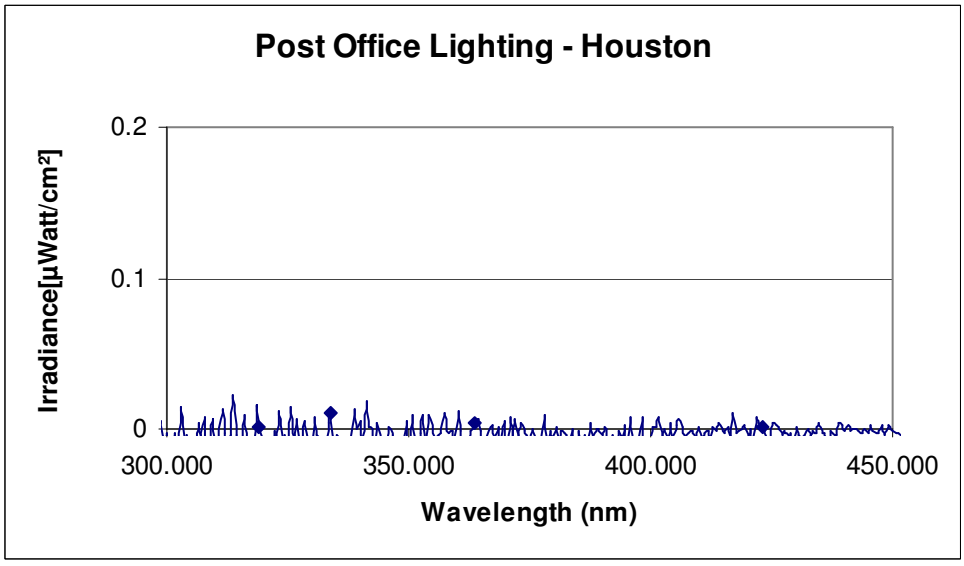

Figure 7.33: Post Office Lighting – Houston

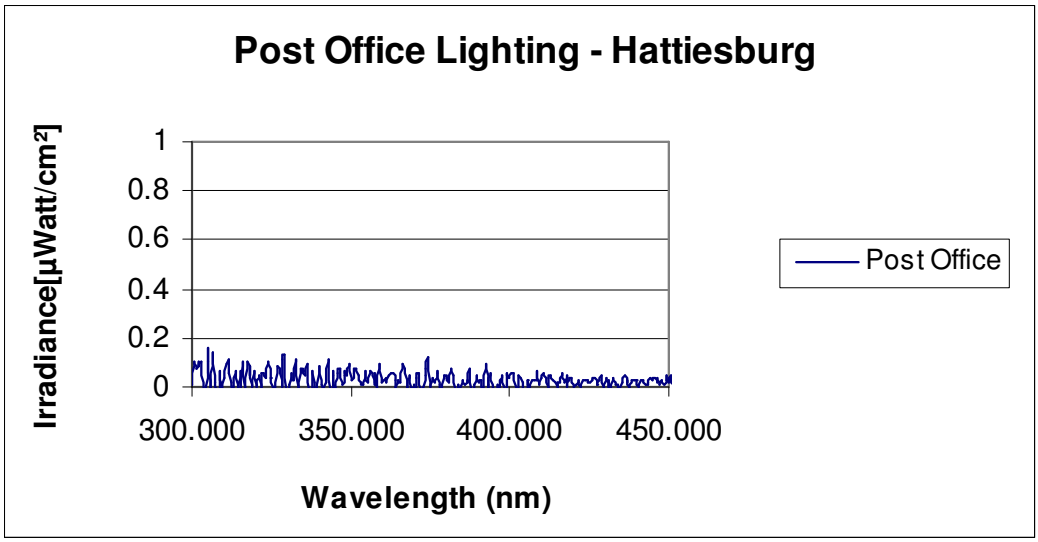

Figure 7.34: Post Office Lighting – Hattiesburg

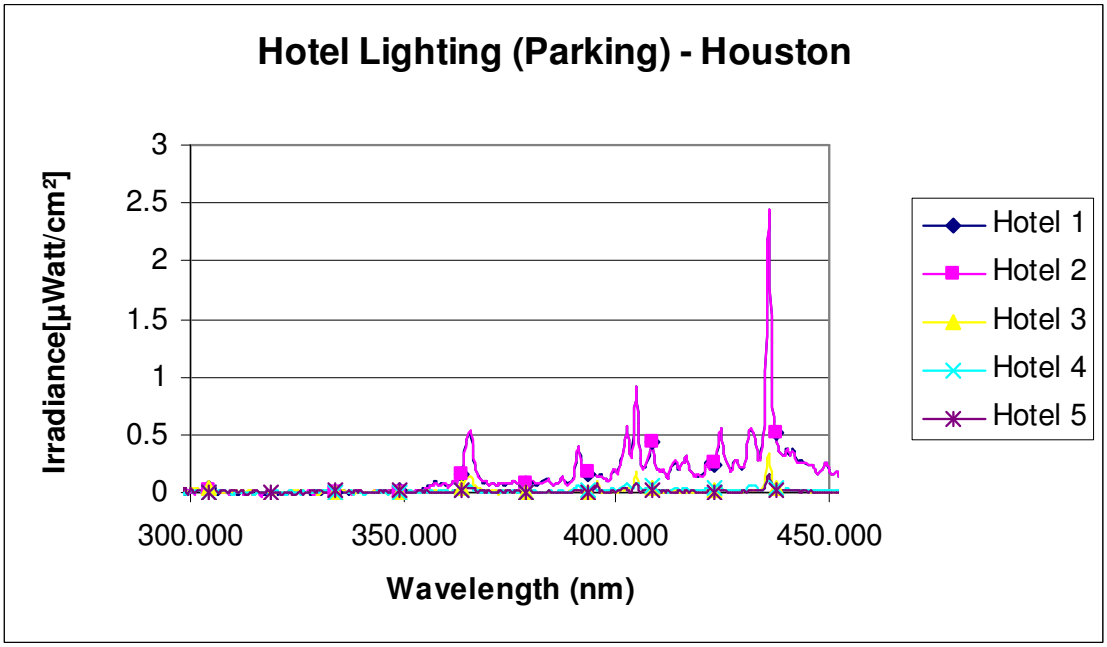

Figure 7.35: Hotel Lighting (Parking) - Hattiesburg

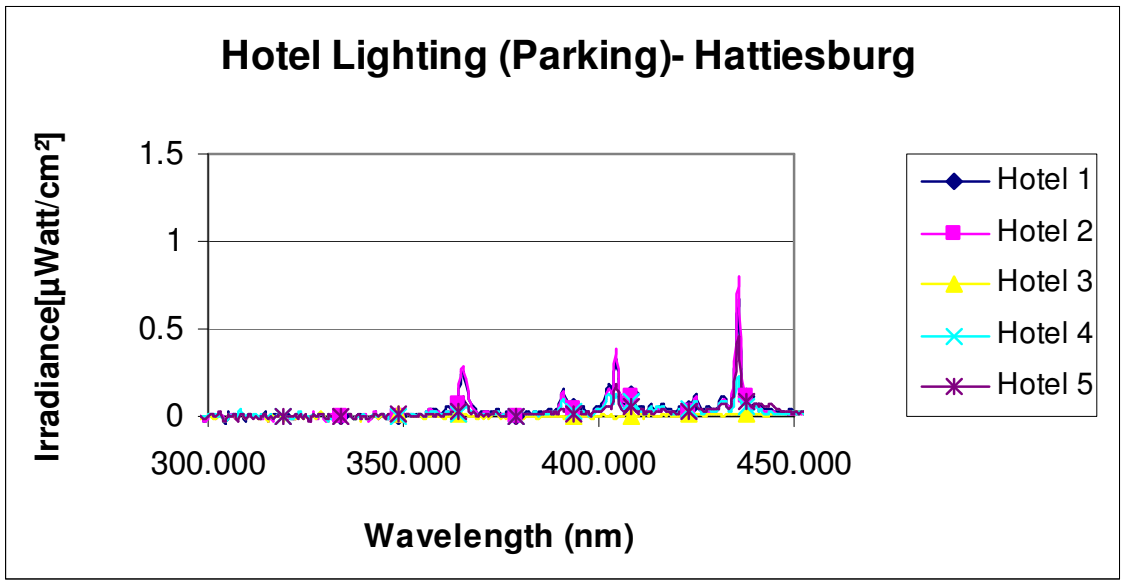

Figure 7.36: Hotel Lighting (Parking)- Hattiesburg

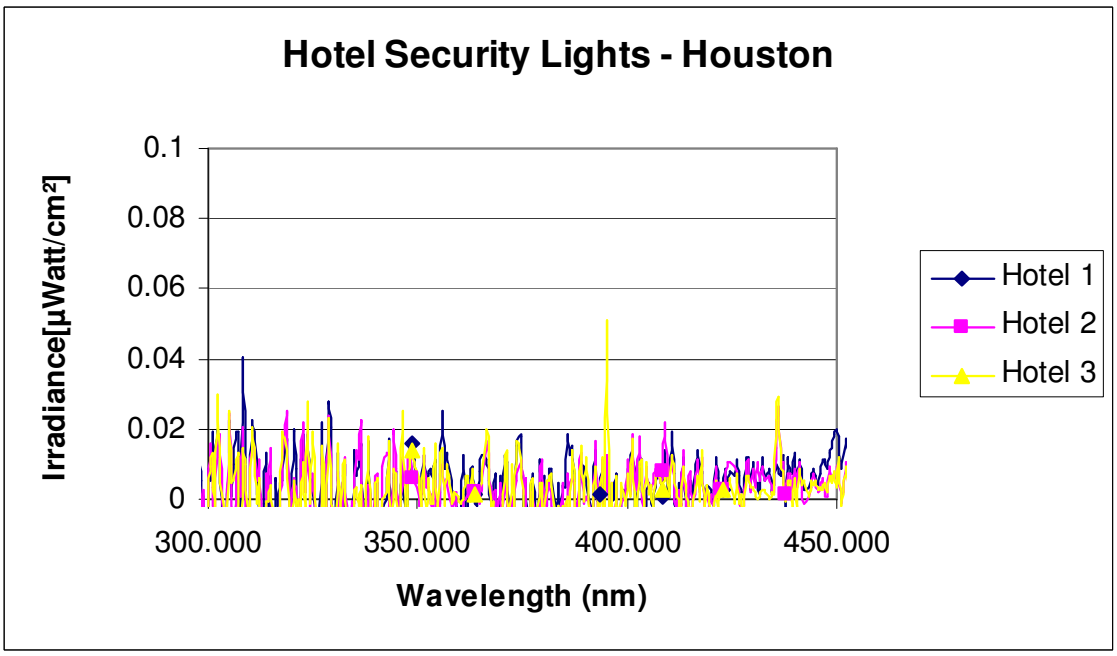

Figure 7.37: Hotel Security Lights - Hattiesburg

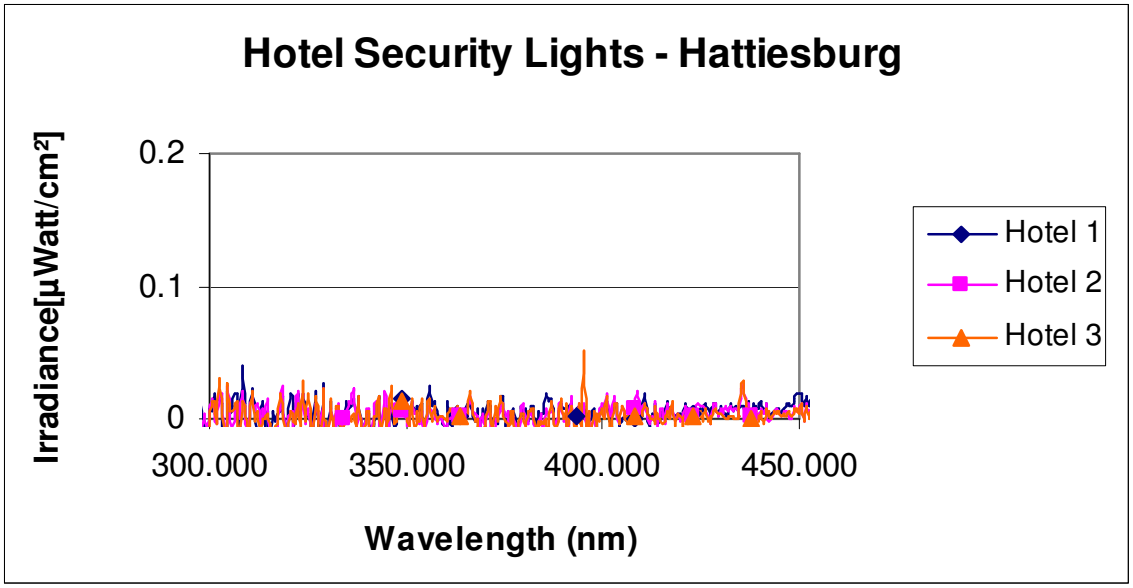

Figure 7.38: Hotel Security Lights - Hattiesburg

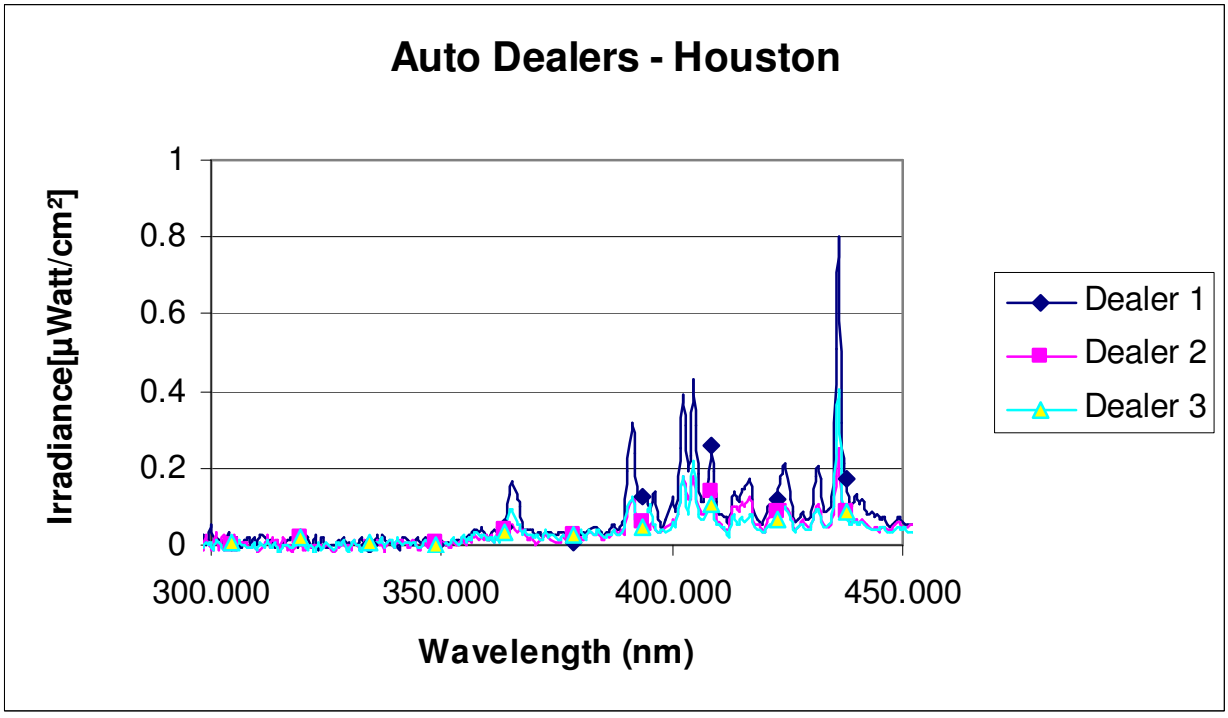

Figure 7.39: Auto Dealer Lighting – Houston

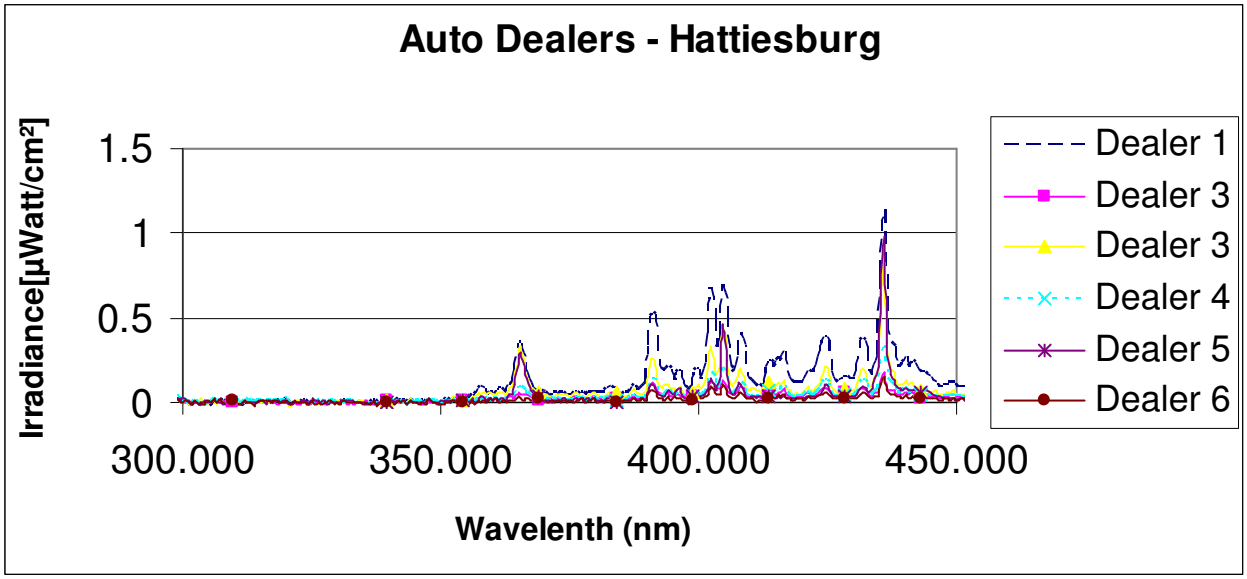

Figure 7.40: Auto Dealer Lighting – Hattiesburg

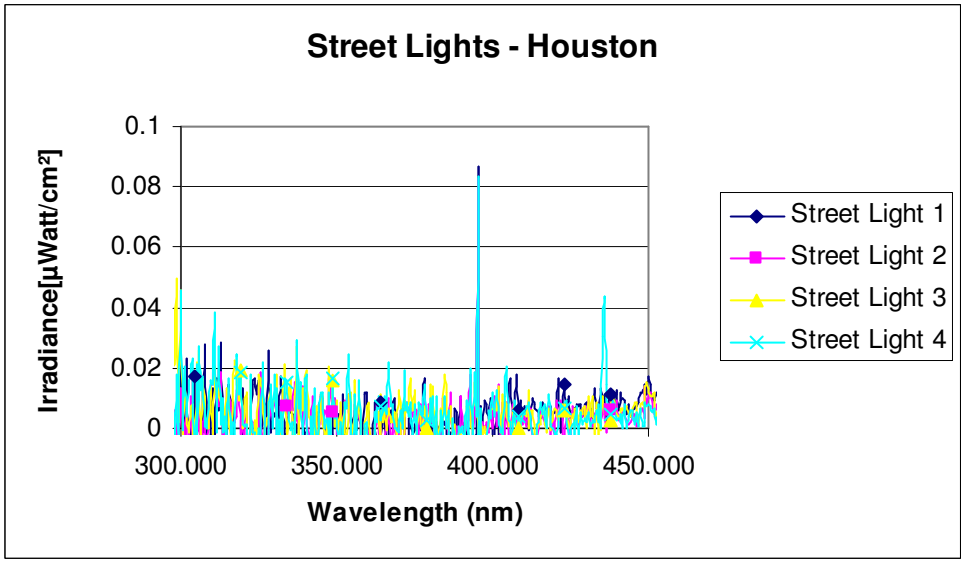

Figure 7.41 Street Lights - Houston

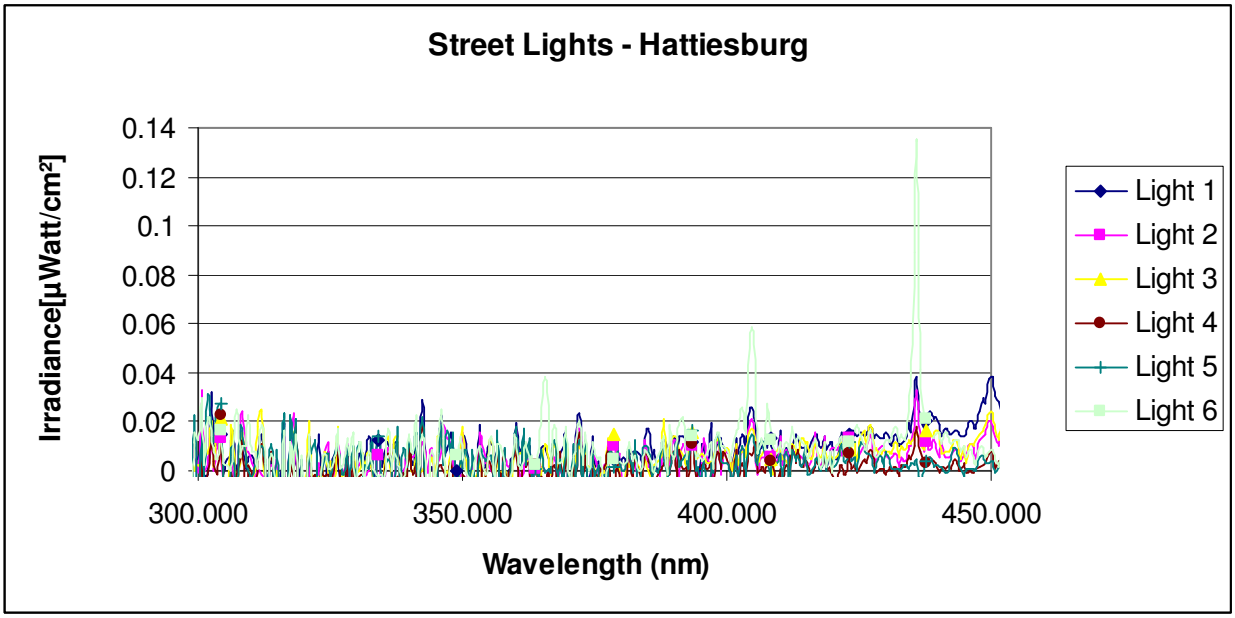

Figure 7.42 Street Lights - Hattiesburg

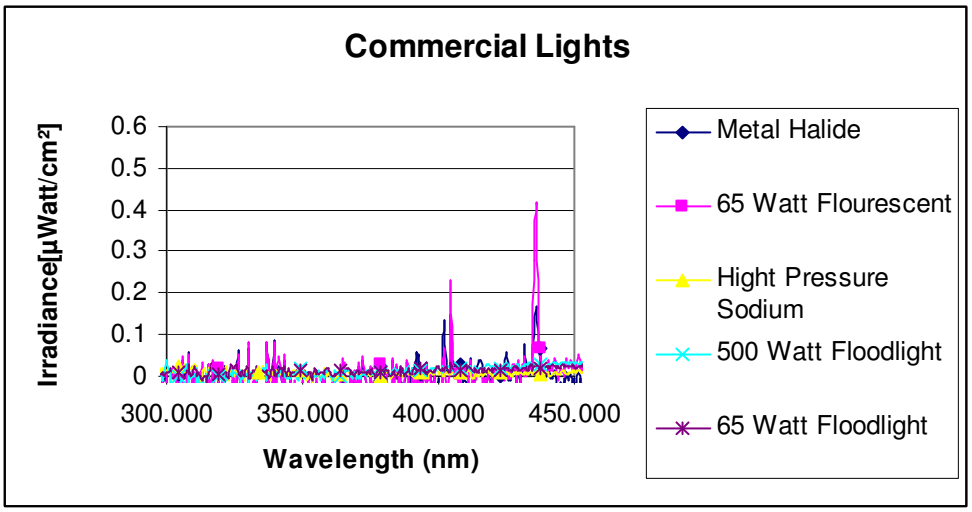

Figure 7.43: Commonly Available Outdoor Lights

7.3 Man-made Clutter Other Than Lighting

Clutter (i.e., UV background), coming from electrical discharges, arcing, corona on utility lines, fires, welding, and insecticide lamps, etc., is often in-band and cannot be filtered with conventional filters. However, where there are certain temporal patterns, which do not last

the entire collection period, the possibility exists to apply filtering techniques. By measuring the time of arrival of photons at the PMT, that portion of the data set where there is a short time intervals between arrivals, lends itself to filtering. The time period, and associated counts in which the temporal pattern occurred, can be filtered from the total collection time interval, leaving the constant count rate from the radiation source relatively unchanged. Figure 7.44 shows the clutter from a stun gun arc, a lighter, and a propane flame. The noise is apparent from 300 nm to 400nm and above.

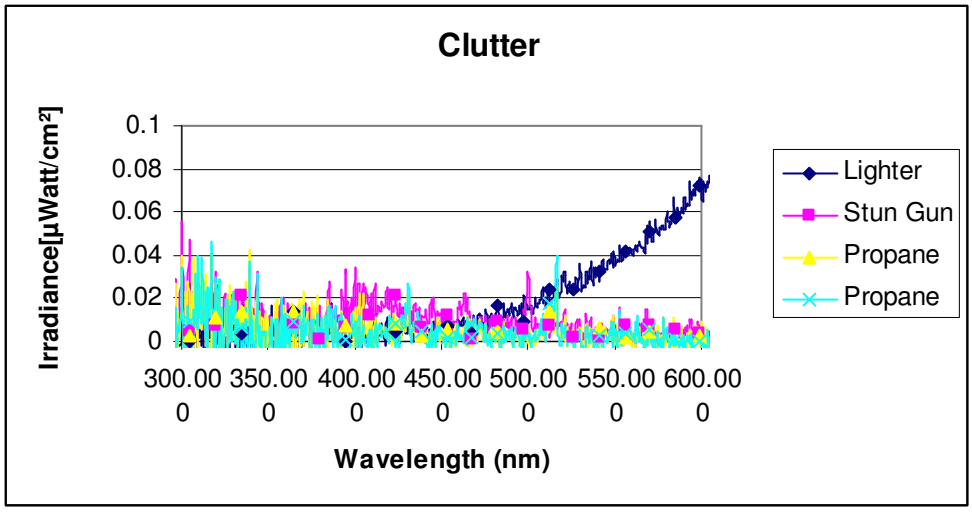

Figure 7.44: Clutter from a Stun Gun Arc, a Lighter, and a Propane Flame

7.4 Conclusion

The outside background surveys of commercial establishments indicate that man-made background lighting above 350 nm prohibits the use of optical detection techniques during evening hours in such locations unless the lighting can be turned off. Additionally, the natural background levels from 300 to 400 nm during daylight and nighttime hours, shown in Tables 7.3 and 7.4, respectively, require such a large minimum detectable number of photons from the radioactive target, that small (i.e., millicuries) radioactive source targets, outside, at extended

ranges are undetectable under many conditions using optical methods. Clutter, where it exists, can spread across the 300 to 400 nm region, making optical detections difficult. The spectral output, shown in Figure 7.44, for a stun gun arc, a lighter and a propane burner, indicate these sources can provide additional UV background noise.

Like establishments in the same city have similar lighting. This is indicated by the lighting at Auto Dealers (Figure 7.40), Fast Food Establishments (Figure 7.30), Hotels (Figure 7.35), Strip Malls (7.4), Supermarkets (Figure 7.7), Banks (Figures 7.24) and Restaurants (Figures 7.13) in Hattiesburg, Mississippi. Additionally, like establishments, in different geographic locations, generally, have similar lighting. This is indicated by the lighting at Strip Malls (Figures 7.3, 7.4 and 7.5), Supermarkets (Figures 7.6, 7.7 and 7.8), Drug Stores (7.9, 7.10, and 7.11) and Restaurants (Figures 7.12, 7.13, and 7.14) in Houston, Texas; Hattiesburg, Mississippi; and Tuscaloosa, Alabama.

CHAPTER 8

CONCLUSIONS AND OPPORTUNITY FOR FUTURE WORK

8.1 Conclusions

The problem statement in Chapter 1 sought the answer to two questions: (1) Can the air fluorescence signal of a radioactive source in the UV from 300 to 400 nm be distinguished from other background UV, suggesting the possibility of a decision support matrix to distinguish radioactive sources from other UV sources for particular background scenarios (e.g., background conditions that include a radioactive source in the presence of common materials and UV from solar and commercial lighting)? (2) Can material scintillation in the UV due to the presence of radioactive sources be used to enhance the detection of the radioactive material?

The answer to the first question is that it is "possible" that the UV air fluorescence from radioactive sources can be distinguished from the background UV in outside detection scenarios. Outside in-band background levels are often too high to permit sensitive detections with a 95% degree of confidence between 300 and 400 nm. However, in certain situations, such as low moonlight, overcast skies, or shaded environments, some useful detections may be possible, especially in areas where radiation is known to exist, and the area can be overlaid with a scintillator. Inside, where the UV background light can be controlled, the optical detection of UV air fluorescence from radioactive sources is promising.

As for the second question, some common materials (e.g., polypropylene, high density polyethylene, and low density polyethylene) can be used to enhance the detectability of

radioactive sources. Laboratory measurements indicate gains as high as 2.5×10^2 can be achieved, in certain bands, with a ^{90}Sr source in close proximity to the scintillating material. This could be useful in nuclear facilities where pipe fittings, walls, etc., can be constructed or overlaid with a scintillator to increase the chances of detection. However, when the tests materials are exposed to ^{241}Am, none of the tested material provided much scintillation value in the 10 nm bands centered on 313, 337, 355, 380 , and 390 nm.

The ability of materials to transmit light is of particular significance in detection scenarios requiring observation of the air fluorescence through a window or package cover. Of special interest is the "Hefty" plastic bag, also called the TSA plastic bag for purposes of this research. The bag is able to transmit over 50 % of the light from 300 to 400 nm and has scintillation/air fluorescence ratios of over 2 at 313, 337, 355, and 380 nm, and a value of 3.81 at 390 nm. This indicates the material has value in the detections of ^{90}Sr radioactive materials at security checkpoints, especially where a person's belongings are placed in such plastic bags prior to screening. Extruded acrylic and polycarbonate are commonly used as windows or covers for various boxes and packages. The extruded acrylic tested is a poor scintillator at 313, 337 and 355 nm, but shows value at 380 and 390 nm having scintillation/air fluorescence ratios above 50. However, unless the extruded acrylic (Plexiglas) is manufactured to pass UV light (i.e., UV-T), it is a poor transmitter of UV light. The polycarbonate tested is a poor scintillator and transmitter of UV light.

The best wavelength is sought to determine the activity of a source (i.e., an alpha source for this study) that would be required to achieve the MDNP at the collector. Based on the fluorescence efficiency curve in Figure 1.1, the outdoor background surveys in Chapter 7, and ASTM G173-03, a wavelength of 316 nm is selected as the wavelength that provides the best

fluorescence efficiency while minimizing the optical in-band UV background. To determine the activities of alpha sources that are required to overcome various optical backgrounds and achieve detections with 95% confidence, theoretical alpha activities are calculated for the background levels at 316 nm in Tables 7.3 and Tables 7.4. The theoretical values are based on an instrument that has a circular collector, with a 0.25 meter radius (r). The distance (*d*) from the collector to the source is 20 meters. Since d >>r, a solid angle is approximated by Equation 7.3.

In the 316 nm peak region, there are approximately 5.5 photons created per particle (Bunner 1964). Actually, the number will probably be less, since the band in which Bunner (1964) calculated the photons is larger than 1 nm. However, for purposes of this theoretical calculation, a value of 5.5 photons per particle is used. The activity required per nanometer at 316 nm is determined using Equation 7.3 to compute the solid angle, which is the portion of photons emitted by the source that are received by the collector. Dividing the MDNP by the solid angle gives the number of photons that must be emitted.

$$Emitted\#\ Photon = \frac{MDNP}{Solid\_Angle} 10^4 cm/m \tag{8.1}$$

The number of particles emitted by the source is the number of photons emitted divided by the number of photons created by each alpha particle. Since there are 3.7E+10 particles per curie, the activity per nanometer is given by Equation 8.2 and displayed in Table 8.1 and Table 8.2.

$$\text{Activity} = \frac{(MDNP)(10E4)}{Solid\_Angle}\left[\frac{1}{(photons\_per\_particle)(3.7E10)}\right] \tag{8.2}$$

The location of the source (e.g., against a barrier, capable of emitting in ½ of a sphere, 2π geometry, or in the open, capable of emitting in all directions, 4π geometry) can alter the activity required for a detection. For this study we will assume 2π geometry, doubling the value obtained using Equation 8.2.

Table 8.1

Prediction of ^{241}Am Activity
Required at 316 nm for Daytime Scenarios

Sky Condition	**Daytime Background-Solar (Photons*s^{-1}cm^{-2})**	**CDL (Photons*s^{-1}cm^{-2})**	**MDNP at 95% Confidence (Photons*s^{-1}cm^{-2})**	**Activity per nm Required to get MCNP (Curies)**
Clear	1.9510E+13	1.0276E+07	2.0551E+07	1.015E+04
Overcast	1.9510E+11	1.0276E+06	2.0551E+06	1.015E+03
Twilight	1.9510E+09	1.0276E+05	2.0551E+05	1.015E+02

A moonless clear night reduces the light by a factor of at least 10 (i.e., 10^{-1} from a full moon), and a moonless, overcast night sky reduces the light by an additional factor of 10 (i.e., 10^{-2} overall from a full moon) (Schlyter 2010). Table 8.2 shows the results of nighttime scenarios considering a full moon and moonless conditions.

Table 8.2

Prediction of ^{241}Am Activity
Required at 316 nm for Nighttime Scenarios

Sky Condition	**Nighttime Background (Photons*s^{-1}cm^{-2})**	**CDL (Photons*s^{-1}cm^{-2})**	**MDNP at 95% Confidence (Photons*s^{-1}cm^{-2})**	**Activity per nm Required to get MCNP (Curies)**
Full Moon	1.9510E+07	1.0276E+04	2.0554E+04	1.015E+01
Moonless Clear (at horizon)	1.9510E+06	3.2494E+03	6.5016E+03	3.212E+00
Moonless Overcast (at horizon)	1.9510E+05	1.0276E+03	2.0578E+03	1.017E+00

Results of the theoretical calculations in Table 8.1 show that large ^{241}Am sources equal to or greater than 1.015E+02 curies, using 2π geometry, can be detected during twilight hours when background scenarios only contain only solar radiation. Looking at Table 8.2, at night, with a full moon, an activity of 1.015E+01 curies is required. This value is reduced to 3.212E+00 curies with no moon, and 1.017E+00 curies on a moonless night with overcasts skies. If a sicintillator can be found similar to those found for ^{90}Sr (i.e., polypropylene, HDPE, or LDPE) with scintillation to air fluorescence ratios of at least a 100, the required activities in Tables 8.1 and 8.2 are divided by 100. Of course, the location and type of radioactive material must be known, and the area must allow the material to be overlaid with the scintillator material. In such cases, the activities in Tables 8.1 are reduced to 100.15, 10.15, 1.015 curies for a clear, overcast, and twilight background light, respectively. Additionally, the values for nighttime conditions in Table 8.2 can be reduced to 100.15 mCi for a full moon, 32.12 mCi for no moon, and 10.17 mCi for no moon with an overcast sky. Scintillation is a powerful addition to the detection toolbox, making possible the detections of 10s to 100s of millicuries of radioactive materials in some nighttime background conditions in the 300 to 400 nm region.

8.2 Opportunities for Future Work

Future opportunities for work on optical techniques for the detection of radiation induced air fluorescence in outside scenarios in the 300-400 nm region should focus on increased efficiencies of the collector system, the identification and use of scintillators, and the examination of the background signal for harmonic and temporal components.

Better photomultiplier tubes with increased efficiencies (i.e., 40% compared to 20%) can increase the overall collector system efficiency by a 100 percent. Additionally, PMTs with lower dark counts would be of great value in scenarios where the background UV can be controlled or limited to certain wavelengths. In these situations, the background of the collector system is the major source of background noise.

The reflective and refractive characteristics of the collector system should be explored. The use of multiple transmissive filters, required to achieve low out of band transmission values, often come at the expense of lower in-band transmission values (e.g., 90 %) for transmissive filters compared to reflective filters which often have efficiencies in the 99% range. The maximum use of reflective filters will increase the system's efficiency.

High in-band outside natural and man-made UV background levels often preclude the use of optical techniques for the detection of small radioactive sources (i.e., with activities smaller than 10s to 100s of millicuries per nanometer) without scintillators. More research is needed to identify additional common materials for beta scintillation, and materials that are good alpha scintillators. This study shows that where ^{90}Sr radiation is known to exist, and the area can be overlaid with a scintillator (e.g., the polypropylene, high density polyethylene, and low density polyethylene), the signal can be increased by a factor of over a 100 in the 10 nm bands centered on 313, 380 and 390 nm. More research is needed to identify scintillator characteristics (e.g., thickness, density, internal transmissions at various wavelengths, etc.) that maximize scintillators' potential. Additionally, doping additives, that increase the scintillation value, similar to those listed in Table 2.3, should be explored.

A Fourier analysis of the background signal should be explored, and if possible, an algorithm developed to identify and filter out background contributions with harmonic

components. Additionally, the temporal characteristics of the signal should be examined to determine if there are periods with short time intervals between photons arrivals (i.e., a condition common to arcing and fires) that can be filtered and the remaining signal used to provide detections at the desired confidence level.

References

Ave M., M. Bohacova, B. Buonoma, N. Busca, L. Cazon, S. Chemerisov, M. Conde, R. Crowell, P. Di Carlo, C. Giulio, M. Doubrava, A. Esposito, p. Facal, F Franchini, J. Horandel, M. Hrabovsky, M. Kleifges, S. Kuhlmann, G. Mazzitelli, L. Nozka, A. Obermeier, M. Paltaka, S. Petrers, P. Privitera, J. Ridky, V. Rizi, G. Rodriguez, F. Salamida, P. Schovanek, H. Spinka, E. Strazzeri, A. Ulrich, Z. Yusof, V. Vacek, P. Valente, Verzi, T. Waldenmaier, 2007, Measurement of the pressure dependence of air fluorescence emission induced by electrons. arXiv:astro-ph/0703132v1 6 March. 4, 14, 32.

Ave, M., M. Bohacova, B. Buonoma, N. Busca, L. Cazon, S. Chemerisov, M. Conde, R. Crowell, P. Di Carlo, C. Giulio, M. Doubrava, A. Esposito, p. Facal, F Franchini, J. Horandel, M. Hrabovsky, M. Kleifges, S. Kuhlmann, G. Mazzitelli, L. Nozka, A. Obermeier, M. Paltaka, S. Petrers, P. Privitera, J. Ridky, V. Rizi, G. Rodriguez, F. Salamida, P. Schovanek, H. Spinka, E. Strazzeri, A. Ulrich, Z. Yusof, V. Vacek, P. Valente, Verzi, T. Waldenmaier. 2007. Temperature and Humidity Dependence or Air Fluorescence Yield measure by Air Fly. 2008. Nuclear Instruments and Methods in Physics Research A 597 28 November. 52.

Bachelor, Paula P., David v. Jordan, Warren W. Harper, Bret D. Cannon, and Erin C. Finn. 2009. Self-absorption effects on Alpha-induced atmospheric nitrogen fluorescence yield. *Journal of Radioanalytical Nuclear Chemistry* 282. 872-876.

Baschenko, S. M. 2004. Remote Detection of Alpha Particle Sources. *Journal of Radiological Protection*, Vol. 24. 75-82.

Bergman ,R. S. , T. S. Parham, and T. K. McGowan. 1994. UV Emissions form General Lighting Lamps. Paper presented at the IES Conference, Miami, FL. August 7-11. 1-3, 14-15.

Bias, C. 2008. Enhanced Detection of Induced Fluorescence From Residual Radioactive Materials, PhD diss., University of Nevada.

Birks, J.R. , 1964, *The Theory and Practice of Scintillation Counting*, NewYork: The Macmillan Company. 235-265.

Bunner , A. N., 1964, The Atmosphere as a Cosmic Ray Scintillator, Master's Thesis, Cornell University. 106.

Bunner, A. N., 1967, Cosmic Ray Detection by Atmospheric Fluorescence, PhD diss., Cornell University. 26.

Clark ,R. N. and G. A. Swayze, R. Wise, K. E. Livo, T. M. Hoefen, R. F. Kokaly, and S. J. Sutley, 2007, USGS Digital Spectral Library splib06a, *U.S. Geological Survey, Data Series 231*: 49-54. http://speclab.cr.usgs.gov/spectral.lib06/ds231/datatable.html [Accessed July 18, 2010]

Davidson, G. and R. O"Neil. 1964. Optical Radiation from Nitrogen and Air at High Pressure Excited by Energetic Electrons, American Science and Engineering, Inc., Cambridge, Massachusetts, *The Journal of Chemical Physics* Vol 41, No 12: 3946-3955.

General Electric. 2008. "Spectral Power Distribution Curves". www.gelighting.com/na/business_lighting/education_resources/learn_about_light/distribution_curves [Accessed 21 April, 2008].

Hannuksela, Ville, and Juha Toivonen, Harri Toivonen. 2010. Optical remote detection of alpha radiation. *Proceedings of Third European IRPA Cpngress*, June 14-18, Helsink, Finland. 1-7.

"History of Air Fluorescence Technique," 2007, http://www.telescopearray.org/outreach/history.html. [Accessed October 2010].

Huntemeyer, Petra. 2003. An Experiment to Measure the Air Fluorescence Yield in Electromagnetic Showers. 28th International Cosmic Ray Conference. Universal Academy Press, Inc. 845-848.

IUPAC Compendium of Chemical Terminology, 1997, 2nd Edition http://old.iupac.org/oldbook/L03540.pdf [accessed April 27, 2010].

Kakimoto, F. , E. C. Loh, M. Nagano, H. Okuno, M. Teshima, and S. Ueno, 1996, A Measurement of the Air Fluorescence Yield. *Nuclear Instruments and Methods in Physics Research* Section A, Vol. 372, Issue 3, April. 527-533.

Knight, Randall D and Brian Jones and Stuart Field. 2006. *College Physics: A Strategic Approach*. San Francisco: Pearson Addison-Wesley. 585-586.

Knoll ,G. F. 1979. *Radiation Detection Measurement.* New York: John Wiley & Sons. 774-775, 776.

Knoll, G.F. 1999. *Radiation Detection Measurement*. Hoboken, New Jersey: John Wiley & Sons, Inc. 94-96, 4, 44-45, 117-118, 219-234.

Kozlowski, C. 2001. UV Radiation Emitted by Selected Sources at Work Stands. *Internatioal Journal of Occupational Medicine and Environmental Health*, Vol. 14, No. 3; 287-292.

Lamadie F. ,, J. R. Costes, F. Delmas, C. Mahe, P. Girones, C. Le Goaller, 2004, Alpha imaging; first results and prospects. *Nuclear Science Symposium Conference Record*, 2004 IEEE Vol. 3, Issue, 16-22 Oct. 2004. 1594-1598.

Leybourne, A.E., S. Creasey, J. Dixon, J. Lee, G. Messer, S. Neal, G. H. Rayborn, D. Speaks, J. Stephens, T. Strange, C. D. Walker, W.C. West, H. F. Woodruff, and C. B. Winstead,. Long Range Detection of Radiation-Induced Air Fluorecence. Proceedings of the Institute of Nuclear Materials Management 51st Annual Meeting, July 11-15, 2010, Baltimore, MD. 1-9.

McCluney ,W. R., 1994, *Introduction to Radiometry and Photometry*, Boston: Artech House, Inc.

Nagano,M., K. Kobayakawa, and N. Sakaki, 2001, "*Fluorescence Efficiency of Electrons in the Atmosphere Above Oceans*," Proceedings of the ICRC 2001, pp. 675-678.

O'Neil,R. and G. Davidson, 1968, "The Fluorescence of Air and Nitrogen Excited by Energetic Electrons," Final Report for Contract AF 19(628)-4080 Prepared for the Air Force Cambridge Research Laboratories, AFCRL-67-0277. 18-37.

Reece, R., 2005, "Air Fluorescence Photon Yield in Cosmic Ray Showers," The University of Texas, Austin.

Runkle, Robert C., and L. Eric Smith, and Anthony J. Peurrung. 2009. The photon haystack and emerging radiation detection technology. *Journal of Applied Physics* 106, 041101, 24 August.

Sigma Aldrich. 2008. http://www.azom.com/details.aps?ArticleID-2960 [Accessed January 8, 2008].

Sokolsky, P, 2003, *The High Resolution Fly's Eye and the FLASH Experiment*. AAPPS Bulletin Vol. 13. February 11-17.

Saleh, Bahaa E .A. and Malvin Carl Teich, 1991. *Fundamentals of Photonics*. New York: John Wiley & Sons, Inc. 399-400, 673-675.

Shapiro , J. 1995, 2002, *Radiation Protection, A Guide for Scientists, Regulators, and Physicians*, 4th Rd., Harvard University Press, Cambridge, Massachusetts, and London, England. 26-31, 51-53, and 181.

Sigmore, A.C. 1968. Protection of light-sensitive products. *Modern Packaging*, New York: McGraw-Hill, June. 243-245.

Schlyter, Paul. 2010. Radiometry and Photometry in Astronomy: 10-12. http://stjarnhimlen. se/comp/ radfaq.html#10 [Accessed October 13, 2010].

Tsoulfanidis, N, 1995, *Measurement and Detection of Radiation*, Washington, DC: Taylor and Francis. 45, 52-54, 69-73, and 160.

Tuma, Jan J. 1976. *Handbook of physical Calculations.* New York: McGraw-Hill, Inc. 320-328.

Waldenmaier, T, J. Blumer, H. Klages, 2008, Spectral resolved Measurement of the Nitrogen Fluorescence Emissions in Air induced by Electrons, arXiv:0709.1494v2 [astro-ph]. 17-19.

Wilner, Kalman and Nissim Ben-Yosef. 1998. Clutter in the solar blind ultraviolet urban areas. Society of Photo-Optical Instrumentation Engineers, *Optical Engineering*, Vol 37, No. 3. March.

Ziock, Klaus. P., William W. Craig. Lorenzo Fabris, Richard C. Lanza, Shawn Galagher, Berthold K. P. Horn, and norm W. Madden. 2004. Large Area Imaging Detector for Long-Range, Passive Detection of Fissile Material. *IEEE Transactions on Nuclear Science*, Vol. 51. No. 5. October; 2238.